UNIVERSITA' DI PISA

Dipartimento di Chimica e Chimica Industriale

"Scuola di Dottorato Galileo Galilei"

PhD course in Chemical Science (CHIM/03)

XXV cycle

(2010-2012)

Metal clusters as organometallic synthons

Veronica Bonuccelli

Supervisor:

Prof. Piero Leoni

External supervisor:

Prof. Clifford P. Kubiak

Table of contents

Abstract

The achievement of molecular assemblies containing transition metal clusters inserted in the main chain of a polymer, especially if the cluster-cluster connection is made through conjugated spacers covalently bonded to the metal atoms is a poorly explored field of modern organometallic chemistry and nanotechnology. This Thesis deals with the synthesis, and the spectroscopical, electrochemical and spectroelectrochemical characterization of systems containing cluster units derived from $[\{Pt_6\}(CO)_2](CF_3SO_3)_2$, **3**$(CF_3SO_3)_2$ $\{Pt_6\}$ = $[Pt_6(\mu\text{-}PBu^t_2)_4(CO)_4]$, an hexanuclear cluster with 82 valence electrons, of compounds containing one or two [60]fullerene molecules linked to one cluster unit derived from **3**$(CF_3SO_3)_2$ or from the $44e^-$ trinuclear cluster $[\{Pt_3\}(CO)_3](CF_3SO_3)$, **2**$(CF_3SO_3)$ $\{Pt_3\}$ = $[Pt_3(\mu\text{-}PBu^t_2)_3(CO)_2]$, and of new tris-phosphido bridged palladium clusters suitable to be used as synthons for ordered molecular assemblies.

Clusters **2**(CF_3SO_3) and **3**$(CF_3SO_3)_2$ have a stable internal core (a Pt_3 triangle in the former and a Pt_4 tetrahedron with two opposite edges bridged by two "apical" Pt atoms in the latter) enveloped, respectively, by 3 or 4 bulky di-*t*-butylphosphides, which leave only a few and well-located reactive positions, mutually directed, respectively, at 120° and 180°. The study of the general reactivity of these compounds has shown that, leaving unchanged the $\{Pt_3\}$ or the $\{Pt_6\}$ cores, it is possible to substitute all the three or only one carbonyl ligand in the trinuclear cluster and that the substitution reactions occur selectively on the two "apical" platinum atoms in the hexanuclear cluster. For example, **2**(CF_3SO_3), reacts with an excess of an halide salt achieving the monosubstituted derivative $\{Pt_3\}X$, and, in the same reaction conditions, **3**$(CF_3SO_3)_2$ gives the dihalo cluster $\{Pt_6\}X_2$; moreover, the reaction of $\{Pt_6\}Cl_2$ (**4**) with $NaBH_4$ affords the dihydride derivative $\{Pt_6\}H_2$ (**5**), which is a useful precursor for the introduction of other functionalities in the apical positions. Thanks to these features, these clusters are suitable synthons for the synthesis of ordered molecular assemblies.

Starting from the knowledge of the general reactivity of these derivatives, we prepared the asymmetric derivative $\{Pt_6\}(H)(OSO_2CF_3)$ (**6**), by treating a solution of **5** in dry Et_2O with triflic acid, and the alkynyl derivatives $[\{Pt_3\}(CCC_6H_4CHO)]$ (**13**) and

[{Pt_6}($CCC_6H_4CHO)_2$] (**17**), by reacting the corresponding chloro-derivative with 4-ethynyl-benzaldehyde (**12**), under Sonogashira-type conditions (NEt_3 as the solvent and a catalytic amount of CuI). Moreover, **6**, **13** and **17** were employed as precursors for the synthesis of the "dicluster" compounds [{Pt_6}(H)]$_2$(μ-Y) [**9**$(CF_3SO_3)_2$, Y = 4,4′-bipyridine; **10**$(CF_3SO_3)_2$, Y =1,4-dicyanobenzene], which were prepared by reacting **6** with a stoichiometric amount of the appropriate bifunctional ligand, and of the neutral compounds [{Pt_3}$CCC_6H_4C_2H_3N(C_8H_{17})C_{60}$] (**16**) and [{$Pt_6$}{$CCC_6H_4C_2H_3N(C_8H_{17})C_{60}$}$_2$] (**18**), achieved by refluxing a chloro-benzene solution of [60]fullerene, *N*-octylglycine and, respectively, **13** or **17**. All new derivatives were characterized by IR and multinuclear NMR spectroscopies and the structure of cluster **13** was confirmed by a single crystal X-ray diffraction study.

In addition, cyclovoltammetric and spectroelectrochemical measurements on CH_2Cl_2 solution of **9**$(CF_3SO_3)_2$, **10**$(CF_3SO_3)_2$, **13** and **16** were performed, in order to evaluate the intramolecular electron delocalization.

The cyclovoltammetric profile of **9**$(CF_3SO_3)_2$ and **10**$(CF_3SO_3)_2$ shows a number of reduction processes higher than in the "single" hexanuclear derivatives, which undergo two reversible monoelectronic reduction processes. This may suggest a possible electron transfer, and the IR spectra recorded during their stepwise reduction allowed the characterization of the reduced species.

Furthermore, **13** and **16** undergo two oxidation processes, typical of the trinuclear derivatives, and the voltammogram of **16** shows, also, three reduction processes, due to the presence of the fullerene unit. Also in this case, the oxidation products of **13** and **16** were characterized by IR, UV-Vis and NIR spectroelectrochemical measurements.

In order to enlarge the library of clusters usable as synthons for ordered molecular structures, the trinuclear monohalide clusters {Pd_3}$(CO)_2$X [{Pd_3} = Pd_3(μ-$PBu^t_2)_3$; X = Br (**20**), I (**21**)] were prepared by reacting stoichiometric amounts of the proper *t*-butylammonium halide and the dinuclear complex [Pd(PBu^t_2H)(μ-PBu^t_2)]$_2$ (**19**). The reaction of **21** with $CNBu^t$, leads to the substitution of all the terminal ligands affording the symmetrical cluster [{Pd_3}($CNBu^t)_3$]I, **26**(I). Metathesis of the anion, obtained by treating **26**(I) with $AgCF_3SO_3$ or $AgPF_6$, afforded cleanly the new salts **26**(CF_3SO_3) or **26**(PF_6), respectively. The cationic clusters [{Pd_3}$(CO)_2(NCCH_3)$](PF_6), **24**(PF_6), [{Pd_3}$(CO)_2$(Py)](PF_6), **25**(PF_6) and [{Pd_3}$(CO)_3$](PF_6), **23**(PF_6), were respectively

obtained by reacting **21** with $TlPF_6$ under nitrogen in acetonitrile or in pyridine solution or under 1 atm of carbon monoxide in THF. Finally, $\{Pd_3\}(CO)_2Cl$ (**22**) was achieved by the reaction of **23**(PF_6) with $[(PPh_3)_2N]Cl$. All clusters have been obtained in good yields and purity and have been characterized by microanalysis and IR and multinuclear NMR spectroscopies. Single crystal X-ray diffraction studies on **20** and $[\{Pd_3\}(CNBu^t)_3](CF_3SO_3)$, **26**($CF_3SO_3$), confirmed the structures suggested on the basis of the spectroscopical characterization.

The cyclovoltammetric profile exhibited in dichloromethane solution by the palladium clusters prepared in this work is characterized by the presence of two oxidation processes, whose reversibility and potentials depend on the ligands' nature. Moreover, UV-Vis and IR spectroelectrochemical studies on **21**, **23**(PF_6) and **26**(PF_6) provide the spectroscopical characterization of the stable electrogenerated oxidized species and details for the redox-coupled reactions of metastable products.

1 Introduction

In 1964 F. A. Cotton introduced the term "*Cluster*", in substitution of terms like "*Staphylonuclear*" and "*Cage*" used previously to define compounds for which the presence of direct bonds between a finite number of metal centers was unquestionably established.[1] Thus, a polynuclear transition metal complex is not necessarily a cluster complex. An even more strict definition describes a metal cluster[2] as a finite number of metal atoms (at least three) held together among themselves by direct metal-metal bonds. Besides the set of metal centers, a molecular cluster contains a certain number of terminal or bridging ligands, and may contain one or more elements of the principal groups, localized inside or on the surface of the polymetallic unit. Since the seminal papers published by Cotton[1] on Re(III) dimers and trimers with multiple metal-metal bonds, clusters chemistry has grown exponentially, thanks also to the essential contribution given by the continuous improvement of X-ray crystallography.

Transition metal clusters could be subdivided in two main classes:[2d] *organometallic clusters*, in which the metals are in a low oxidation state (around zero, or also negative) and are coordinated to π-acidic ligands (mainly carbon monoxide) and *inorganic clusters*, with the metals in medium oxidation state and coordinated to σ-donor (and often π-donor) ligands as halides, alkoxides, carboxilates or amides. Generally, clusters belonging to the first class have nuclearity (number of metal atom) that can either be very low (< 6) or very high (up to 154) and single or fractional metal-metal bond order. The others, on the contrary, have low nuclearity and often contain multiple metal-metal bonds.[3,4]

Clusters with a low nuclearity frequently have highly symmetrical structures. Metal atoms tend to aggregate in regular deltahedra (polyhedra with equilateral triangular faces) like tetrahedra, trigonal bipyramids and octahedra. There are also other less symmetrical structures, which may be considered as derived from deltahedra by rupture of one or more metal-metal bonds (Figure 1). Clusters with higher nuclearity have less regular structures arising from the progressive addition of metal centers to bridge bonds or to cap faces of the simpler deltahedral structures, or by condensation by atom-, bond- or face-sharing of smaller structures. Pseudo-spheric structures (eg. cube, icosahedron) are common only in the presence of interstitial atoms.

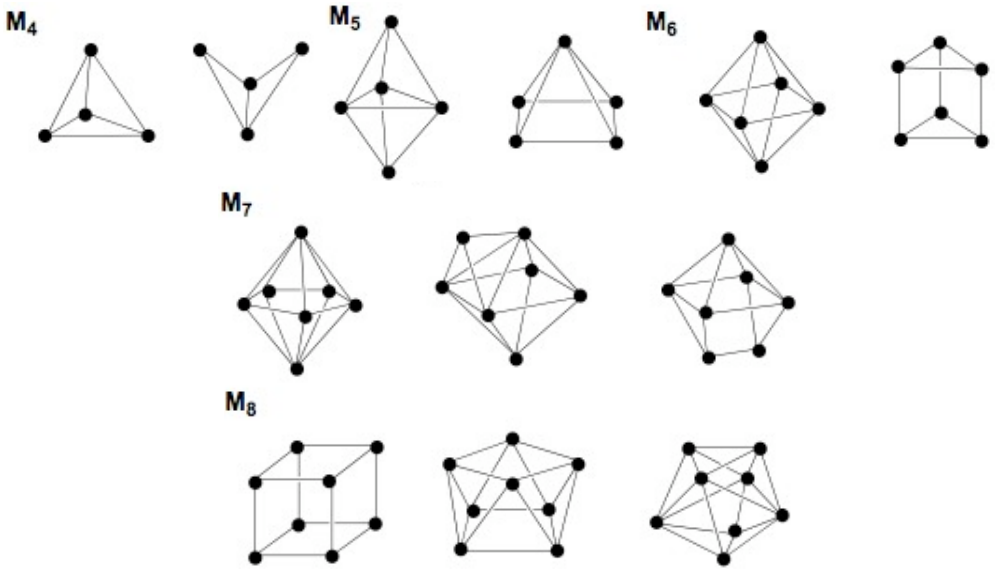

Figure 1. Examples of cluster structures.

Often, the disposition of the metal centers is similar to those observed in close-packed bulk metals. This is frequent if the cluster nuclearity is high, even if triangular, tetrahedral and octahedral geometries may be considered as fragments of the hexagonal close-packing.[2a]

Cluster structures may be correlated with the number of valence electrons (NVE) and the nuclearity of the cluster itself. Small clusters (five or less metal atoms) often obey the 18-e$^-$ rule; in this case, the NVE of the cluster is correlated to the nuclearity x and to the number of metal-metal bonds y by equation (1):

$$NVE = 18x - 2y \qquad (1)$$

When the number of metal atoms increases, the 18-e$^-$ rule is no more obeyed;[5] for this reason, new rules have been proposed. The most general are the PSEP (Polyhedral Skeletal Electron Pair, or Wade-Mingos, rules),[5,6] based on a molecular orbital treatment of the bond which adapt the rules stated before for boranes and carboranes to transition or post-transition metal clusters with pseudo-spherical (closo) or more open (nido or arachno) structures, as well as with other less regular structures.

Without entering into the details of these rules, they allow to assign a typical NVE to each of the most commonly found cluster structures, for example a tetrahedral or an octahedral cluster are respectively expected to have 60 or 86 valence electrons (see

Table 1 for other NVE-structure relationships). Two electrons must be added to each number when one metal-metal bond is broken, for example, by breaking one of the six metal-metal bond of a tetrahedral cluster we obtain the butterfly structure with NVE = 62, the opening of a further MM bond affords the square-planar geometry with NVE = 64.

Table 1. Example of correspondence between cluster structures and NVE.

Cluster geometry	NVE	Examples
Triangle	48	$Os_3(CO)_{12}$
Tetrahedron	60	$Rh_4(CO)_{12}$
Square plane	64	$Pt_4(MeCO_2)_8$
Trigonal bipyramid	72	$Os_5(CO)_{16}$
Square pyramid	74	$Fe_5(CO)_{15}C$
Octahedron	86	$Ru_6(CO)_{17}C$
Trigonal prism	90	$[Rh_6(CO)_{15}C]^{2-}$
Square antiprism	114	$[Co_8(CO)_{18}C]^{2-}$
Cube	120	$Ni_8(PPh)_6(CO)_8$

The PSEP rules are generally valid only for clusters with 12 or less metal centers. Other rules are stated for larger clusters, but their reliability is inversely proportional to the nuclearity of the cluster.[7] Indeed, upon increasing the number of metal centers, the molecular orbitals become more numerous and closer and closer in energy, also in the frontier area. As the number of non-bonding or weakly bonding or anti-bonding orbitals increases, the cluster becomes relatively stable with a variable number of electrons and may behave as an electron reservoir (molecular capacitor).

In the last years, the interest for the properties of this latter type of clusters has contributed to the development of an active research on the synthesis and the characterization of high-nuclearity clusters, the so called “giant clusters”. Until now, a lot of giant clusters have been prepared and crystallographically characterized;[8] to the best of our knowledge, the largest structurally characterized cluster is presently

$Pd_{154}(CO)_{60}(PEt_3)_{30}$, which has been prepared by Dahl *et al.*.[9] These clusters are interesting also because: a) it is not fully clear where is the threshold above which electronic structure of the cluster becomes similar to the one typical of bulk metals; b) since molecular clusters become larger, and nanoparticles and colloids (which, differently from molecular clusters, are polydispersed particles with undefined composition and structure) are getting smaller and smaller, soon it will not be possible to differentiate them in terms of nuclearity. The knowledge of the properties of giant molecular clusters will be helpful to understand the properties of nanoparticles, especially as concerns quantum effects, which are correlated to their dimensions.[10]

Another field investigated in detail recently is the search for new compounds containing linear metal-metal bonded chains.[11,12,13] These compounds are considered as molecular models of an ordinary wire, which is a long and thin piece of metal covered with a flexible organic or polymeric insulator. In the molecular models, a single linear chain of metal atoms is coordinated to proper bridging ligands which, in addition to force to linearity (that is an unusual arrangement for polymetallic systems), behave as "insulators" (Figure 2).[11m]

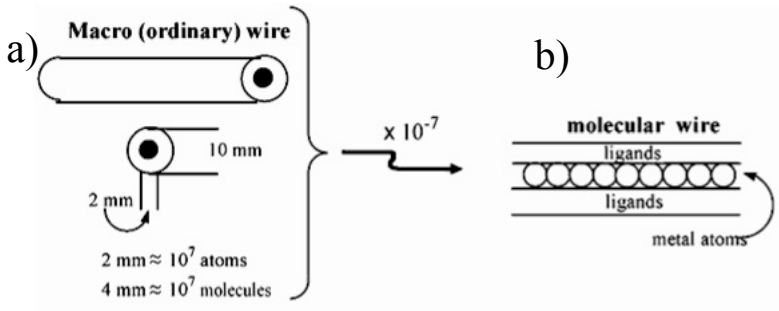

Figure 2. Schematic representation of a a) macrowire and a b) molecular wire.

Along these lines, extended metal atom chain (EMAC) systems, with up to 9 metal centers kept together by polypyridylamido ligands, have been developed independently by Cotton[11] and Peng.[12] For example, Cotton has studied linear trinuclear complexes of general formula $M_3(dpa)_4L_2$ (dpa = 2,2′-dipyridylamide, Figure 3).[11g] By chemically or electrochemically varying the oxidation states of the metal centers, these compounds show a remarkable variation of the metal-metal bond order and of the electron delocalization across the metal chain.

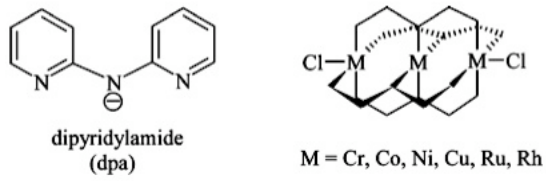

Figure 3. Linear trinuclear complexes of the type $M_3(dpa)_4L_2$.

Peng and co-workers have synthesized mono-dimensional polymers in which linear trinuclear complexes as $Ni_3(dpa)_4(PyCOO)_2$ are linked to the axial sites of metalloporphyrins (Figure 4). Due to the optical, electronic and photophysical properties of the porphyrin moieties, these co-polymers are good candidates for several applications as sensors, magnetic materials and catalysts.[12c]

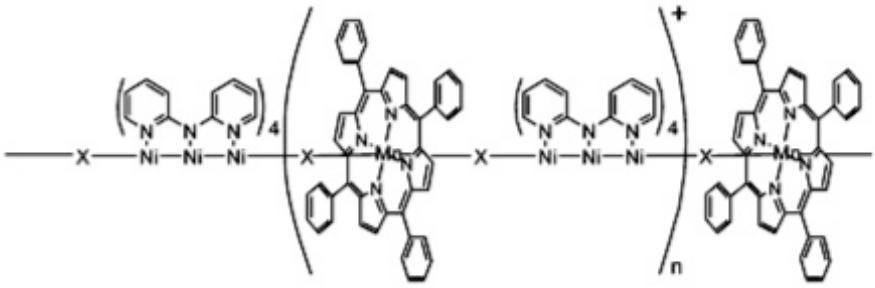

Figure 4. Example of trinickel EMACs and metalloporphyrins co-polymer.

During the last years, systems containing non-linear polymetallic compounds as charge- and electron-transfer materials, such as functionalized ionic materials obtained by assembling functional anionic molecular clusters with suitable cations, have been prepared.[14] For example, Longoni and co-workers prepared different viologen salts of bimetallic carbonyl clusters, in particular $[EtV]_2[Fe_4Pt(CO)_{16}]$, $[EtV][Fe_4Au(CO)_{16}]_2 \cdot 2THF$ and $[EtV][Fe_3Pt_3(CO)_{15}] \cdot THF$, (where EtV = 1,1´-diethyl-4,4´-bipyridilium cation), in which the redox-active organic cation has formal redox potentials comparable to those of the metal cluster anions. Resistivity measurements showed that the mixed $[EtV][Fe_3Pt_3(CO)_{15}] \cdot THF$ salt displays a resistivity in pressed pellets that is three/four orders of magnitude smaller than the one of similar salts containing a nonredox cation, $[NMe_2CH_2Ph]_2[Fe_3Pt_3(CO)_{15}]$, and typical of a semiconductor.[14b]

Possible developments in the fascinating new field of molecular electronics are expected for these and similar structures, as well as for high nuclearity metal clusters that behave as electron reservoirs, and are being studied as molecular nanocapacitors.[15,16]

A new type of synthetic application is recently attracting considerable and increasing interest; according to this approach small metal clusters are used as the precursors of large molecular "polycluster" aggregates in which two or more cluster units are not connected by new metal-metal bonds but by firmly bonded organic, inorganic or organometallic spacers.

1.1 Cluster-containing molecular assemblies.

1.1.1 "Small" assemblies.

An attractive development of molecular cluster chemistry concerns the synthesis of molecular assemblies containing transition metal cluster units kept together via bridging ligands in predefined patterns (polycluster derivatives). Although a systematic research in this field has grown up only in the last decade, a relevant number of dicluster structures is now available. As far as the cluster-bridging ligand connection is concerned, this is more frequently made with coordinative bonds with bifunctional ligands with P, O, N, S donors (especially with bridging diphosphines) than with metal-carbon bonds; in the latter case bis-carbynes,[17] bis-alkyne[18] and bis-alkynyl[19] ligands are of common use. Most of these derivatives contain M_3 units with M = Co,[20] Os,[21] Mo,[22] W[23] and Ru[24]. As concerns bridging bis-alkynyls, only in a few examples, the alkynyl-cluster bond is of the σ, η^1,μ_3 type,[25] while more generally it involves also the π-electrons of the CC triple bond.

Surprisingly, since Pt_3 clusters are relatively common, only a very few Pt_3 dicluster derivatives have been reported until now. To the best of our knowledge, these are limited to $[Pt_3](\mu\text{-}SiMe_2\text{-}R\text{-}Me_2Si)[Pt_3]$ ($[Pt_3] = Pt_3(\mu\text{-}PPh_2)_3(PEt_3)_2$, R = 1,4-diphenylene, 1,1'-ferrocenylene), recently reported by Osakada,[26] and to the interesting class of derivatives $Pt_6(\mu_2\text{-}CO)_6(\mu_2\text{-}PP)_2(PP)_2$ or $Pt_6(\mu_2\text{-}CO)_6(\mu_2\text{-}PP)_3$ ($PP = Ph_2P\text{-}(CH_2)_n\text{-}PPh_2$, n = 1-3) described by Puddephatt in the middle 90ties, which contain two separate triangular $Pt_3(\mu_2\text{-}CO)_3(PP)$ units bridged by two or three PP ligands.[27]

Depending upon the length of the bridging diphosphine, these derivatives act as encapsulating agents (those containing four PP ligands after dissociation of one chelating diphosphine) for metal centres as $Tl^{(I)}$, $Hg^{(0)}$ [27b,c] or, when the cage between the two triangles is too small (n = 1, 2), they bind $Hg^{(0)}$ or $Tl^{(I)}$ "externally" (Figure 5).[27d]

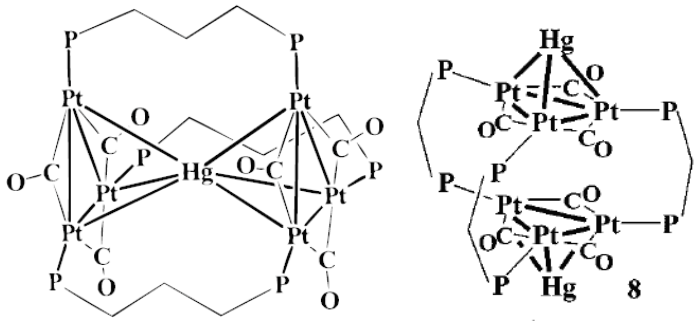

Figure 5. Examples of Pt_3 dicluster derivatives.

Also the Pd_3 unit is not common in this type of compounds. In the few examples reported up to now,[28] the most commonly used bridging ligands are the halides,[28c-f] as in $[Pd_6(\mu\text{-}Br)_4(\mu\text{-}CO)_4(PBu^t_3)_4]$ (Figure 6a), prepared by Mingos *et al.*[28d] by reacting the dinuclear complex $[Pd_2(\mu\text{-}Br)_2(PBu^t_3)_2]$ with $[Fe_2(CO)_9]$. Holah and co-workers,[28a] described the synthesis of $[Pd_6(\mu_2\text{-}CO)_6(\mu\text{-dppm})_3]$, with two almost planar and nearly eclipsed $Pd_3(\mu_2\text{-}CO)_3P_3$ units connected by three dppm (1,1-Bis(diphenylphosphino)methane) ligands (Figure 6b).

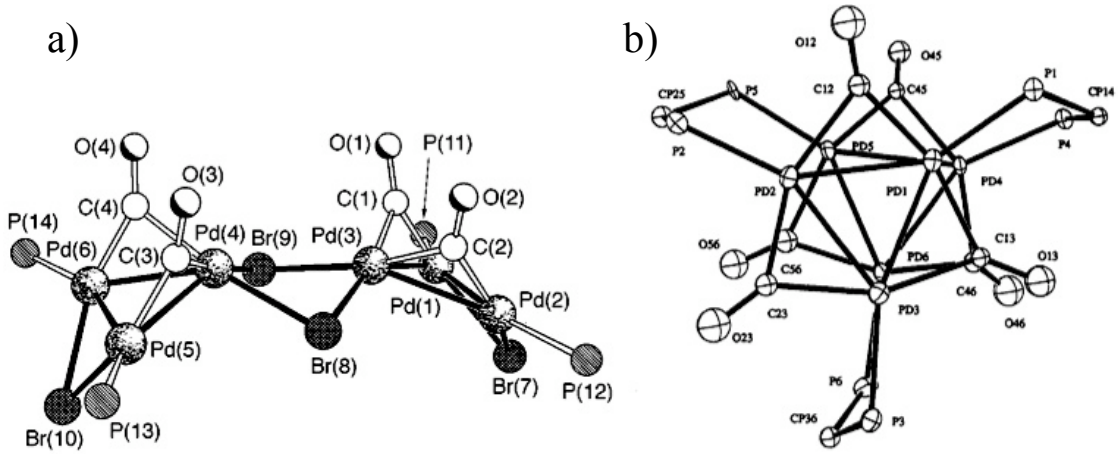

Figure 6. Molecular structure of a) $[Pd_6(\mu\text{-}Br)_4(\mu\text{-}CO)_4(PBu^t_3)_4]$ and b) $[Pd_6(\mu_2\text{-}CO)_6(\mu\text{-dppm})_3]$.

Other compounds with interesting electronic properties, although they do not contain M-M bond in the polymetallic unit, are the dimers of oxo-bridged triruthenium clusters $Ru_3(\mu_3\text{-}O)(\mu\text{–}CH_3CO_2)_6(CO)(L)(\mu_2\text{–}BL)Ru_3(\mu_3\text{-}O)(\mu\text{–}CH_3CO_2)_6(CO)(L)$ (Figure 7 with BL = pyrazine) prepared by Kubiak *et al.*[29].

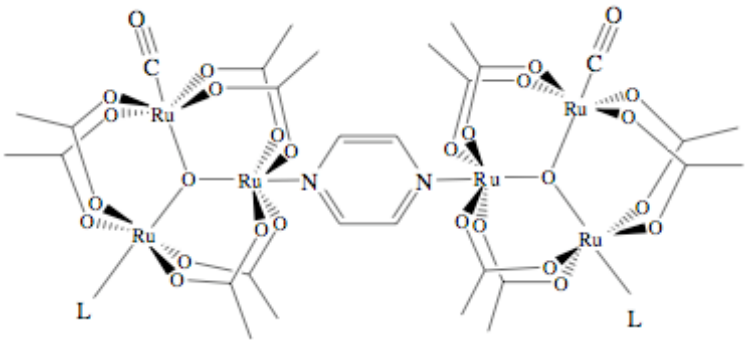

Figure 7. Structure of a dimer of trinuclear ruthenium clusters.

In these compounds, the adjustment of the ancillary ligands L and of the bridging ligands allows a fine control of their electrochemical and spectroscopic properties. Thus, depending on the nature of the ligand set, either largely charge localized, moderately coupled (Class II in the Robin-Day classification of intervalence charge-transfer complexes), or delocalized (Class III) systems have been prepared. Detailed experimental and theoretical studies on these systems shed light on fundamental aspects of the border between localized and delocalized systems, *i. e.* on the criteria that help distinguishing how the systems cross the "late" Class II, Class II/III borderline, "late" borderline, and Class III boundaries.

Polycluster derivatives with more than two cluster units are by far less common. Fehlner and co-workers[30] have utilized the $[(CO)_9Co_3(\mu_3\text{-}C\text{-})]$ cluster, functionalized with a carboxylate group, to prepare a variety of branched arrays with up to six Co_3C units, and related derivatives have been described recently by Bruce[31] (Figure 8a,b) and others.[32]

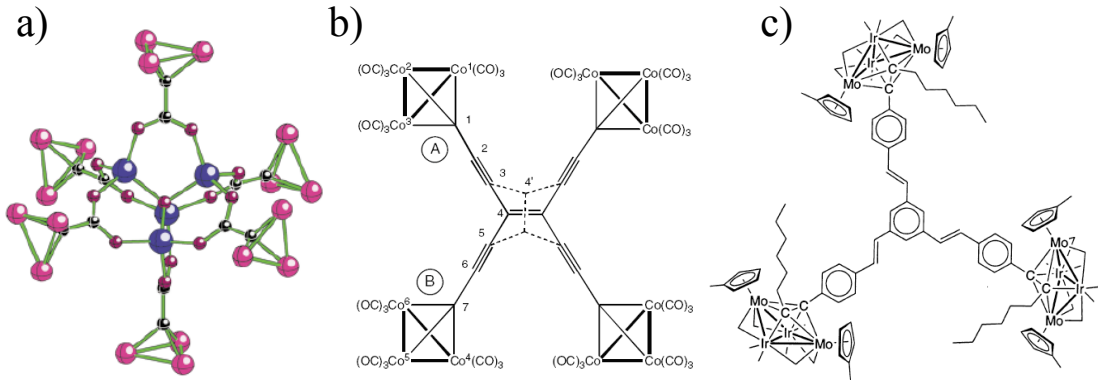

$[M_4O\{(CO)_9Co_3(\mu_3\text{-}CCO_2)\}_6]$ (M = Zn, Co)

Figure 8. Example of polycluster derivatives with more than two cluster units.

A few interesting derivatives, containing up to three cluster units, have been recently prepared by Humphrey and co-workers,[33] who exploited the tendency of the CC triple bonds of polyalkynes to form M_4C_2 octahedra when reacted with M_4 butterfly clusters (Figure 8c). Some other systems bridged by As, Te, O, S atoms, or triphosphine, hydroxy, CN or trimercapto- or tripyridyl-triazine ligands, with 3-8 cluster units, have also been described.[34]

1.1.2 Clusters-containing Polymers.

Placing transition metal centres into polymers offers a convenient way to significantly modify their properties and to achieve advanced materials. The metal may exist in various oxidation states, allowing to tune charge-transport properties, and may form stable compounds with unpaired electrons. The existence of co-operative interactions, and the alignment of the magnetic moments of transition metal ions in the solid state, may result in several kinds of magnetic materials with ferromagnetic, antiferromagnetic or superparamagnetic properties. Areas like non-linear optics and photonics, that require processable material with electron delocalization and polarizability, may also have impact from metallopolymers. Metal centres bring in close proximity many molecular "objects" with various types (and strength) of interactions allowing the supramolecular engineering of large aggregates whose shape may often be planned in advance, for example to obtain structures ordered in 1-, 2- or 3-dimensions, they often play a vital role in catalysis and in several drugs and bio-active materials. Based on these premises, the chemistry and interesting applications of coordination polymers are being

developed, but are often limited to the solid state. In organometallic polymers the problem of low solubility may be surpassed by inserting suitable substituents, generally long alkyl chains, in the molecular framework. In particularly interesting cases there is strong coupling between the orbitals of the transition metals and those of the conjugated spacers. These bridging groups are primary components of the polymer backbone and strongly influence the mechanical characteristics and the electronic, optical, catalytic and physical properties of the resulting material.

The vast majority of organometallic oligomers contain single metal centres scattered in the macromolecule and connected to each other by ditopic ligands.[35] A few recent studies concern oligomers with alternated bimetallic centres and conjugated organic spacers,[36] but analogous derivatives with transition metal molecular clusters replacing the mononuclear units are synthetically very challenging and therefore uncommon. However, for the peculiar properties of molecular clusters, which may behave as electron reservoirs and molecular capacitors, single electron tunnel effect (SET) transistors or as solid superconductors, these materials might have an excellent potential for the preparation of processable, functional materials with intriguing properties.[37,38,39]

Metal clusters can be found in three different positions relative to the backbone of the main polymer (Figure 9):

a. clusters units are embedded into the main polymeric chain;

b. clusters are directly bonded to a pre-formed polymeric chain;

c. clusters can be bonded to side arms of the main chain.

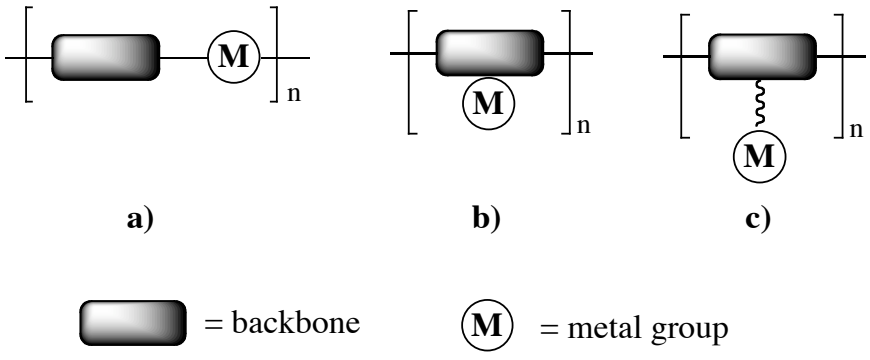

Figure 9. Possible structures of cluster-containing polymers.

While in the first case the cluster is essential for the existence of the polymer, in cases b) and c) the polymer, in principle, can exist also after cluster detachment.

Only a few examples of polymers belonging to class a) and b) are known. Generally, they contain M_n units linked by bifunctional P-, N- or isocyanide ligands. In 1994, Puddephatt and co-workers[40] described the synthesis of $\{[Pt_3(\mu_2\text{-dppm})_3(\mu\text{-CN-Ar-NC})](PF_6)_2\}_{n.}$, the first polymer with metal clusters embedded in the main chain. These short oligomers have been incompletely characterized since they are soluble only in acetone or DMSO, in which, however, extensive fragmentation of the oligomeric structure was observed.

More recently, Johnson *et al.*[41] reported the preparation of $[Ru_6C(CO)_{15}(Ph_2PC_2PPh_2)]_n$ (Figure 10), the first encompassing carbonyl clusters. The polymer is well soluble and, therefore, more easily characterizable.

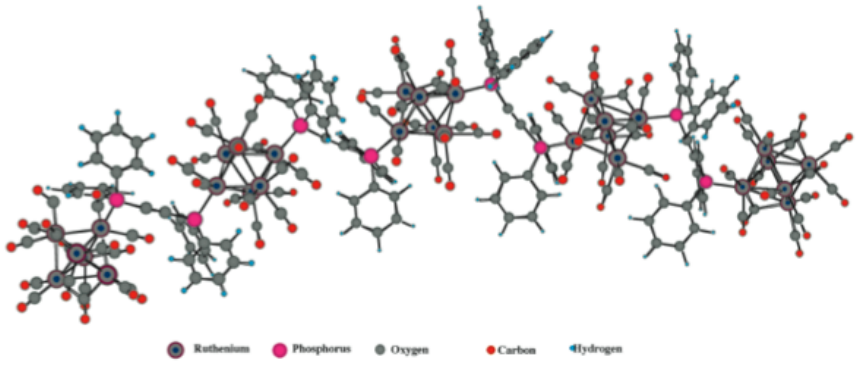

Figure 10. The proposed structure of $[Ru_6C(CO)_{15}(Ph_2PC_2PPh_2)]_{n.}$

By processing this material by electron beam exposure, nanowires with tunable conduction characteristics were produced. The polymer was prepared by reacting $[Ru_6C(CO)_{17}]$ with the diphosphine linking reagent $[Ph_2PC_2PPh_2]$ and was isolated as a dark brown powder soluble in dichloromethane. Its degree of polymerisation was estimated to be around 1000. An example of a bimetallic cluster-containing polymer has been reported by Humphrey and co-workers,[42] who synthesized a range of oligourethanes incorporating dimolybdenum-diiridium (Mo_2Ir_2) units into the oligomeric backbone, by using a step growth polycondensation approach (Figure 11).

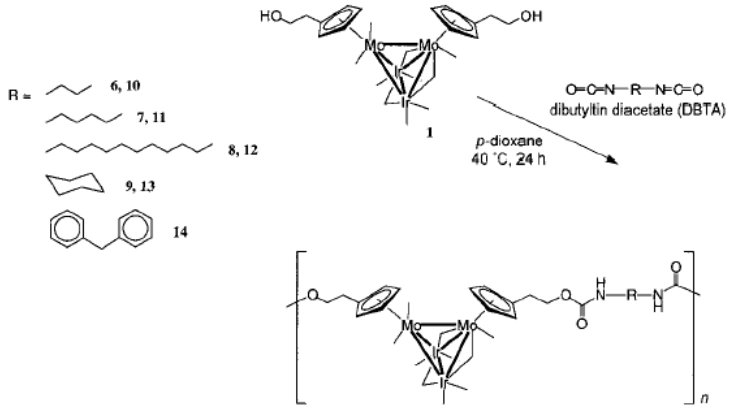

Figure 11. Preparation of oligourethanes incorporating dimolybdenum-diiridium (Mo_2Ir_2) units in the oligomeric backbone.

Han and co-workers[43] reported the synthesis of soluble organometallic conjugated polymers with multinuclear ruthenium clusters [{$Ru_x(CO)_y$}, x = 2-4] (Figure 12) bonded to azulene moieties. The composition of the clusters was found to govern the electronic and optical properties of the polymers, which were obtained by oxidative copolymerization in the presence of $FeCl_3$ of poly(bithienyl-azulenyl) derivatives with different side chains (R = $C_{10}H_{21}$ or $OC_{12}H_{25}$) followed by coordination of the cluster units, that was achieved by refluxing the conjugated polymers with $Ru_3(CO)_{12}$ in xylenes.

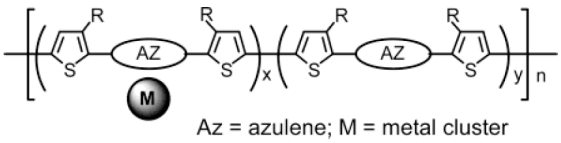

Figure 12. Azulene-based conjugated polymers with multinuclear ruthenium clusters [{$Ru_x(CO)_y$}, x = 2-4].

Hurst and co-workers[44] reported the synthesis and the characterization of a series of polymeric complexes based upon central "sandwich" tripalladium ditropylium (Tr) units [Pd_3Tr_2] connected through different halide ligands (Figure 13). Other derivatives have been prepared in our laboratories, and will be discussed in following sections.

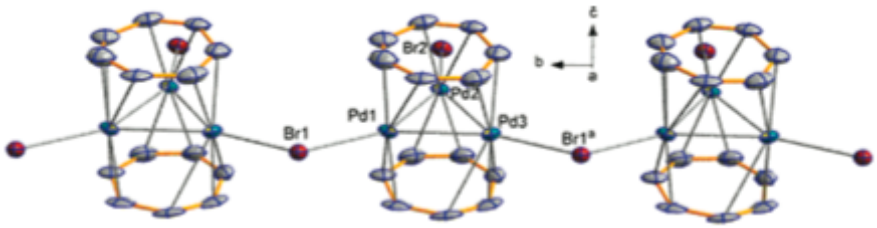

Figure 13. Structure of the polymeric palladium complexes.

On the other hand, several examples of polymers with pendant metal clusters have been reported.[45] Again, the polymer-cluster linkage is generally made through dative linkages with neutral P, O, N bifunctional donors, and has been effected either by linking the cluster units to the preformed functionalized polymers or by polymerization of a cluster unit containing an olefin moiety as a substituent in one of the ligands.

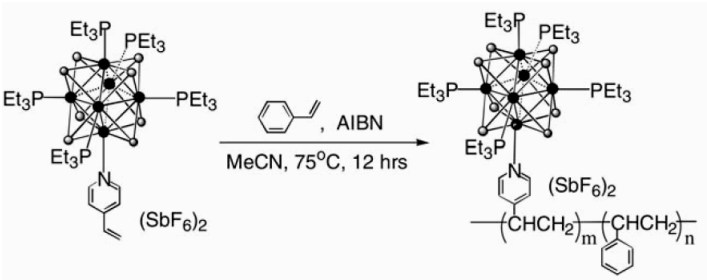

Figure 14. Synthesis of the styrene-$[Re_6(\mu_3\text{-}Se)_8(PEt_3)_5(4\text{-vinylpyridine})](SbF_6)_2$ copolymers.

For example, Zheng and co-workers[45d] reported the copolymerization of styrene with $[Re_6(\mu_3\text{-}Se)_8(PEt_3)_5(4\text{-vinylpyridine})](SbF_6)_2$ (Figure 14). The procedure afforded a novel inorganic-organic hybrid composite of high molecular weight and a low polydispersity index. This type of polymers suffers a general problem of possible leaching of the cluster units.

1.2 Phosphido-Bridged platinum clusters as building blocks for the synthesis of ordered molecular assemblies.

The 44 e^- trinuclear cluster $[Pt_3(m\text{-}PBu^t_2)_3(CO)_3](CF_3SO_3)$, **2**$(CF_3SO_3)$[46] and the 82 e^- hexanuclear cluster $[Pt_6(m\text{-}PBu^t_2)_4(CO)_6](CF_3SO_3)_2$, **3**$(CF_3SO_3)_2$,[47] have been prepared in our laboratories in the frame of a research project on the utilization of di- or trinuclear platinum derivatives as the precursors of clusters with a higher nuclearity.

More recently the same derivatives have been shown to be suitable synthons for the synthesis of ordered molecular assemblies. In fact, they: a) can be prepared in good yields and purity; b) have a remarkably stable polynuclear *core* which remains unchanged under the reaction conditions needed to build the final structures; c) together all their derivatives shown below, they exhibit a notable thermal, air and moisture stability and d) have a few sites with the proper reactivity, well positioned to give the expected shape to the final structures.

Both are prepared from the trinuclear hydride $[Pt_3(\mu\text{-}PBu^t_2)_3(CO)_2H]$ (**1**),[48] which may be synthesized in a few steps from K_2PtCl_4 (overall yield = 45%).

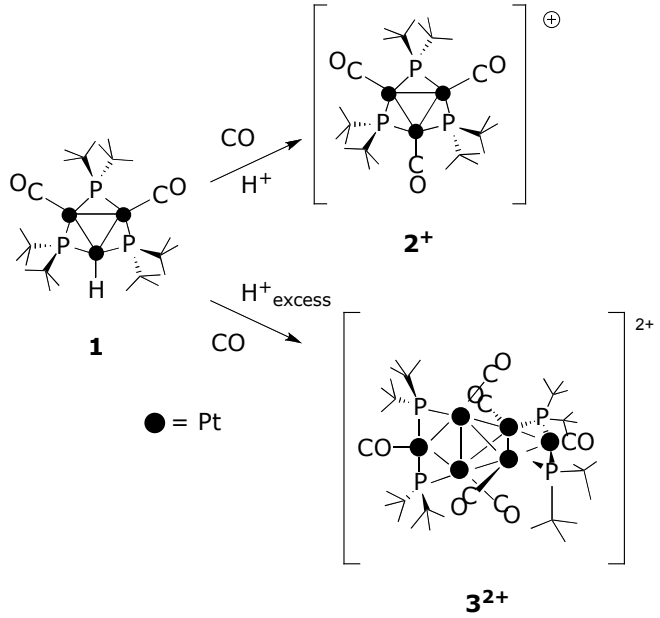

Scheme 1. Synthesis of **2**(CF_3SO_3) and **3**$(CF_3SO_3)_2$.

The trinuclear cluster **2**(CF_3SO_3) was obtained in good yield (78%) as a green solid by treating **1** with an equimolar amount of triflic acid, under a CO atmosphere. Following the same procedure, but using an excess of triflic acid, the hexanuclear cluster **3**$(CF_3SO_3)_2$ was isolated as a red crystalline solid (yield = 56%, Scheme 1).

The solution and solid state structure of both clusters[46] has been determined by spectroscopic and crystallographic studies. The structure of **2**(CF_3SO_3), and of its derivatives, shows that the platinum and phosphorus atoms lie all on the same plane, and that the six *t*-butyl groups are placed half above and half below this plane, completely hiding the $Pt_3(\mu\text{-}P_3)$ core. As shown in Figure 15 by the space filling molecular model of the structure of cation $\mathbf{2}^+$, only the terminal carbonyl ligands,

mutually directed at 120°, emerge from this shield, and, indeed, these are the distinctive reactive sites of cation $\mathbf{2}^+$ in most conditions.

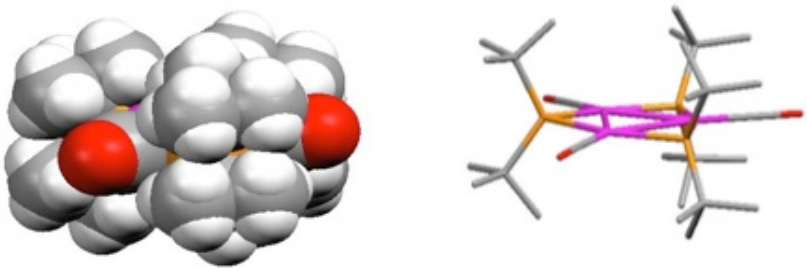

Figure 15. Space filling molecular model of the structure of $\mathbf{2}^+$.

The triangular cluster $[Pt_3(\mu\text{-}PBu^t_2)_3(CO)_3](CF_3SO_3)$, $\mathbf{2}(CF_3SO_3)$ is the precursor of many other derivatives;[49] since generally the reaction occurs to one of the sites bearing a carbonyl ligand, leaving unchanged the whole $[Pt_3(\mu\text{-}PBu^t_2)_3(CO)_2]$ unit, from now on this unit will be briefly indicated by the notation $\{Pt_3\}$. For example, versatile monohalo-derivatives may be achieved by reacting $\mathbf{2}(CF_3SO_3)$ with NBu_4X (X = Cl, Br, I, Scheme 2), and, starting from the chloro-derivative $\{Pt_3\}Cl$, (**11**), the corresponding σ-alkynyl derivatives $\{Pt_3\}CCR$ were obtained after condensation with terminal alkynes. The reactions have been performed under Sonogashira-type conditions, *i.e.* in $NHEt_2$ in the presence of a catalytic amount of CuI (Scheme 2).

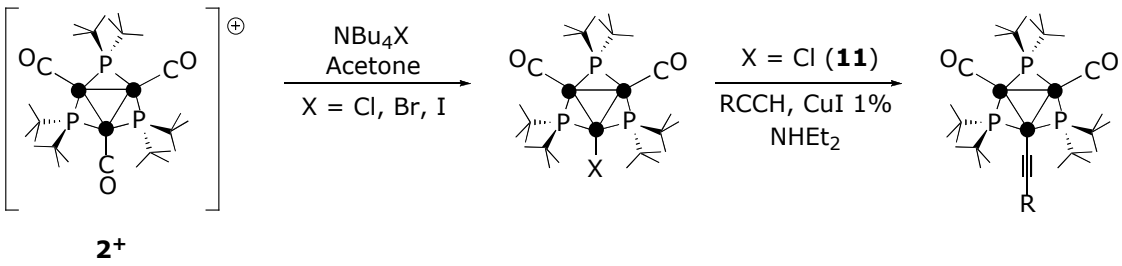

Scheme 2. Reactivity or tris-phosphido-bridged trinuclear clusters.

The alkynyl function is of widespread use in the organometallic chemistry of mono- and polynuclear derivatives. The linear geometry of the alkynyl unit and its π-unsaturated character have led to metal alkynyls becoming attractive building blocks for molecular wires[50] and polymetallaynes[51] of general formula $[ML_m\text{-}CC\text{-}R\text{-}CC]_n$, which are deeply investigated for their luminescence, photovoltaic or liquid crystalline behaviour, and their uses as semiconductors and triplet emitters, light-emitting diodes and polymer-

based lasers. When bonded to a polymetallic unit, the alkynyl ligand is very rarely bonded terminally, as in mononuclear complexes, since also the π-electrons of the triple CC bond are quite generally directly involved in the bond. For this reason, the ligand is more often found to bridge two or even three or four metal centers, with loss of linearity and of π-conjugation.[52] In our systems, the high steric encumbrance above and below the triangular metal framework seriously hinders the π coordination of the alkynyl ligand and promotes the formation of σ,η^1-alkynyls, thus ensuring a better electronic communication between the cluster unit and the substituent of the alkynyl ligand.

It is also worth noting that many reactions leave intact the whole $\{Pt_3\}$ unit, which reacts as a single metal center, thus allowing its employment as an end-cap for larger structures; however, there are also methods that permit to insert the cluster as a branching point. For example all the terminal carbonyl ligands of cation $\mathbf{2}^+$ can be easily and cleanly exchanged with isocyanides, affording clusters of general formula $[Pt_3(\mu\text{-}PBu^t_2)_3(CNR)_3]^+$.

From the point of view of the steric hindrance, the hexanuclear cluster $\mathbf{3}(CF_3SO_3)_2$ is also severely encumbered. From crystallographic studies, we know that $\mathbf{3}(CF_3SO_3)_2$ (D_{2d} simmtery) contains a tethraedral *core* of four platinum atoms with the opposite edges bridged by other two ("apical") platinum centers; four bridging di-*t*-butylphosphido ligands and a carbonyl group terminally bonded to each platinum complete the structure of the cluster. A space filling molecular model (Figure 16) shows that the high steric bulkiness of the eight *t*-butyl substituents completely wraps the central $[Pt_6(\mu\text{-}PBu^t_2)_4(CO)_4]^{2+}$ fragment (hereafter $\{Pt_6\}$), thus inhibiting to potential reagents the access to the internal atoms.

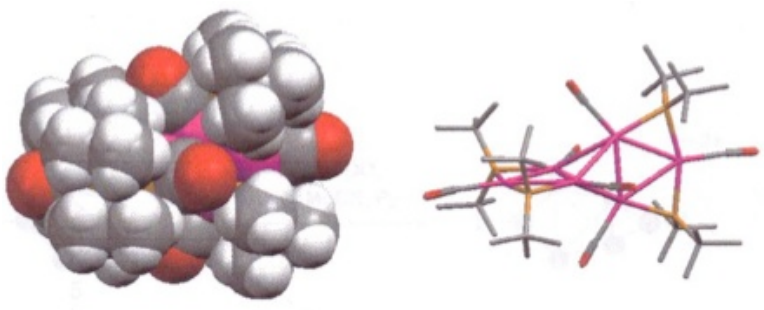

Figure 16. Space filling molecular model of the structure of $\mathbf{3}(CF_3SO_3)_2$.

In the great majority of cases, only the two apical platinum atoms and/or their CO ligands are selectively functionalized while the internal structure of the cluster remains unchanged. Furthermore, the two reactive sites are roughly co-linear and point in opposite directions, which represents an advantage for the preparation of compounds containing two spacers mutually oriented at 180°. The utilization of rigid and linear bifunctional spacers was expected to afford strictly linear oligomers.

The procedures summarized in (Scheme 3) show how a large number of derivatives of **3**$(CF_3SO_3)_2$, arising from the substitution or the nucleophilic attack involving exclusively the apical carbonyls, have been prepared in high yields. The formation of other regioisomers, deriving from reactions at the internal carbonyl ligands, has never been observed.[53]

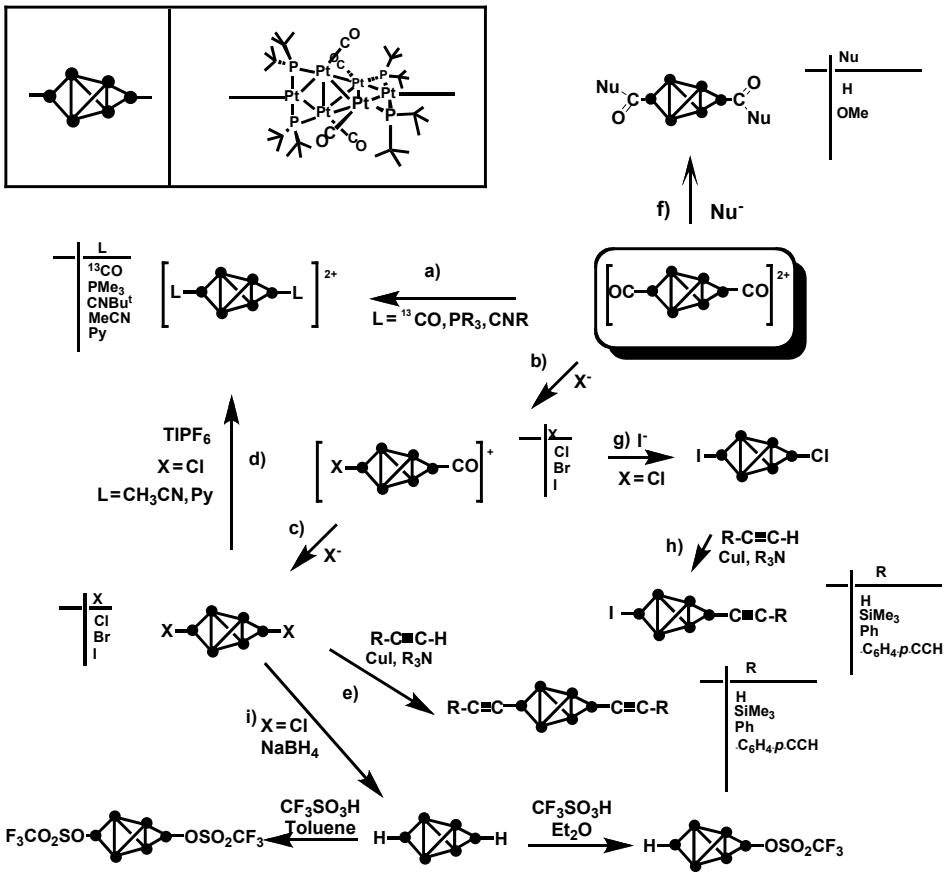

Scheme 3. Reaction involving hexanuclear clusters derivatives.

Useful mono- or bis-halo derivatives were obtained by stepwise substitution the two "apical" carbonyl ligands with halide ions. For example, the reaction of $[\{Pt_6\}(CO)_2](CF_3SO_3)_2$, **3**$(CF_3SO_3)_2$ with an equimolar amount of NBu_4Cl affords

cleanly the monosubstituted derivative [{Pt_6}(CO)Cl](CF_3SO_3) [Scheme 3, reaction b)], while by treating **3**(CF_3SO_3)$_2$ with a 3-6 fold excess of the appropriate halide salt, the symmetrical disubstituted clusters {Pt_6}X_2 [X = Cl, Br, I; Scheme 3, reaction c)] were obtained in high yields. Furthermore, the reaction of [{Pt_6}(CO)Cl](CF_3SO_3) with an equimolar amount of KI gives the asymmetrically disubstituted cluster {Pt_6}ClI [Scheme 3, reaction g)], which may be successfully employed to prepare the differently substituted clusters by exploiting the diverse reactivity of the two halogen ligands.

Actually, in the symmetrically and asymmetrically substituted dihalo-derivatives, the apical halo-ligands may be easily substituted. For example {Pt_6}Cl_2 (**4**) reacts with an excess of $NaBH_4$ yielding the bis-hydride {Pt_6}H_2, (**5**) [Scheme 3, reaction i)]. Moreover, clusters with one or two "apical" chloro-ligands, {Pt_6}ClI and {Pt_6}Cl_2, (**4**), react with terminal alkynes under Sonogashira-type conditions, to give mono- [Scheme 3, reaction h)] or bis- [Scheme 3, reaction e)] alkynyl derivatives.

The substitution of the whole set of carbonyl ligands was observed only when cluster **3** was reacted with an excess of isocyanides, in which case we isolated the persubstituted derivatives [Pt_6(μ-PBu^t_2)$_4$(CNR)$_6$](CF_3SO_3)$_2$ (R = alkyl or aryl).

The general reactivity of **2**(CF_3SO_3) and **3**(CF_3SO_3)$_2$, and the structure of their derivatives, encouraged their utilization as synthons for extended structures containing the {Pt_3} and/or the {Pt_6} units and conjugated alkynyl spacers. Recently, a linear derivative (Figure 17a)[54] and a dendrimer (Figure 17b),[55] with a nearly-planar structure have been prepared starting from the chloro-derivatives **4** and **11**.

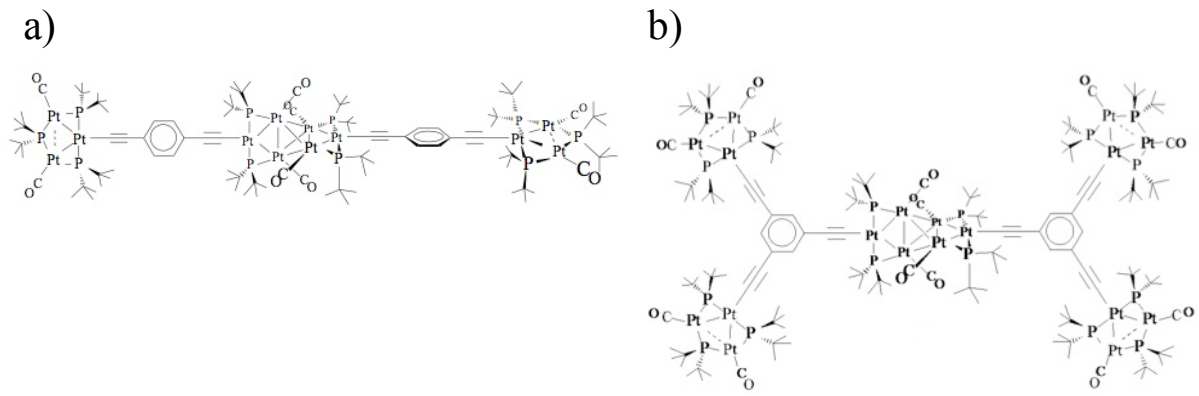

Figure 17. Structures of a) a linear tricluster derivative and b) a dendrimer containing the {Pt_3} and {Pt_6} units.

As in the latter cases, cluster **11** can be used to introduce the trinuclear fragment $\{Pt_3\}$ as an end-cap moiety in linear or branched oligomers or, by exploiting also the substitution of the carbonyl ligands with bifunctional neutral bis-isocyanides, can become a branching point for dendrimeric structures. Moreover, the chloro-derivatives shown in Scheme 4 can afford dicluster derivatives, which may be considered as simple models of larger oligomeric structures (Scheme 4).

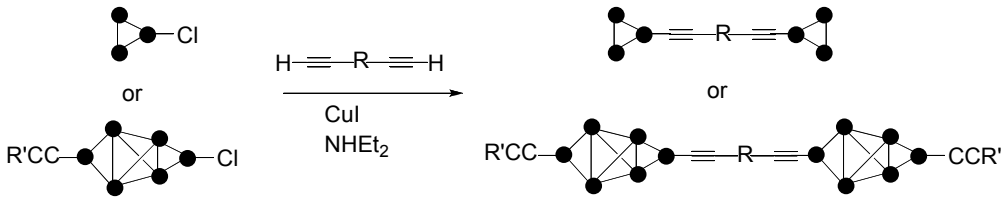

Scheme 4. Examples of simple tri- and hexanuclear "dicluster" compounds.

Finally, our group has recently described the synthesis of the family of oligomers of general formula (E-[({Pt_6}CCArCC)]$_x${Pt_6}-E, [E = Cl, I, CCArCCH, Ar = 1,4-C_6H_2(2,5-$C_{12}H_{23}$), x = 1-15], with a linear structure in which up to 16 molecular clusters are connected by alkynyl spacers, and of a series of shorter monodisperse oligomers, with precise composition and length (x = 0, 2, 4; from 3 to 10 nm, depending upon the number of units). The alkynylic bond is remarkably robust and the oligomeric structure is maintained in solution; the solubility in organic solvents is granted by the long aliphatic chains, and flexible thin films can be simply obtained by evaporation of the solutions (Scheme 5).[56]

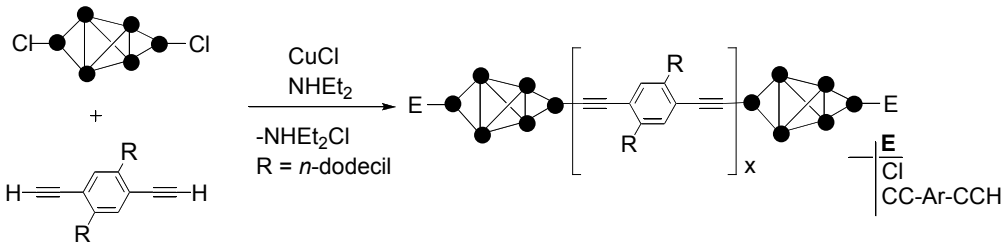

Scheme 5. Preparation of polymers containing the {Pt_6} unit connected by σ-alkynyl spacers.

As we have shown by preparing short model systems containing two cluster units, the Ar group in the bis-alkynyl spacer is not forced to be a phenyl ring as in the previous examples but may be selected in a broad library of aromatic fragments (biphenyls, anthranyls, thienyls or polythienyls, ferrocenyls or diferrocenyls). The terminal group E

can also be the triangular unit $\{Pt_3\}$, a phenylethynyl group variously substituted in *para* (H, *n*-C_5H_{11}), a carbonyl ligand or a weakly bonded triflate anion, which can easily be substituted by neutral (phosphines, isonitriles, pyridins, nitriles) or anionic ligands (thiolates, carboxylates, phenols).[57] On the other hand, it is well possible to prepare derivatives with one electron-donor and one electron-acceptor as terminal groups, to increase electron mobility along the chain by "push-pull" effects.

The electrochemical properties of the trinuclear and hexanuclear cluster precursors are under scrutiny. All the triangular clusters studied until now undergo two sequential reversible monoelectronic oxidations, which substantially typify their redox fingerprint. The two oxidation processes are much more positive for $[\{Pt_3\}CO]^+$, **2**(CF_3SO_3) than for all its neutral derivatives; this can be explained by the presence of the positive charge and of three strongly π-acidic CO ligands in cation $\mathbf{2}^+$. Also a monoelectronic reduction process, followed by fast chemical reactions has been observed in the halo-derivatives $\{Pt_3\}X$ (X = Cl (**11**), Br, I).[49] The voltammogram of a CH_2Cl_2 solution containing the dication $[\{Pt_6\}(CO)_2]^{2+}$, $\mathbf{3}^{2+}$, shows two reversible one-electron reduction processes followed by a partially chemically reversible two-electron reduction at more negative potentials.[46] The neutral halo-derivatives, $\{Pt_6\}X_2$ (X = Cl (**4**), Br, I), show similar waves, although with the expected large cathodic shifts, so only the first two reductions become detectable, and an irreversible oxidation process appears.[53]

The stability of the cluster units in different oxidation states should allow to alter the charge delocalization along the oligomer chains by chemically or electrochemically modifying the oxidation states of the cluster units. The comprehension of charge delocalization in the oligomers should be facilitated by electrochemical studies on model systems $\{Pt_6\}$-spacer or $\{Pt_6\}$-spacer-$\{Pt_6\}$, or the equivalent with $\{Pt_3\}$ in place of $\{Pt_6\}$, that can be prepared for each type of spacer that will be successfully introduced in the oligomers. Some preliminary information on this aspect was given by model systems with a $\{Pt_6\}$ unit bonded through an ethynyl (C≡C) spacer, to one or two ferrocenyl redox-probes (Figure 18).[58]

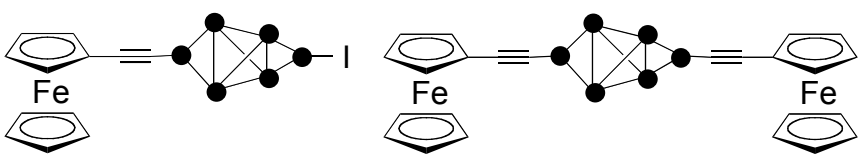

Figure 18. Mono- and bis(ferrocenylethynyl)-substituted hexanuclear clusters.

The biferrocenylic cluster has been designed to inspect possible charge transfer interactions between the ferrocenyl units through the C≡C-{Pt_6}-C≡C "spacer". Actually, electrochemical measurements suggest the lack of a significant iron to iron charge transfer; however, spectroelectrochemical analyses made on CH_2Cl_2 solutions of both compounds shown in Figure 18, indicate that the Fe(II)-Fe(III) oxidation induces the growth of diagnostic absorptions in the near infrared (NIR) region, which may be assigned to a cluster-Fe(III) charge transfer. Theoretical analysis (ab initio DFT methods) have confirmed that the charge transfer to Fe(III) occurs from a molecular orbital mainly centered on an apical platinum atom, rather than on the entire cluster. This can explain the lack of communication between the ferrocenyl units of the disubstituted cluster. Derivatives absorbing in the NIR region can, in principle, be used in optical devices, especially when the absorption is triggered by external stimuli (chemical, photochemical or electrochemical). The intensities of the absorptions of the compounds shown in Figure 18 are too weak for these applications, but several opportunities to its optimization are given by the synthetic methods, which allow substantial modifications of the cluster, spacer and redox-probe units. These will also provide sufficient information useful to plan the synthesis of new structures where the direction of the charge transfer can be predetermined as shown in Scheme 6.

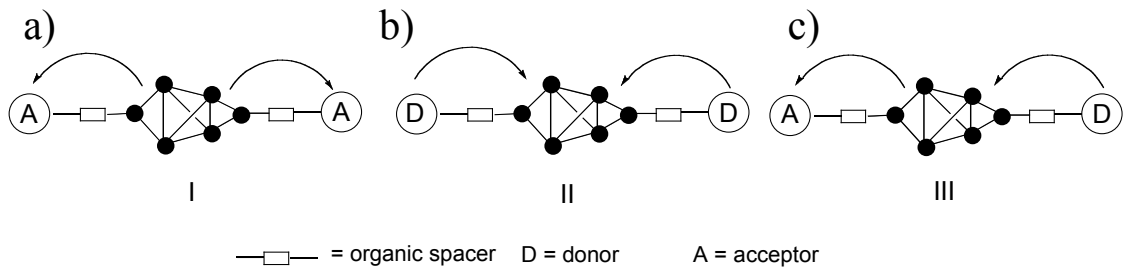

Scheme 6. Electron transfer a) from, b) to and c) across the {Pt_6} cluster unit.

To obtain type-III systems we will have to understand why the tetrahedral *core* of diferrocenylic cluster does not allow the electronic communication between the ferrocenyl units. Therefore, we will prepare new model complexes by varying the structures of both the spacers and the cluster units, and for all the new derivatives the charge transfer mechanism will be investigated by electrochemical, spectroelectrochemical and theoretical analysis. The information gained on the model

systems will then be transferred to the engineering of extended structures with predetermined shape (for example linear or dendrimeric molecules) and type of electronic communication (for example systems where the cluster units are isolated or communicate only with the spacer or also with the adjacent cluster units).

It is also worth noting that the charge mobility across a molecular framework can also be evaluated by measuring the single molecule electrical conductivity by Scanning Tunneling Microscopy (STM). To this purpose, we have shown that the hexanuclear derivatives $\{Pt_6\}[S(CH_2)_4SH]_2$ and $\{Pt_6\}(SCN)_2$ can be absorbed on a gold surface without decomposition and that the single molecule conductivity of $\{Pt_6\}[S(CH_2)_4SH]_2$ (2.4 nS, molecular major axis 2.4 nm), measured by STM, is five orders of magnitude greater than the one estimated for the insulating α,ω-alkanedithiol of similar length (1,18-$HS(CH_2)_{18}SH$). The acquired data suggest that the $\{Pt_6\}$ unit has a resistivity similar to the one of a 1,4-phenylenediyl ring, generally employed as a structural unit in organic conducting or semiconducting oligomers. Moreover, the cluster $\{Pt_6\}[S(CH_2)_4SH]_2$ behaves as a double tunneling barrier, with the $\{Pt_6\}$ core acting as a "well", and is therefore suited to function as a resonant tunneling diode. It has also been shown that $\{Pt_6\}(SCN)_2$ has a conductance of 50 nS, 20 times larger than the one of $\{Pt_6\}[S(CH_2)_4SH]_2$.[59]

Along these lines, during my PhD Thesis we have:

- prepared and spectroscopically, electrochemically and spectroelectrochemically characterized new dicationic model systems containing two $\{Pt_6\}$ units connected by bifunctional nitrogen ligands.
- Synthesized and spectroscopically, electrochemically characterized compounds containing the $\{Pt_3\}$ or $\{Pt_6\}$ units connected to a C_{60} unit, in order to start an investigation on their properties.
- Prepared and fully characterized new phosphido-bridged palladium triangular clusters, in order to start an investigation on new model systems containing these new cluster units.

2 Results and discussion.

2.1 Model systems containing two hexanuclear platinum cluster units.

The synthesis of molecular assemblies containing two cluster units kept together by different species acting as bridging ligands is an attractive field of investigation. These relatively simple systems could be useful for evaluating the influence of the nature of the spacer on the electronic communication between the two polymetallic units, and may be considered as models for extended structures (dendrimers or polymers) containing more than two cluster units. In fact, as discussed previously, the presence of transition metal centers in the backbone of organic conjugated polymers leads to new advanced materials with interesting properties, and there are only a few examples of polymers in which the metal-containing repeating component is a cluster unit.[43, 60]

As fully described in section 1.2, the hexanuclear clusters prepared in our laboratories may be inserted in linear polymeric chains. Furthermore, a worthwhile issue to be remarked is related to the electron mobility within the whole hexanuclear structure of these clusters. As confirmed by the simultaneous oxidation at the same potential (+0.3 V *vs* SCE)[58] of the two ferrocenyl redox probes in Fc-C≡C-{Pt_6}-C≡C-Fc (Figure 18), the two apical platinum centres are not mutually communicating in the *ground state*. This may be due to the shape of the HOMO (Figure 19), which, at least in the dication $[\{Pt_6\}(CO)_2]^{2+}$, is mainly localized in the internal tetrahedral core, with some contribution from the bridging phosphides but a null contribution from the two apical metal centres. However, the same study revealed that the *oxidation* of the ferrocenyl groups induces a metal-to-metal charge-transfer (from the apical Pt atoms to the adjacent Fe) in the near infrared (NIR). Moreover, other results obtained in recent studies suggest that, also *upon reduction*, this class of clusters may acquire a connecting behaviour, and that a wide library of ligands that may be positioned in the apical positions may allow the selection of the redox potentials at which the insulator-conductor behaviour can be switched.[61]

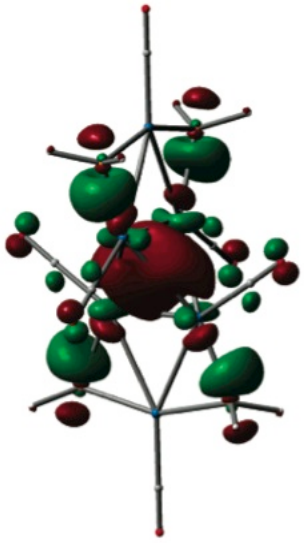

Figure 19. HOMO of $\{Pt_6\}^{2+}$.

Along these lines, the achievement of new model-compounds containing two $\{Pt_6\}$ units connected by non-alkynyl bifunctional conjugated spacers seemed very much desirable. Below are described the synthesis and the electrochemical and spectroelectrochemical characterization of new systems in which the ditopic nitrogen ligands 4,4′-bipyridine (**7**) or 1,4-dicyanobenzene (**8**) (Figure 20) have been used as the spacers.

7 **8**

Figure 20. Molecules used as spacers in systems containing two $\{Pt_6\}$ units.

These have been chosen because: a) they are conjugated organic molecules, in which, the presence of one or two aromatic rings may assist electron transfer and b) they are neutral ligands, which allow to prepare *polycationic* "dimers" or oligomers. Both the different spacer and the different charge should substantially help in modifying the redox potentials, compared to those exhibited by the bis-alkynyl derivatives prepared previously.[54,55,56] Moreover, the synthesis of systems in which the bifunctional ligand is coordinated to the hexanuclear cluster through its N-atoms seemed easily accessible,

since dicationic clusters of general formula $[\{Pt_6\}L_2]^{2+}$, with L = pyridine or acetontrile were already known.[53]

2.1.1 Preparation and spectroscopic characterization of H-$\{Pt_6\}$-OSO_2CF_3 (6).

The mono-hydride $\{Pt_6\}(H)(OSO_2CF_3)$ (**6**), which may be prepared by reacting the known dihydride $\{Pt_6\}H_2$ (**5**)[53] with triflic acid in dry Et_2O (Scheme 7) contains a very weakly bonded triflate anion. The latter may be easily substituted by many monodentate or ditopic anionic or neutral ligands and may thus be employed as the precursor of model systems containing two $\{Pt_6\}$ units connected by different types of bridging ligands.

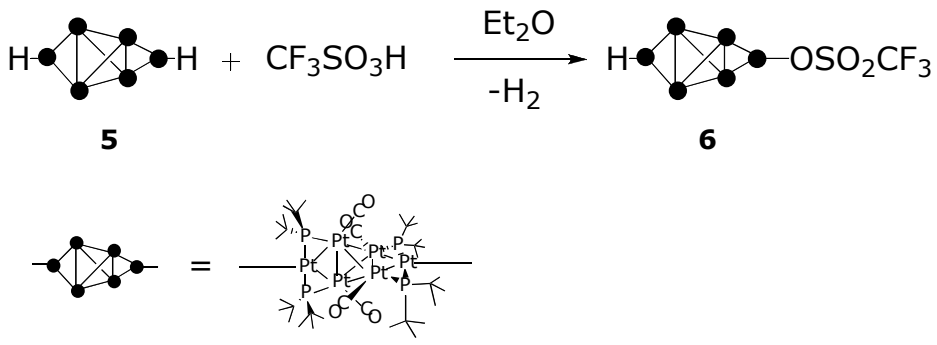

Scheme 7. Synthesis of cluster **6**.

Since we knew that triflic acid may also convert **5** into the bis-triflate derivative $\{Pt_6\}(OSO_2CF_3)_2$, we performed the reaction by mixing strictly equimolar amounts of the reagents; moreover, the choice of the solvent is crucial to avoid the formation of mixtures. Actually, the final product **6** is only sparingly soluble in diethyl ether and precipitates out as a pure microcrystalline red solid as soon as it is formed (isolated yield 73%).

Compound **6** is quite insoluble in most organic solvents except CH_2Cl_2, in which, however, it is slowly converted into the well-known dichloride $\{Pt_6\}Cl_2$ (**4**). Thus, in this solvent we were able to collect significant NMR spectra only for the more sensitive nuclei (^1H and ^{31}P). The $^{31}P\{H\}$NMR (CD_2Cl_2, 293K) shows two singlets, which confirmed that the two apical platinum atoms are coordinated to two different ligands

(the phosphorus atoms are two by two equivalent). The signals are centered at 352.2 and 320.8 ppm, the first being due to the two equivalent P atoms closer to the hydride ligand [δ_P = 342.0 ppm in **5**][53] and the second to the other two phosphorus centers [δ_P = 333.7 ppm in $\{Pt_6\}(OSO_2CF_3)_2$].[62] As more fully described in the Appendix A, the $^{31}P\{H\}$NMR signals are flanked by satellites due to the coupling with the NMR active ^{195}Pt nuclei (isotopic abundance 33.8%). The complex spectrum is originated by the sum of many different subspectra; in fact, each hexanuclear cluster is constituted by 22 groups of non-equivalent isotopomers, nearly all giving subspectra that cannot be interpreted with simple first-order approximations. For these reasons, it was not possible to estimate the value of all the coupling constants; however, the main features of the complex shape of the signal remain constant and may be taken as a fingerprint of the hexanuclear $\{Pt_6\}(L)(L')$ structure (where L = L′ or L ≠ L′).[47] Actually, these signals, and of those of all the other $\{Pt_6\}$ derivatives prepared in this Thesis, are similar to the ones observed for the other $\{Pt_6\}(L)(L')$ derivatives prepared previously. They are diagnostic for isomers bearing the L/L′ ligands in the apical positions,[47] and rule out all other possible isomeric structures, deriving from the attack of L/L' to the inner position of the central Pt_4 tetrahedron.

The ^1H NMR (CD_2Cl_2, 293K) spectrum shows two virtual triplets (see Appendix A) at 1.50 ppm ($^3J_{H\text{-}P} + {}^5J_{H\text{-}P}$ = 7.6 Hz, 36 H) and 1.37 ppm ($^3J_{H\text{-}P} + {}^5J_{H\text{-}P}$ = 7.3 Hz, 36 H), which were assigned to the 72 *t*-butyl protons of the two sets of phosphido ligands. The presence of the Pt-*H* bond is confirmed by the existence of a broad singlet at –0.27 ppm, with a large $^1J_{HPt}$ coupling (1154.4 Hz, from the satellite peaks), as expected for the terminal Pt–H function.[53]

The absorptions at 1322, 1228, 1169 and 999 cm^{-1} in the solid state IR spectrum confirm the presence of a coordinated triflate; it is in fact known that complexes containing the metal bonded Pt-OSO_2CF_3 unit absorb at 1280-1420, 1210-1270, 1100-1180 and 1000-1100 cm^{-1} [63] while ionic triflates give signals at *ca* 1270, 1160, 1030 cm^{-1}.[64]

2.1.2 Preparation of dicationic compounds containing two $\{Pt_6\}$ units.

The reactions of cluster **6** with the appropriate ligand (**7** or **8**) in dry CH_2Cl_2 (Scheme 8) give the desired products **9**$(CF_3SO_3)_2$ or **10**$(CF_3SO_3)_2$.

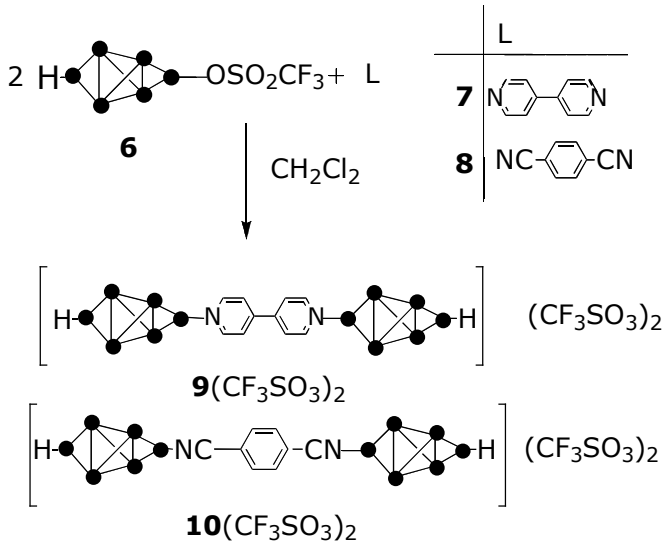

Scheme 8. Synthesis of "dicluster" compounds **9**$(CF_3SO_3)_2$ and **10**$(CF_3SO_3)_2$.

In order to obtain only the dicluster compounds, we used a strict stoichiometric ratio of the reagents (cluster/ligand 2:1); in fact, on decreasing the cluster/ligand ratio, we observed also the formation of the monocationic cluster $[\{Pt_6\}(H)(L)](CF_3SO_3)$ [L = **7** and **8**]. Reaction timing is also very important because both the reagent and the product are stable only for a short period in CH_2Cl_2 solution. Thus, after stirring the reaction mixture for 2 hours and evaporating the solvent under vacuum, the final product was dissolved in acetone, some unreacted starting cluster, was filtered away, and the new derivatives **9**$(CF_3SO_3)_2$ and **10**$(CF_3SO_3)_2$ were obtained as brown solids in good purity and yield (64-67%) after solvent evaporation.

2.1.3 Spectroscopical characterization of 9$(CF_3SO_3)_2$.

The ^{1}H NMR spectrum (Acetone-d_6, 293K) of **9**$(CF_3SO_3)_2$ confirms the presence of a system containing two cluster units and **7** as the conjugated spacer. In fact, the spectrum shows two doublets at 9.68 ($^3J_{H\text{-}H}$ = 5.3 Hz, 4 H) and 8.67 ppm ($^3J_{H\text{-}H}$ = 5.3 Hz, 4 H) attributable to the protons of 4,4′-bipyridine (δ_H = 8.70 and 7.49 ppm for uncoordinated

7).[65] As shown in Figure 21, if 4,4′-bipyridine was coordinated to only one cluster in a terminal mode, we would have expected four doublets instead of two

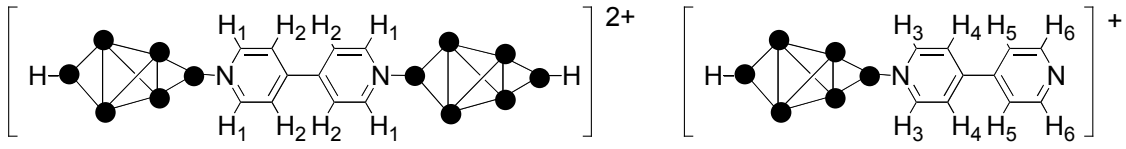

9$(CF_3SO_3)_2$

Figure 21

This spectrum contains also two partially overlapped virtual triplets at 1.50 ($^3J_{H\text{-}P} + {}^5J_{H\text{-}P}$ = 7.3 Hz, 72 H) and 1.45 ppm ($^3J_{H\text{-}P} + {}^5J_{H\text{-}P}$ = 7.3 Hz, 72 H), due to the *t*-butyl protons of the phosphido ligands, as a further confirmation of coordination of two different ligands to the two apical platinum atoms. The Pt–H bonds are still present, as confirmed by the broad singlet at –0.37 ppm ($^1J_{H\text{-}Pt}$ = 1209.4 Hz). The presence of 4,4′-bipyridine is also confirmed by the signals at 156.8, 146.5 and 126.3 ppm (δ_C = 150.0, 120.8 and 144.8 ppm for uncoordinated **7**)[65] in the $^{13}C\{^1H\}$ NMR spectrum (Acetone-d_6, 293K).

The $^{31}P\{^1H\}$ NMR spectrum (Acetone-d_6, 293K) contains two singlets, accompanied by satellites due to the coupling with ^{195}Pt, at 356.6 and 316.2 ppm, that were respectively assigned to the four equivalent *P*–Pt–H phosphorus atoms [δ_P = 342.0 ppm in $\{Pt_6\}H_2$ (**5**)][53] and to the four equivalent *P*-Pt-N nuclei nuclei [δ_P = 327.8 ppm in $\{Pt_6\}(C_5H_5N)_2$].[53] The $^{195}Pt\{^1H\}$ NMR (Acetone-d_6, 293K) spectrum is compatible with the structure suggested for **9**$(CF_3SO_3)_2$ and shows four multiplets of the expected shape (see Appendix A). The two signals at –2953 and –3327 ppm are attributable to the platinum atoms of the internal tetrahedra and were, respectively, assigned to the four platinum centers closer to the hydride ligands [δ_{Pt} = –2822 ppm in **5**][53] and to the four Pt nuclei closer to the spacer [δ_{Pt} = –3406 ppm $\{Pt_6\}(C_5H_5N)_2$].[53] The other two signals, at –4361 ppm (2 *Pt*-N, δ_{Pt} = –4343 ppm $\{Pt_6\}(C_5H_5N)_2$)[53] and at –5080 ppm [2 *Pt*-H, δ_P = –5146 ppm in $\{Pt_6\}H_2$ (**5**)],[53] are due to the apical platinum atoms.

The IR (solid state) spectrum shows the CO stretching absorptions at 2024 and 2005 cm^{-1} and the signals due to the non-bonded $CF_3SO_3^-$ counterion at 1259, 1171 and 1029 cm^{-1}.[63]

2.1.4 Spectroscopical characterization of $10(CF_3SO_3)_2$.

The IR (solid state) spectrum of **10**$(CF_3SO_3)_2$ shows one absorption at 2166 cm^{-1} for the stretching of the coordinated CN moiety, two bands at 2022 and 2000 cm^{-1}, assigned to the stretching of the carbonyl ligands, and bands at 1258, 1172 and 1030 cm^{-1} for the triflate counterion.[63]

The ^1H NMR spectrum (Acetone-d_6, 293K) contains one singlet at 8.54 ppm, two virtual triplets (Figure 22) at 1.58 ($^3J_{P\text{-}H} + {}^5J_{P\text{-}H}$ = 7.6 Hz, 72 H) and 1.43 ppm ($^3J_{P\text{-}H} + {}^5J_{P\text{-}H}$ = 7.1 Hz, 72 H) and one broad singlet at –0.52 ppm ($^1J_{H\text{-}Pt}$ = 1148.2 Hz). The first signal, assigned to the four aromatic protons of **8**, is compatible with a symmetrical system; the remaining ones are respectively due to the *t*-butyl protons of the phosphides and to the hydride ligand.

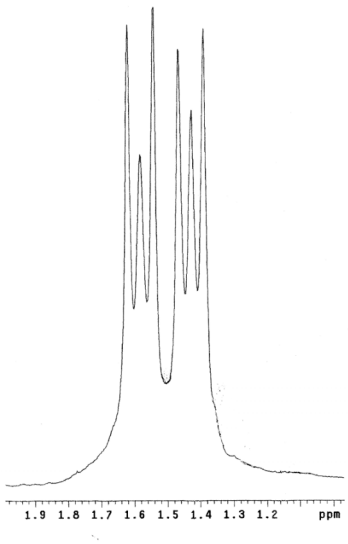

Figure 22. Portion of ^1H NMR (Acetone-d_6, 293K) spectrum of compound **10**$(CF_3SO_3)_2$, showing the virtual triplets assigned to the *t*-butyl protons.

The $^{31}P\{^1H\}$ NMR (Acetone-d_6, 293K), reported in Figure 23, shows two signals at 362.2 and 334.5 ppm, with the usual shape observed in related hexanuclear clusters, that confirm the presence of two different "apical" ligands on each cluster. The signals are, respectively, assigned to the four *P*–Pt–H [δ_P = 342.0 ppm in **5**] [53] and to the four *P*-Pt-NC nuclei.

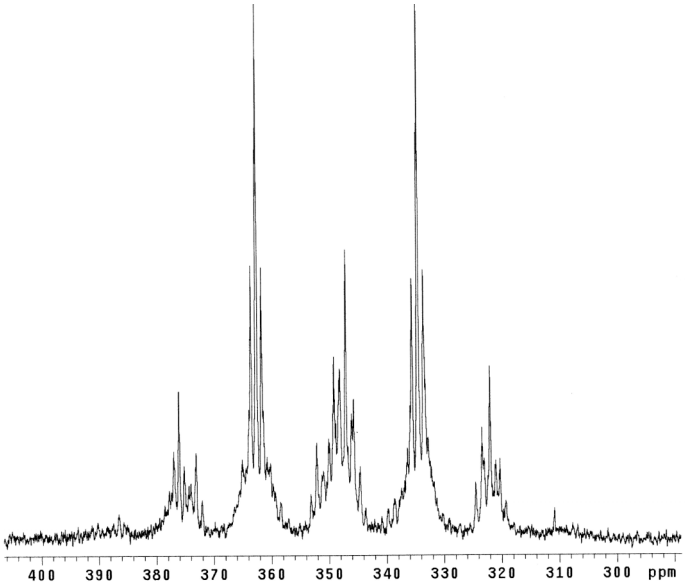

Figure 23. $^{31}P\{^{1}H\}$ NMR spectrum (Acetone-d_6, 293K) of compound **10**$(CF_3SO_3)_2$.

The $^{13}C\{^{1}H\}$ NMR and $^{195}Pt\{^{1}H\}$ NMR (Acetone-d_6, 293K) spectra (see Experimental part) show signals with the expected chemical shift and intensities, in full agreement with the structure given in Scheme 8.

2.1.5 UV-Vis spectra of 9$(CF_3SO_3)_2$ and 10$(CF_3SO_3)_2$.

Qualitative UV-Vis measurements ($250 < \lambda < 800$ nm) were carried out on CH_2Cl_2 solutions of cluster **6**, and of the new dicluster derivatives **9**$(CF_3SO_3)_2$ and **10**$(CF_3SO_3)_2$. All the spectra show two broad bands at *ca.* 300 and 445 nm (Table 2), the latter of which was assigned to the hexanuclear cluster.[56]

Table 2. UV-Vis absorptions of **6** and of **9**$(CF_3SO_3)_2$ and **10**$(CF_3SO_3)_2$.

Compounds	λ_{max}/nm
6	445, 304
9$(CF_3SO_3)_2$	447, 304
10$(CF_3SO_3)_2$	443, 302

The absorption at *ca*. 300 nm was straightforwardly attributed to the cluster in compound **6**. Conversely, in **9**$(CF_3SO_3)_2$ and **10**$(CF_3SO_3)_2$, which contain aromatic ligands (absorptions at $\lambda = 270$ and 239 nm for free **7** [66] and at $\lambda = 287$, 278, 247 and

235 nm for free **8** [67]), this broad band is probably due to the overlap of two or more electronic transitions. In fact, in addition to the transitions attributed to the cluster, ligand-centered and MLCT (metal-to-ligand charge-transfer) transitions may be present in this region.[68]

2.1.6 Electrochemistry and spectroelectrochemistry of $9(CF_3SO_3)_2$ and $10(CF_3SO_3)_2$.

As explained in more detail in Appendix B, cyclic voltammetric and IR and UV-Vis spectroelectrochemical studies may be useful to verify the presence of electronic communication in systems as those described above.

In cyclic voltammetry, the presence of electronic communication in systems containing two metal centers (the same is valid for polymetallic units) connected by a conjugated spacer, is generally correlated with the increase of the number of redox processes in comparison with those found in complexes containing only one metal center, with the obvious restriction that the mono- and the dinuclear systems should be as similar as possible in terms of charge, metal oxidation state and ligand set. In fact, if the two metal "feel" each other, after the reduction (or oxidation) of the first metal center, the second is reduced (or oxidized) at a more negative (or more positive) potential. Thus, two separated processes occur and two separated peaks appear in the voltammogram (Scheme 9). In the absence of electronic communication, the two metal atoms behave as if they were isolated and they are reduced (or oxidized) at the same potential, giving only one peak, with double intensity, in the voltammogram.

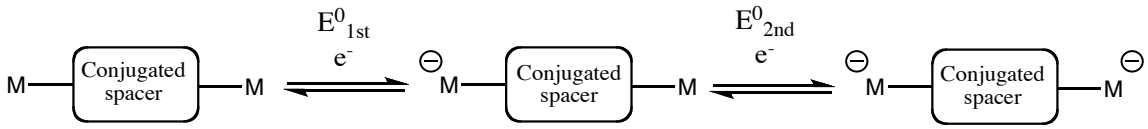

Scheme 9

We have seen in section 1.2, that the hexacarbonyl cluster $[\{Pt_6\}(CO)_2]^{2+}$ ($\mathbf{3}^{2+}$) and its derivatives have an interesting electrochemical behavior. For this reason, we carried out a series of cyclovoltammetric studies on the dicationic cluster $\mathbf{3}^{2+}$, on the monocationic chlorocarbonyl cluster $[\{Pt_6\}Cl(CO)]^+$ and on the neutral bis-halide-derivatives

$\{Pt_6\}X_2$.[46,53] All these derivatives exhibit two reversible monoelectronic reduction waves that typify their redox fingerprint. In the voltammogram of $\mathbf{3}^{2+}$ also a bielectronic quasi-reversible reduction process is observed at more negative potential values.[46] The monocation $[\{Pt_6\}Cl(CO)]^+$ and the neutral derivatives, for example $\{Pt_6\}Cl_2$ (**4**), show an expected cathodic shift for all the processes, due to the decreasing positive charge of the complexes. Moreover, they show an irreversible oxidation, while the third irreversible bielectronic reduction at more negative potential is no longer detectable (Figure 24). [53]

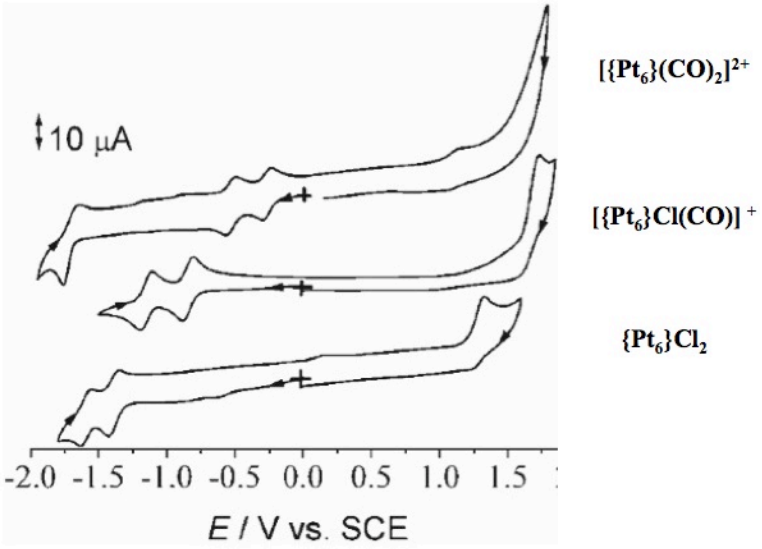

Figure 24. Cyclic voltammograms recorded at a platinum electrode in CH_2Cl_2 solution of $[\{Pt_6\}(CO)_2]^{2+}$ ($\mathbf{3}^{2+}$), $[\{Pt_6\}Cl(CO)]^+$ and $\{Pt_6\}Cl_2$ (**4**), respectively, using NBu_4PF_6 (0.2 M) as the supporting electrolyte. Scan rate 0.2 Vs^{-1}.

We have also carried out some preliminary cyclovoltammetric studies on clusters $\mathbf{9}(CF_3SO_3)_2$ and $\mathbf{10}(CF_3SO_3)_2$. The measurements were performed in CH_2Cl_2 solution for both compounds and in THF only for $\mathbf{10}(CF_3SO_3)_2$, using NBu_4PF_6 0.2 M as the supporting electrolyte. The voltammograms of $\mathbf{9}(CF_3SO_3)_2$ and $\mathbf{10}(CF_3SO_3)_2$ are respectively shown in Figure 25 and in Figure 26. The corresponding redox potentials, together with those of $\mathbf{3}^{2+}$ and $[\{Pt_6\}Cl(CO)]^+$,[53] (the second is used as a reference because in $\mathbf{9}(CF_3SO_3)_2$ and $\mathbf{10}(CF_3SO_3)_2$ each cluster unit is formally monocationic), are summarized in Table 3.

Table 3: Formal electrode potentials (V *vs* SCE) and peak-to-peak separations (mV) for the redox processes exhibited in CH_2Cl_2 solution by $\mathbf{9}^{2+}$ and $\mathbf{10}^{2+}$ and, for comparison, by $\mathbf{3}^{2+}$ [53] and $[\{Pt_6\}Cl(CO)]^+$.[53]

Compounds	Solvents	Reductions processes	Oxidation processes
		$E^{0\prime}$ [a] (ΔE_p)[b]	$E^{0\prime}$ [a] (ΔE_p)[b]
$\mathbf{3}^{2+}$	CH_2Cl_2	-0.54 (60); -0.84 (58)	/
$[\{Pt_6\}Cl(CO)]^+$	CH_2Cl_2	-0.84 (78); -1.14 (82)	+1.65[c]
$\mathbf{9}^{2+}$	CH_2Cl_2	-0.91 (69); -1.17[c]; -1.21[c]; -1.37 (86)	/
$\mathbf{10}^{2+}$	CH_2Cl_2	-1.72[c] ; -1.86[c]	/
$\mathbf{10}^{2+}$	THF	-1.18[d]; -1.36[d]; -1.66[d]	/

[a,b] Measured at 0.1 $V \cdot s^{-1}$. [a] Measured in V, vs SCE. [b] Measured in mV. [c] Peak potential value for irreversible processes. [d] Peak potential value for quasi-reversible processes.

The data in Table 3 show that cations $\mathbf{9}^{2+}$ and $\mathbf{10}^{2+}$ have a different redox behavior compared to the model cluster $[\{Pt_6\}Cl(CO)]^+$. The bipyridine-spaced system $\mathbf{9}^{2+}$ shows four different monoelectronic reduction processes, the first two at potentials similar to those exhibited by $[\{Pt_6\}Cl(CO)]^+$. The processes at −0.91 and −1.37 V are reversible on the cyclic voltammetry time scale (i_{pc}/i_{pa} = 1 at 0.2 $V \cdot s^{-1}$), while the other two, at −1.17 and −1.21 V, are irreversible (Figure 25). The process at −1.21 V may be assigned to a 4,4′-bipyridine-centered reduction; in fact, a similar process was found in the cyclic voltammogram of $[(Pt(pip_2NCN))_2(\mu\text{-}4,4'\text{-bipyridine})]^{2+}$ [pip_2NCNH = 1,3-bis(piperidyl-methyl)benzene, $E°$ = −1.22 V vs. Ag/AgCl ($E°$ = −1.28 V vs. SCE)].[68a] In the anodic region, no oxidation processes have been observed.

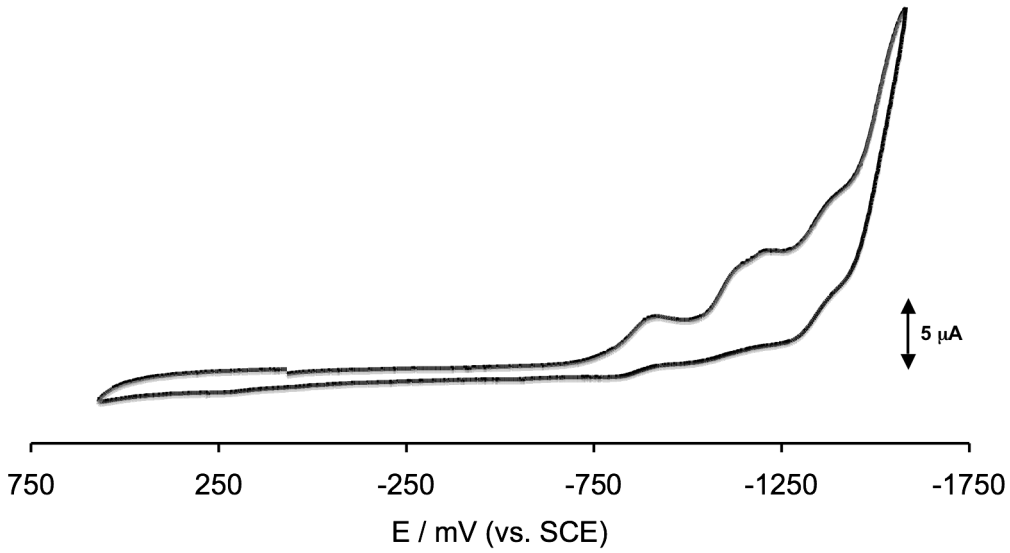

Figure 25. Cyclic voltammogram of $\mathbf{9}^{2+}$ recorded at a platinum electrode in CH_2Cl_2 solution, using NBu_4PF_6 (0.2 M) as the supporting electrolyte. Scan rates: 0.1 V s^{-1}.

The voltammogram of **10**$(CF_3SO_3)_2$ in CH_2Cl_2 solution shows two irreversible reduction processes at very negative potentials ($E°$ = –1.72 and –1.86 V vs. SCE, Figure 26a). The cathodic shift may be due to the decomposition of **10**$(CF_3SO_3)_2$ under these conditions. In fact, by repeating the CV measurements in the non-chlorinated solvent THF, which has a wider solvent window in the cathodic region, three quasi-reversible reduction processes were detected ($E°$ = –1.18, –1.36 and –1.66 V *vs*. SCE, Figure 26b)

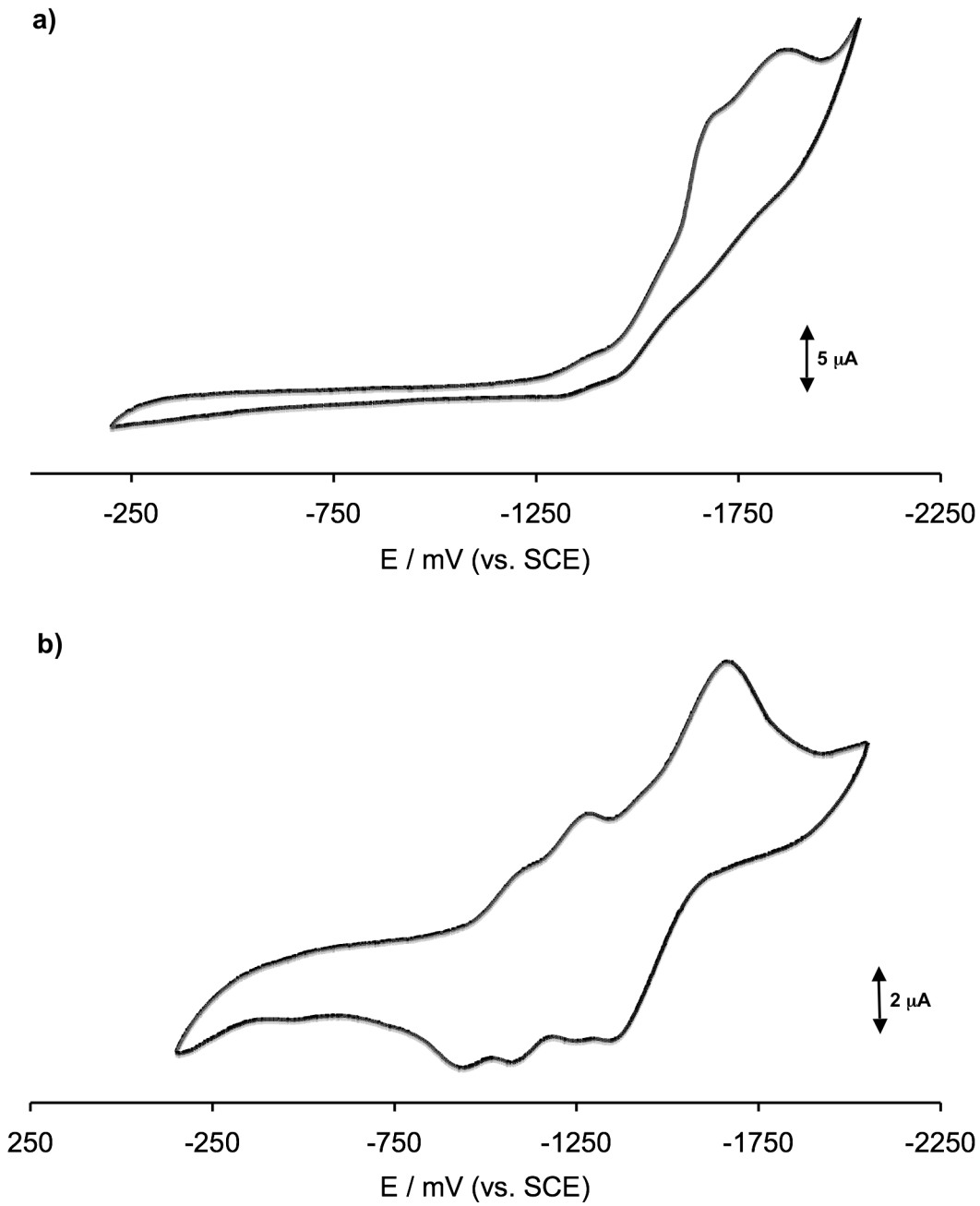

Figure 26. Cyclic voltammogram recorded at a platinum electrode in a) CH_2Cl_2 and b) THF solutions of $\mathbf{10}^{2+}$; using NBu_4PF_6 (0.2 M) as supporting electrolyte. Scan rates: 0.1 V s^{-1}.

The processes at −1.18 and −1.36 V are monoelectronic, conversely the reduction at −1.66 V is multielectronic, but could be due to the overlap of two or more processes, as also suggested by the shape of the peak. As discussed above for $\mathbf{9}^{2+}$, also in this case the number of redox processes increases on passing from the monocluster model to the dicluster derivative. However, it is not yet possible to confirm the presence of electronic

communication, since reduction processes attributable to the bridging ligand might be present; for example the CV profile of $[((MeC(O)S^{-}4\text{-}NCN)Pt)_2(\mu\text{-}1,4\text{-}dicyanobenzene)]^{2+}$ (NCN = $[C_6H_2(CH_2NMe_2\text{-}2,6)_2]^-$) shows two irreversible reduction processes, assigned to the 1,4-dicyanobenzene ligand, at −1.32 and −1.58 V vs. SCE.[69]

Useful indications could have been obtained by an IR spectroelectrochemical study. Actually, the hexanuclear clusters are ideal candidates for this type of analysis due to their rich electrochemistry and to the presence of the carbonyl ligands acting as strong IR chromophores. It is in fact well known that the ν_{CO} absorption is progressively shifted to lower frequencies upon increasing the electron density at the metal to which the carbonyl ligand is coordinated.

This technique may have different applications, among which the investigation of ultrafast electron transfer processes in mixed-valence complexes. Turner and co-workers[70] were the first to use dynamic IR spectroscopy to calculate rate constants and self-isomerisation barrier heights in the case of a "turnstile"- type exchange of the carbonyl ligands, observed in the trigonal bypiramidal complex $[Fe(CO)_3(\eta^4\text{-}norbornadiene)]$. Kubiak and co-workers[71] used this method to study the rate of the electron transfer in trinuclear ruthenium "dimers" of the type $\{[Ru_3O(CH_3COO)_6(CO)(L)]_2(\mu\text{-}BL)\}^n$ (L = 4-dimethylaminopyridine, pyridine or 4-cyanopyridine; BL = 1,4-pyrazine, 4,4'-bipyridine). These compounds exhibit four reversible redox processes, two bi-electronic oxidation waves at +0.43 ÷ +0.58 (n = +2/0) and +1.17 ÷ +1.39 V (n = +4/+2) and two mono-electronic reduction processes at −1.11 ÷ −0.68 (n = 0/−1) and −1.33 ÷ −0.91 V (n = −1/−2). From the splitting of the reduction waves, which varies between < 50 to 440 mV it has been shown that the comproportionation constant K_c for the equilibrium $Ru_3^{III,III,II}$-BL-$Ru_3^{III,III,II}$ + $Ru_3^{III,II,II}$-BL-$Ru_3^{III,II,II}$ ⇆ 2 $Ru_3^{III,III,II}$-BL-$Ru_3^{III,II,II}$ falls by seven orders of magnitude from *ca* 10^7 to <10, depending upon the ligands L and the bridge BL. These data and the study of the Intervalence Charge Transfer (ICT) bands in the Near IR region allowed to assign some system to the Class III (delocalized) and some other to the Class II (valence-trapped or localized) of the Robin-Day classification scheme. Reflectance IR spectroelectrochemistry allowed an estimation of the rate constants for the electron transfer processes in the mixed valence states (*ca* 10^{11} s^{-1}).

Since, until now, IR spectroelectrochemical analyses on any member of this family of hexanuclear clusters had never been effected, we first studied the IR spectra of $[\{Pt_6\}(CO)_2]^{2+}$ ($\mathbf{3}^{2+}$).

Thus, the measurements were effected on CH_2Cl_2 solutions of $\mathbf{3}(CF_3SO_3)_2$, on CH_2Cl_2 and THF solutions of $\mathbf{9}(CF_3SO_3)_2$ and on CH_2Cl_2 solutions of $\mathbf{10}(CF_3SO_3)_2$, using NBu_4PF_6 0.2 M as the supporting electrolyte in all cases. The IR spectra recorded in this study are reported in Figure 27 [$\mathbf{3}(CF_3SO_3)_2$], Figure 28 [$\mathbf{9}(CF_3SO_3)_2$] and in Figure 29 [$\mathbf{10}(CF_3SO_3)_2$]; Table 4 summarized the observed data.

Table 4. CO stretching bands of compound $\mathbf{3}^{2+}$, $\mathbf{9}^{2+}$ and $\mathbf{10}^{2+}$ and of their reduction products.

Compounds	Solvent	ν_{CO}/cm^{-1} Initial	ν_{CO}/cm^{-1} Monoreduced	ν_{CO}/cm^{-1} Bireduced
$\mathbf{3}^{2+}$	CH_2Cl_2	2091; 2058	2056; 2020	2021; 1988; 1974
$\mathbf{9}^{2+}$	CH_2Cl_2	2027; 2009	2017	2002
$\mathbf{9}^{2+}$	THF	2024; 2008	2010; 2004	1965
$\mathbf{10}^{2+}$	CH_2Cl_2	2027; 2009	2015	2034; 2019

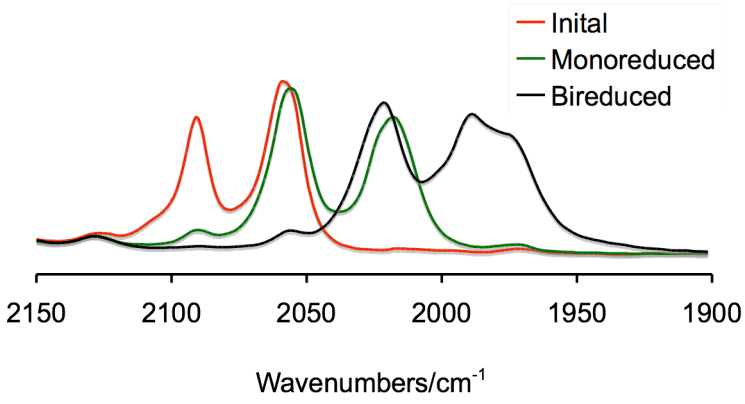

Figure 27. IR spectral changes recorded in a OTTLE cell during the progressive one-electron (green line) and two-electrons (black line) reduction of 3^{2+} in CH_2Cl_2 solution.

The IR spectrum of the hexacarbonyl derivative $\mathbf{3}(CF_3SO_3)_2$ shows two absorption bands at 2091 and 2058 cm^{-1}, respectively assigned to the two apical and to the four inner carbonyl ligands.[53] At the first reduction potential, the two initial bands disappear

and are replaced by two new peaks, at 2056 and 2020 cm^{-1}. As expected, the CO stretching absorptions of the monoreduced species $\mathbf{3}^{+}$ occur at lower frequencies, due to the increase of electron density on the platinum atoms. The presence of only two bands confirms that the symmetry of the cluster remains unchanged after the acquisition of one electron. Going to more negative potentials, the absorptions at 2056 and 2020 cm^{-1} decrease, in favor of new peaks at 2021, 1988 and 1974 cm^{-1}. As also suggested by a theoretical study,[46] the increase of ν_{CO} absorptions may be due to a substantial decrease of the symmetry of the cluster in the neutral bielectronically reduced species **3**. The full reversibility of the processes confirms the remarkable stability of the reduced species $\mathbf{3}^{+}$ and **3**.

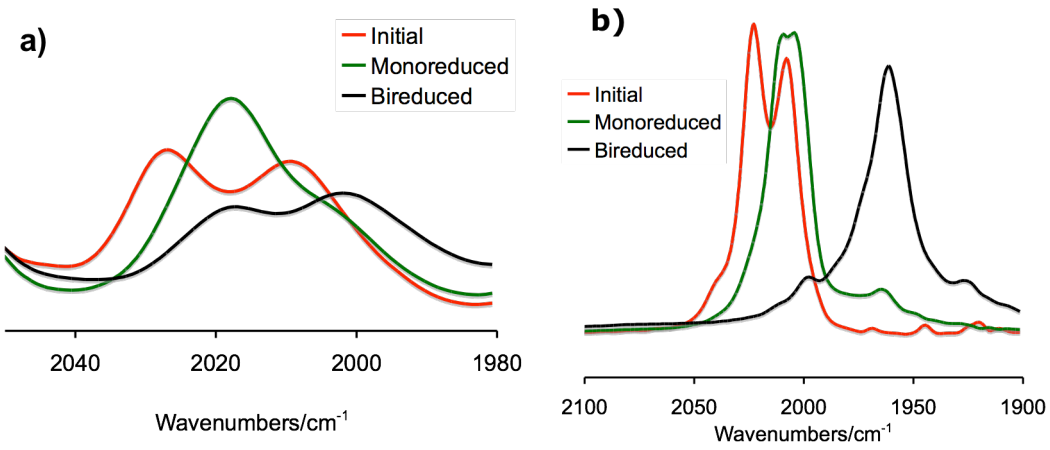

Figure 28. IR spectral changes recorded in a OTTLE cell during the progressive one-electron (green line) and two-electrons (black line) reduction on a) CH_2Cl_2 and b) THF solution of $\mathbf{9}^{2+}$.

Subsequently, we measured the IR spectroelectrochemistry of the dicluster derivatives $\mathbf{9}(CF_3SO_3)_2$ and $\mathbf{10}(CF_3SO_3)_2$. The initial IR spectrum of $\mathbf{9}(CF_3SO_3)_2$ in CH_2Cl_2 shows two ν_{CO} absorptions at 2027 and 2009 cm^{-1}. During the electrolysis of cation $\mathbf{9}^{2+}$, these two peaks decrease in favor of one new broad signal at 2017 cm^{-1}, probably due to the overlap of more absorptions, which decreases on going to more negative potentials, while a new band increases at 2002 cm^{-1}. Unfortunately, the total conversion to the bireduced species was not observed (Figure 28a) due to the interference of the solvent at the working potentials. For this reason, we repeated the measurements in THF (which has a wider solvent window in the cathodic region) (Figure 28b). The starting IR spectrum is very similar to the one recorded in CH_2Cl_2, (ν_{CO} at 2024 and 2008 cm^{-1}). At

the first reduction potential, the initial absorptions disappear and two overlapping bands appear at 2010 and 2004 cm^{-1}. Going through the electrolysis, these two peaks disappear in favor of a new broad peak at 1965 cm^{-1}, probably due to the bireduced species **9**.

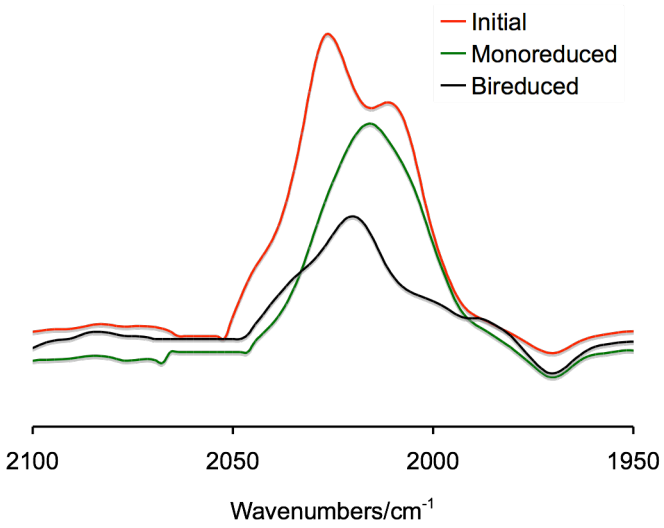

Figure 29. IR spectral changes recorded in a OTTLE cell during the progressive one-electron (green line) and two-electrons (black line) reduction of $\mathbf{10}^{2+}$ in CH_2Cl_2 solution.

The IR spectrum recorded before the electrolysis of a CH_2Cl_2 solution of **10**$(CF_3SO_3)_2$ is quite similar (ν_{CO} = 2027 and 2009 cm^{-1}) to the one discussed above for **9**$(CF_3SO_3)_2$. Again, in the IR spectrum of the monoreduced species we observed one broad band at 2015 cm^{-1}, which is due to the overlap of more CO stretching absorptions. In this case, going to the second reduction potential, the compound starts to decompose and the IR spectrum shows only one weak broad band of difficult attribution at 2019 cm^{-1}, with a shoulder at 2034 cm^{-1}.

2.1.7 Conclusion and future works.

In conclusion, the results obtained in these preliminary cyclic voltammetric and IR spectroelectrochemical studies on **9**$(CF_3SO_3)_2$ and **10**$(CF_3SO_3)_2$ are promising for our purposes because they may suggest some electronic communication between the two $\{Pt_6\}$ units through both the spacers [4,4′-bipyridine (**7**) and 1,4-dicyanobenzene (**8**)]. Unfortunately, the CV profiles of these systems are complicated by the presence the bridging ligands, which are redox active in the region of interest.

Moreover, the IR spectroelectrochemical profiles of the dicluster species **9**$(CF_3SO_3)_2$ and **10**$(CF_3SO_3)_2$ are very complex, due to the presence of four CO ligands on each hexanuclear unit and to the asymmetry of each cluster, caused by the presence of two different ligands on the two "apical" platinum atoms and by possible distortions from the ideal 2d symmetry in the direduced species. Furthermore, also hypothesizing a delocalized singly reduced mixed-valence state, the acquired electron might be delocalized on different portions of the molecules, since the electron transfer might involve only the platinum centers directly bonded to the spacer, or also the central cores of the cluster units. For example, in the alkynyl derivative $\{Pt_6\}(C{\equiv}C{-}Fc)_2$ (Figure 18)[58] theoretical, electrochemical and spectroelectrochemical (NIR, UV-Vis) studies show a lack of electronic communication between the two ferrocenyl units but suggest a metal-to-metal charge transfer, during the stepwise oxidation, from molecular orbitals centered on the apical platinum atoms of the cluster to those centered on the metal atom of the ferrocenyl ligand.

In order to better understand the electronic behavior of **9**$(CF_3SO_3)_2$ and **10**$(CF_3SO_3)_2$, it would be useful to perform other analysis in different conditions (*i.e.* solvent, temperature, supporting electrolyte). Moreover, an exhaustive theoretical study on the nature of the molecular orbitals involved in the reduction processes would help clarifying the details of the redox processes.

In addition, theoretical and electrochemical studies may be extend to new model-compounds containing different organic spacers; for example a system containing a redox probe, such as NC−Fc−CN, may be interesting because the redox behavior of ferrocene derivatives is well-known and would be helpful in the comprehension of a possible electronic transfer.

2.2 C_{60} derivatives of tri- and hexanuclear Platinum clusters.

2.2.1 Introduction to C_{60} and its derivatives.

In 1985 Kroto, Smalley, Curl and co-workers[72] discovered in the gas phase the first molecular allotropes of carbon, the most popular of which is the spherical C_{60} or [60]fullerene. Since then, the attractiveness of C_{60} has grown exponentially and now it

can be considered a widely used and powerful building block for applications in advanced materials,[73] due to a combination of interesting properties, particularly in terms of electron-acceptor capability both in the solid state and in solution. For example, the formation of charge-transfer salts with a number of donor groups or doping with metals has led to ferromagnetic[74] or superconducting[75] materials. Unfortunately, unsubstituted fullerene cannot be easily processed due to its low solubility in most organic solvents; furthermore, it aggregates very easily, becoming even less soluble. This problem may be solved, at least in part, by functionalizing in an appropriate way the C_{60} molecule.[76] In the last two decades, a lot of derivatives of [60]fullerene have been prepared; these, while retaining most of the original properties of the fullerene molecule, became much easier to handle.

The X-ray structural characterization of [60]fullerene revealed the presence of two different types of bonds: "short bonds" (or 6,6 junctions, *ca.* 1.38 Å long) shared by two adjacent hexagons and "long bonds" (or 5,6 junctions, *ca*. 1.45 Å long) in the correspondence of the fusion of a pentagonal and an hexagonal ring. The geometric demand of the spherical cage is such that all the double bonds in C_{60} deviate from planarity.[77] This pyramidalization of the sp^2-hybridized carbon atoms confers an excess of strain to C_{60} which is responsible of its enhanced reactivity. A release of strain is, in fact, associated with the change of hybridization from sp^2 to sp^3 that accompanies most chemical reactions.[78] The chemical reactivity of [60]fullerene is typical of an electron-deficient olefin. In fact, it reacts readily with nucleophiles and it is a reactive 2p component in cycloadditions. Moreover, most of the reactants attack the 6,6 ring junctions of C_{60}, which possess more electron density, giving well-defined, stable and characterizable derivatives.

It is possible to divide single-addition products into a few broad categories, based on the structure of the final derivatives: a) open structures, b) three-membered rings, c) four-membered rings, d) five-membered rings, e) six-membered rings (Figure 30).

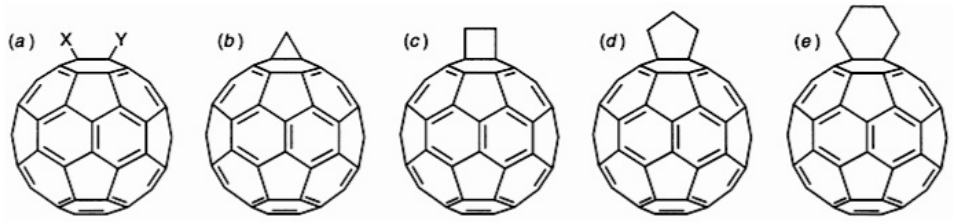

Figure 30. Geometrical shapes built onto a 6,6 ring junction of C_{60}.

Alkynyl derivatives are among the first examples of open structure functionalization. The first derivatives were prepared by Komatsu and co-workers [79] by reacting C_{60} with [(trimethylsilyl)ethynyl]lithium; the final product was obtained by quenching the lithium salt of ethynylated C_{60} with an excess of trifluoroacetic acid (Scheme 10).

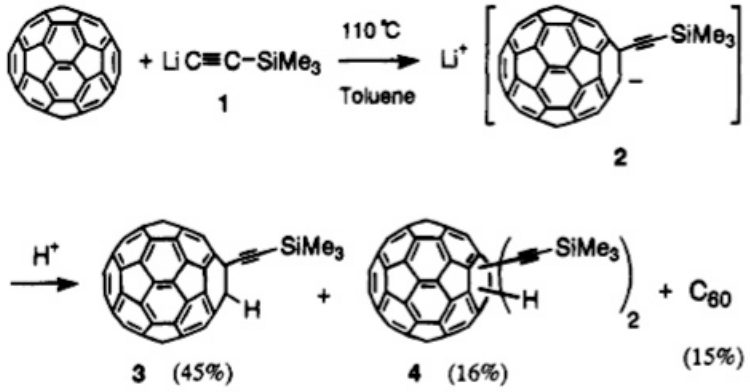

Scheme 10. Synthesis of the first alkynyl derivative of C_{60}.

Subsequently to this work, a lot of [60]fullerene alkynyl derivatives have been prepared, in which different kind of molecular fragments, as, for example, porphyrine,[80] phenothiazine[81] and terthiophene moieties,[82] have been attached to C_{60} through a triple CC bond.

Another well-studied type of functionalization arises from the 1,3-dipolar cycloaddition of azomethine ylides to C_{60}. In this way, it is possible to obtain a wide collection of derivatives in which the fullerene unit is fused to a functionalized five-membered ring (Figure 30d), thus representing a simple approach to a large variety of easily accessible starting materials.[83] The reaction leads to fulleropyrrolidine derivatives in which a pyrrolidine ring is fused with a 6,6 ring junction of C_{60}. Prato *et al.* reported the first synthesis of a N-methylpyrrolidine derivative in 1993.[84] Here, the azomethine ylide was generated by "decarboxylation route",[85] from a mixture of N-methylglycine,

paraformaldehyde and C_{60}, which afforded in good yields the desired product (Scheme 11).

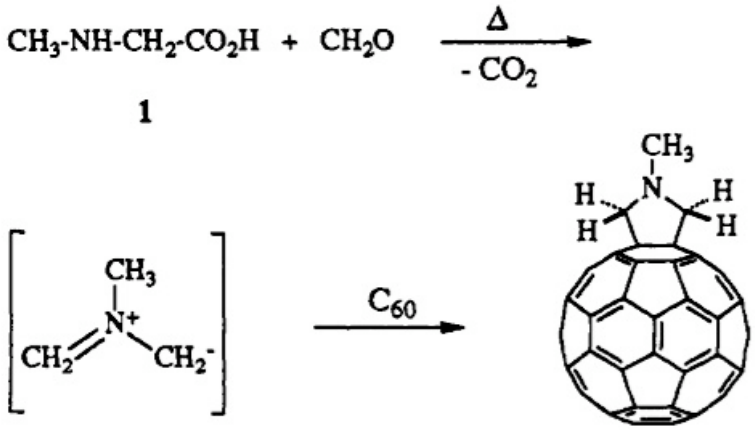

Scheme 11. Preparation of N-methylfulleropyrrolidine derivative.

In this way, a lot of compounds containing C_{60} covalently attached to an additional electroactive group may be prepared, realizing unique redox assemblies which may be considered as donor-bridge-acceptor dyads.[86]

Finally, a part of fullerene chemistry is centered on the synthesis of derivatives containing one or more transition metal atoms directly coordinated to C_{60}.

In particular, exohedral metallofullerenes have attracted a lot of attention concerning the effects of the metal centre(s) on the chemical and physical properties of [60]fullerene. The reactivity and the electrochemical properties of these complexes have been actively investigated, in order to ultimately develop new electronic nanomaterials and nanodevices.[87] The structure of [60]fullerene offers many different possible bonding sites and modes of interaction with metals. These sites are: a) directly over a single carbon atom (η^1-coordination); b) above the midpoint of a 6,6 ring junction ($\eta^{2[6,6]}$-coordination); c) above the midpoint of a 6,5 ring junction ($\eta^{2[5,6]}$-coordination); d) above the center of a pentagonal face (η^5-coordination); e) above the center of an hexagonal face (η^6-coordination) (Figure 31).[88]

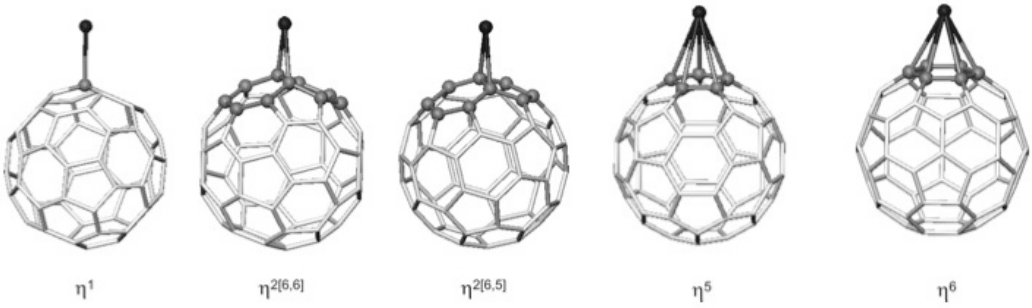

Figure 31. Five possible metal-C_{60} bonding modes.

Interesting examples in which the metal is coordinated η^5 to the fullerene (Figure 31) are the complexes $Ru(\eta^5\text{-}C_{60}Me_5)Cl(CO)_2$ and its derivatives achieved by substitution of the carbonyl and/or the chloro ligands with phosphine, isocyanide, alkyl and alkynyl ligands,[89] $Fe(\eta^5\text{-}C_{60}Me_5)Cp$[90] and $Rh(\eta^5\text{-}C_{60}Me_5)(CO)_2$,[91] prepared by Nakamura and co-workers, which lead an η^5-pentamethylated [60]fullerene ligand, $\eta^5\text{-}C_{60}Me_5$.[92] It was found that in these complexes, there is electronic communication between the metal and the bottom 50-π-electron system through the cyclopentadienide moiety.[93]

In the last years, also metal clusters have been coordinated to the C_{60} molecule. For example Shapley and co-workers and Park and co-workers, independently, prepared various $L_nM_x(C_{60})_y$ complexes, in which a variety of cluster frameworks [$Re_3(\mu\text{-}H)_3$,[94] Ru_3,[95] Os_3,[96] Ru_5C,[97] Os_5C,[98] $PtRu_5C$,[97b] Ru_6C[97a] and Rh_6[99]] are directly coordinated to C_{60}. Studies aimed at clarifying the bonding modes in these complexes have shown that the fullerene molecule is a versatile, multifunctional ligand exhibiting various π- and σ-bonding modes. Moreover, in these complexes, a strong electronic communication between the C_{60} and the cluster units has been found and has been shown to be finely tuned by modifying the ligand set on the metal cluster.[87c, 88]

2.2.2 Preparation and characterization of C_{60} derivatives of tri- and hexanuclear platinum clusters.

As briefly reported above, [60]fullerene has an interesting electron-acceptor capability and the combination of its rich electronic and electrochemical properties with those of other electroactive species is currently a field under intense investigation. In fact, it is believed that chemically modified fullerenes may play a relevant role in the design of

novel molecular electronic devices, in particular for applications to the construction of photovoltaic cells.[100] To this purpose, a number of electron-rich groups have been covalently attached to C_{60}, for the creation of a large variety of dyads. Some examples of donor units used in these compounds include Ru-bipyridine[101] and Ru-terpyridine[102] complexes and ferrocene.[103] Along this line of research, it seemed interesting to bind to C_{60} our trinuclear and hexanuclear platinum clusters, since these compounds are electron rich and may behave as electron donors toward fullerene.

The first problem to solve was how to coordinate the cluster unit to C_{60}. As we have seen above, one of the most suitable way to functionalize [60]fullerene is the 1,3-dipolar cycloaddition of azomethine-ylides (Scheme 11),[84] according to which the final product is obtained by the reaction of C_{60} (**14**) with an aldehyde and a *N*-substituted glycine. Since tri- and hexanuclear cluster derivatives functionalized with one or more formyl groups were supposed to be easily accessible, we decided to start our attempts by applying this method. In particular, we used *N*-octylglycine (**15**), the alkyl chain being deemed useful to increase the solubility of the final products, and the 4-ethynyl-benzaldehyde-derivatives of the tri- and hexanuclear clusters. The 4-ethynyl-benzaldehydic fragment was considered functional to our purposes because it is conjugated and might allow electron transfer from the cluster to the fullerene unit

2.2.2.1 Preparation and spectroscopic characterization of {Pt$_3$}CCC$_6$H$_4$CHO (13).

The first step of the synthesis was the preparation of the precursor {Pt$_3$}[CC–(1,4)C$_6$H$_4$–CHO (**13**) [{Pt$_3$} = Pt$_3$(μ-PBu$^t_2$)$_3$(CO)$_2$]. This was synthesized by reacting the chloro-derivative {Pt$_3$}Cl (**11**) with an equimolar amount of 4-ethynyl-benzaldehyde (**12**) in triethylamine and in the presence of a catalytic amount (1%) of CuI (Sonogashira-type reaction, Scheme 12).

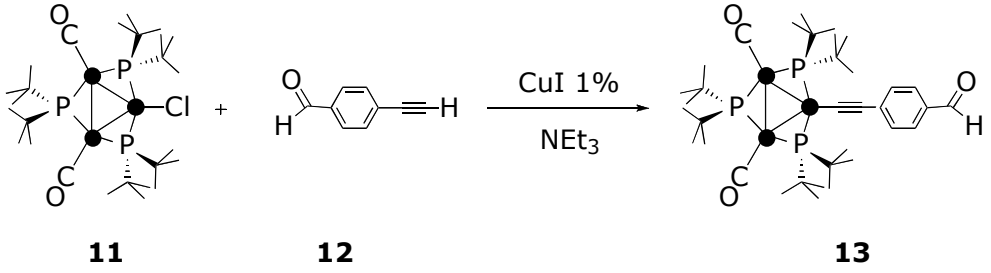

11 **12** **13**

Scheme 12. Synthesis of compound **13**.

The reaction was performed under a rigorously inert atmosphere to avoid the self-coupling of the ethynyl function. After stirring 24 h at room temperature, the solvent was evaporated and toluene was added to the crude product, in order to separate the final product from the insoluble salt (NEt_3HCl) formed during the reaction. Compound **13** was obtained as brown microcrystalline solid in a good yield (83%). Its air and moisture stability, both in the solid state and in solution, and its high solubility in non-polar and in chlorinated solvents, allowed a full spectroscopic characterization. Moreover, its solid state structure was determined by single-crystal X-ray diffraction (see section 2.2.2.1.1) and its redox behavior was studied by electrochemical and spectroelectrochemical (IR, UV-Vis) analyses (see section 2.2.3).

The IR spectrum of **13** in CH_2Cl_2 solution exhibits five significant absorptions at 2097 cm^{-1}, due to the C≡C stretching (ν = 2108 cm^{-1} in $\{Pt_3\}CCPh$)[49], at 2024 cm^{-1} (with a shoulder at 2035 cm^{-1}), due to the C≡O stretching of the carbonyl ligands coordinated to the platinum atoms (ν = 2026 cm^{-1} in $\{Pt_3\}CCPh$) [49], and at 1683, 1589 and 1552 cm^{-1}, the first due to the C=O stretching of the aldehydic carbonyl and the others to the C=C stretching of the aromatic ring of the 4-ethynyl-benzaldehyde ligand (ν = 1680 and 1590 cm^{-1} in the free ligand).[104]

As for hexanuclear clusters, the NMR spectroscopy is a crucial method for the characterization of the family of trinuclear clusters containing the $\{Pt_3\}$ unit. In fact, as fully described in the Appendix A, the presence of eight isotopomers with a different platinum content, gives distinctive features to the shape of the signals (in particular in ^{31}P and ^{195}Pt NMR spectra) which is typical of all the compounds sharing the general formula $\{Pt_3\}X$ described until now[48, 49] and of those prepared in this Thesis.

The $^{31}P\{^1H\}$ NMR (C_6D_6, 293K) spectrum shows two signals at 164.8 and 98.4 ppm, respectively assigned to the two chemically equivalent P_1 and P_3 nuclei (Figure 32a) and to the P_2 nucleus opposite to the alkynyl function (Figure 32b).

The signal centered at δ = 164.8 ppm is composed by a central doublet (the equivalent P_1 and P_3 nuclei couple with P_2) and the signal at higher fields (δ_{P2} = 98.4 ppm) is constituted by a central triplet. Both signals are flanked by satellites due to the coupling with ^{195}Pt (see Appendix A).

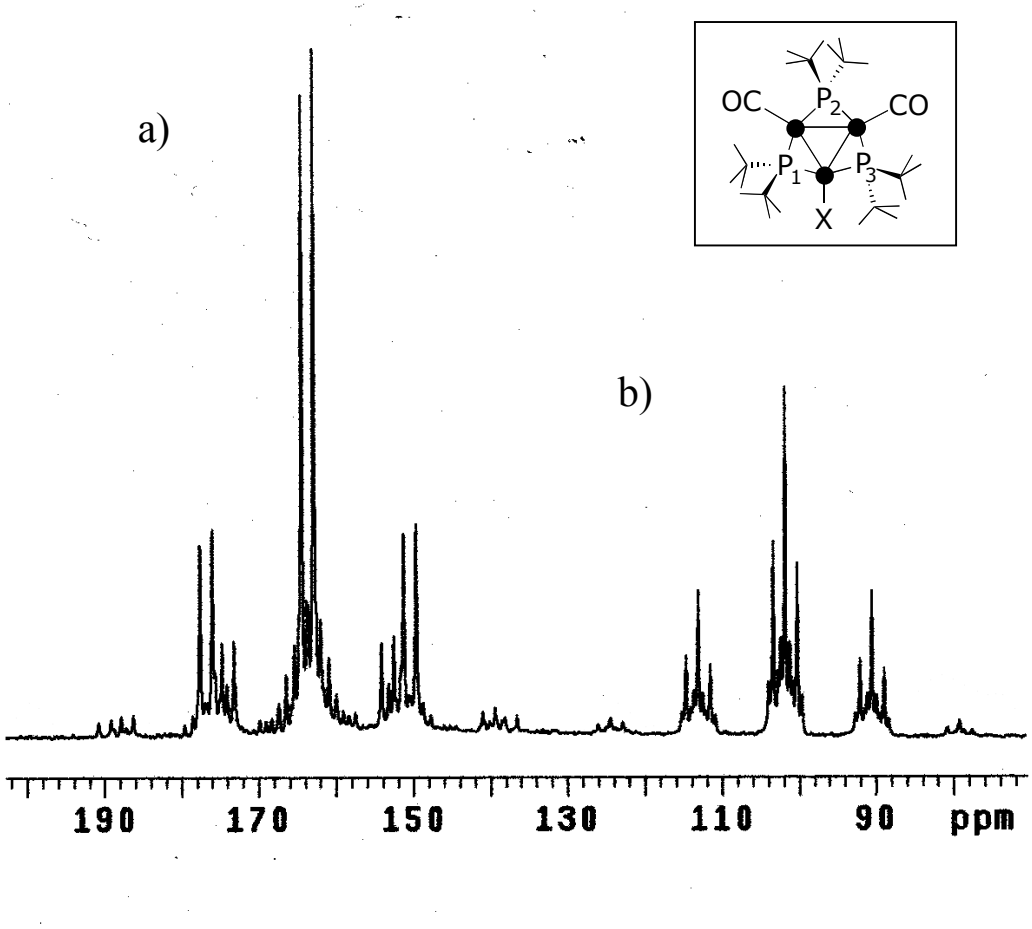

Figure 32. $^{31}P\{^{1}H\}$ NMR (C_6D_6, 293K) of **13**.

The chemical shifts of P_1 and P_3 remain in the range of *ca.* 155-170 ppm for every trinuclear cluster (the only exception is $\{Pt_3\}H$ (**1**), in which $\delta_{P1,3}$ = 220.9 ppm) [48, 49] and may be confidently assigned to phosphido ligands bridging a Pt–Pt bonded edge (see Appendix A). Conversely, the values of δ_{P2} span a wide gap on varying the ligand coordinated to the opposite platinum atom. In particular, the value of δ_{P2} of the final product **13** shifts to lower fields (by *ca*. 50 ppm) in comparison to the corresponding parameter found in the starting chloro-derivative $\{Pt_3\}Cl$ (**11**, δ_{P2} = 46.7 ppm),[55] and its position is close to that found in several alkynyl derivatives previously prepared (*e.g.* $\{Pt_3\}CCPh$ has δ_{P2} = 96.4 ppm).[49]

The considerable fluctuation of the value of δ_{P2} in clusters sharing the $\{Pt_3\}X$ formula may be rationalized by considering in more detail the bonding mode of the bridging phoshides. It is in fact well-known that the values of δ_P shifts of bridging phosphides span from very low fields (up to 450 ppm), typical of bridges on a metal-metal bonded

edge, to the opposite upfield region (up to −150 ppm), when the metal-metal bond is absent.[105a] On the other hand, it is well recognized that the Pt–Pt bond opposite to the anionic ligand X in clusters of general formula $Pt_3(\mu\text{-}PR_2)_3L_2X$ has a very soft deformation potential. This is proved by the skeletal isomerism observed in a platinum cluster which is isoelectronic and strictly correlated to our $\{Pt_3\}X$ derivatives: *i. e.* $Pt_3(\mu\text{-}PPh_2)_3(PPh_3)_2(Ph)$. Braunstein and co-workers[105] have shown that this compound crystallizes from toluene/pentane forming an isosceles Pt_3 triangle with one long [3.586(2) Å (non-bonding)] and two short [2.758(3) Å] Pt–Pt distances. When the crystallization occurs from a CH_2Cl_2/pentane mixture, the complex forms a quasi-equilater Pt_3 triangle: the two short distances are elongated to 2.956(3) Å and the long one is reduced to 3.074(4) Å, (Figure 33), which may still be considered a bonding distance.[106a]

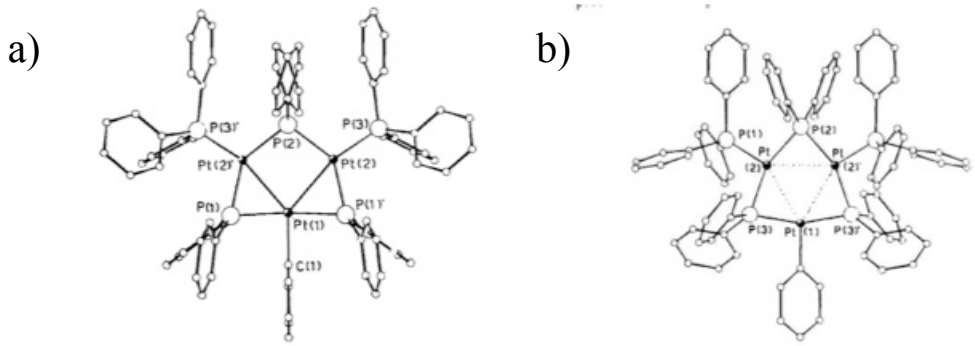

Figure 33. Molecular structures of $Pt_3(\mu\text{-}PPh_2)_3(PPh_3)_2(Ph)$ crystallized from a) toluene/pentane and b) CH_2Cl_2/pentane mixture.

Indeed, theoretical studies[105a] have shown that, when X is a σ-donor ligand, the "open" and the "closed" forms differ in energy by only a few kilocalories per mole. In these cases, the Pt–Pt bond distance opposite to the X ligand, is markedly influenced by relatively small enthalpic contributions, such as packing forces in the solid state or solvent effects in solution, and by the temperature.

We ourselves have observed by diffrattometric studies that the hydride-derivative **1** crystallizes in the "isosceles" manner, with one long [3.6135(6) Å], well above the threshold considered for a Pt–Pt bond (*ca*. 3 Å),[106] and two *ca.* equal [2.7247(6) and 2.7165(6) Å] Pt–Pt distances,[48] Conversely, in its isocyanide analogue $[Pt_3(\mu\text{-}PBu^t_2)_3(CNBu^t)_2H]$[107] the first distance is much shorter [3.0609(3) Å] and may be

considered a bond-distance. In all the alkynyl-derivatives structurally characterized so far, the length of the longer Pt–Pt bond varies between *ca*. 3.6 and 3.0 Å without significantly modifying the stability of the complex. Moreover, it is worth noting that in the four chemically equivalent $\{Pt_3\}$ units of the branched derivative $[(\{Pt_3\}CC)_2C_6H_3CC]_2\{Pt_6\}$, four significantly different values are found for the distance opposite to the alkynyl ligand [3.066(2), 3.179(2), 3.188(3), 3.380(3)]. [55]

The $^{195}Pt\{^1H\}$ NMR (C_6D_6, 293K) of **13** shows two signals at –5715 and –6089 ppm, respectively assigned to the two equivalent platinum nuclei (Pt_2 and Pt_3) coordinated to the carbonyl ligands (Figure 34a) and to the platinum atom (Pt_1) coordinated to the 4-ethynyl-benzaldehyde (Figure 34b) moiety.

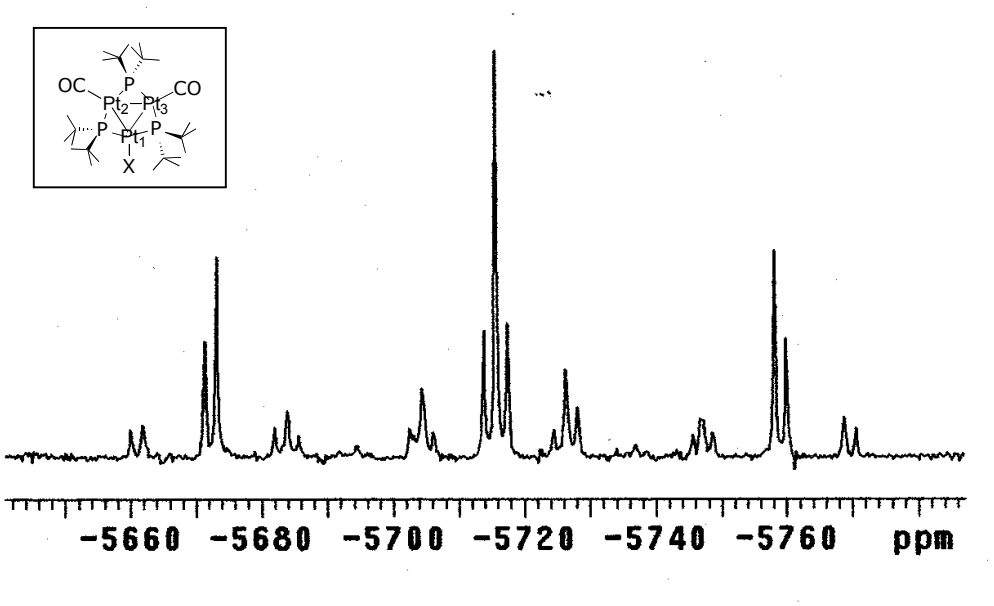

Figure 34a. Portion of the $^{195}Pt\{^1H\}$ NMR spectrum (C_6D_6, 293K) of cluster **13**, showing the signal due to the equivalent nuclei Pt_2 and Pt_3.

Also in this case, the shape of both signals is typical of all the trinuclear clusters with formula $\{Pt_3\}X$,[48,49] the signal centered at –5715 ppm ($Pt_{2,3}$) being a double doublet of doublets and the one at –6089 ppm (Pt_1) a double triplet of triplets (see Appendix A).

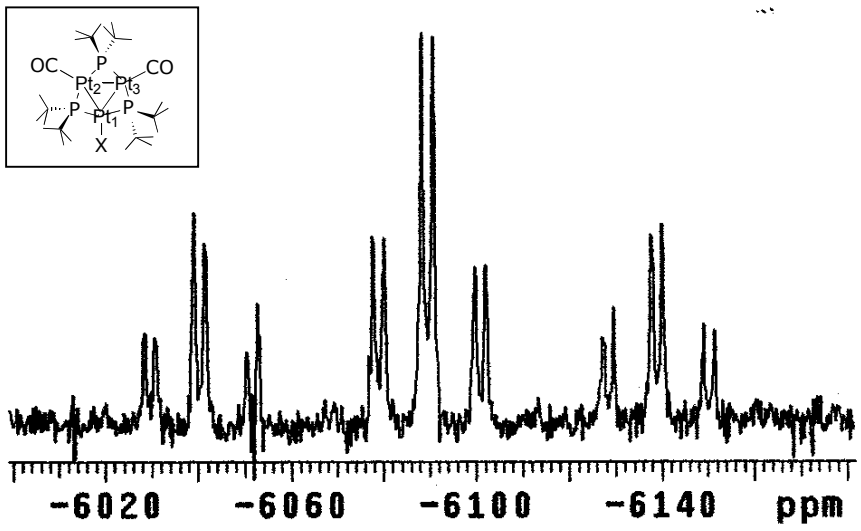

Figure 34b. Portion of the $^{195}Pt\{^{1}H\}$ NMR spectrum (C_6D_6, 293K) of cluster **13**, showing the signal due to Pt_1.

The ^{1}H NMR (C_6D_6, 293K) (Figure 35) spectrum shows, as usual, a virtual triplet (1.47 ppm, $^{3}J_{H\text{-}P} + {}^{5}J_{H\text{-}P}$ = 7.6 Hz, 36 H) and a doublet (1.19 ppm, $^{3}J_{H\text{-}P}$ = 15.2 Hz, 18H), which were assigned to the *t*-butyl protons of the phosphido ligands (see Appendix A).

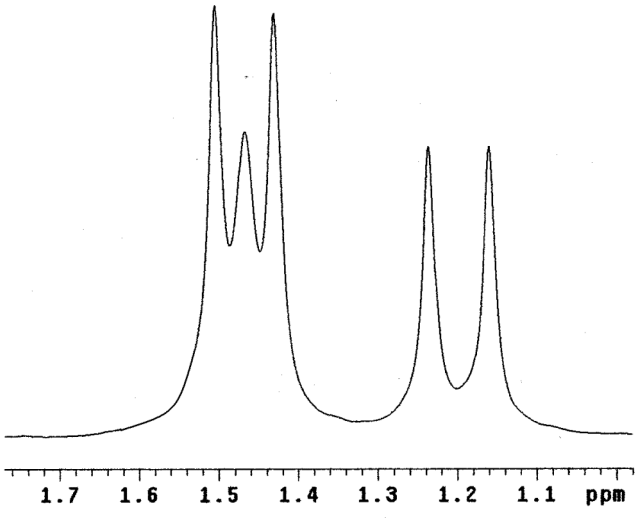

Figure 35. ^{1}H NMR (C_6D_6, 293K) spectrum of **13**.

Moreover, one singlet at 9.69 ppm (1 H) and two doublets at 7.76 ppm ($^{3}J_{H\text{-}H}$ = 8.0 Hz, 2 H) and 7.46 ppm ($^{3}J_{H\text{-}H}$ = 8.0 Hz, 2 H) were respectively assigned to the aldehydic

proton and to the four aromatic protons of the 4-ethynyl-benzaldehyde. The signal of the alkynyl proton (CC-*H*), at 3.21 ppm in the aldehyde precursor,[104] was absent as expected.

The $^{13}C\{^{1}H\}$ NMR (C_6D_6, 293K) shows the signals of both the cluster and the alkynyl ligand (see Experimental part) in full agreement with the structure suggested in Scheme 12.

2.2.2.1.1 Crystal and molecular structure of {Pt$_3$}CCC$_6$H$_4$CHO (13).

Single crystals of **13** suitable for a crystallographic study were obtained by slow evaporation from CH_2Cl_2 solution. The molecular structure is shown in Figure 36, and the more significant geometrical parameters are summarized in Table 5.

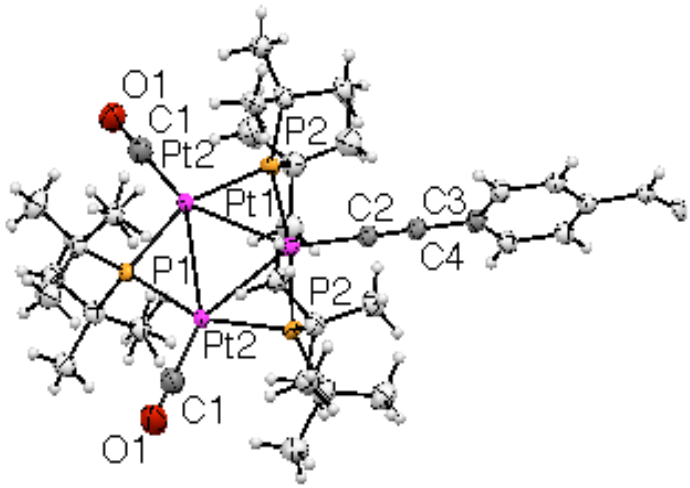

Figure 36. View of the molecular structure of **13**. Hydrogen atoms are omitted for clarity.

The molecule belongs to the C2/m space group (C_{2h}) and exhibits an isosceles Pt_3 triangular core, with one long Pt(2)-Pt(2) [3.1841(6) Å] and two short Pt(1)-Pt(2) [2.8940(7) Å] distances. The former is situated within the very broad range (2.9-3.65 Å) previously found for the Pt–Pt distance opposing the X ligand in other $Pt_3(\mu\text{-}PR_2)_3L_2X$ complexes,[49,105,107] and is very similar to the one found in the cluster $\{Pt_3\}CCC_6H_5$ [3.1181(7) Å] reported previously.[49] Although rather long, it is still shorter than the sum of Pt Van der Waals radii (3.4 Å).[105] The CC triple bond, the phosphorus atoms and the CO ligands approximately lie on the Pt_3 plane; while the phenyl ring and the formyl

group of the alkynyl ligand are perpendicular to this plane. Each pair of *t*-butyl groups lie on either side of the Pt_3 plane, thus offering steric protection to the inner $Pt_3(\mu\text{-}P)_3$ core. The Pt–P distances, between 2.27 and 2.31 Å, are in the range expected on the basis of the $\{Pt_3\}X$ structures determined previously.[48,49,55,107] Due to the presence of a longer Pt–Pt distance in the Pt_3 triangle, one Pt–P–Pt angle is wider than the other two [Pt(1)–P(2)–Pt(2) = 78.66(8)° and Pt(2)–P(1)–Pt(2) = 87.0(1)°]. The P(1) atom bridges the more distant platinum centers, and shows Pt–P distances [Pt(2)–P(1) = 2.313(3) Å] longer than the other ones [Pt(1)–P(2) = 2.270(2) Å and Pt(2)–P(2) = 2.296(3) Å]. The two carbonyl ligands are terminally coordinated, with Pt(2)–C(1)–O(2) angles [180.0(1)°] and Pt(2)-C(1) distances [1.83(1) Å], similar to those found in the previously determined $\{Pt_3\}X$ structures.[48,49,55,107]

Table 5. Significant Bond Lenght (Å) and Angles (°) in **13**.

Pt(1)-C(2)	1.93(2)	Pt(1)-P(2)	2.270(2)
Pt(1)-Pt(2)	2.8940(7)	Pt(2)-C(1)	1.83(1)
Pt(2)-P(1)	2.313(3)	Pt(2)-Pt(2)	3.1841(6)
Pt(2)-P(2)	2.296(3)	Pt(2)-P(1)	2.313(3)
C(1)-O(1)	1.15(2)	C(2)-C(3)	1.22(2)
C(2)-Pt(1)-P(2)	95.5(5)	P(2)-Pt(1)-P(2)	168.9(1)
C(2)-Pt(1)-Pt(2)	146.6(5)	P(2)-Pt(1)-Pt(2)	51.08(7)
Pt(2)-Pt(1)-Pt(2)	66.75(2)	C(1)-Pt(2)-P(2)	103.4(4)
C(1)-Pt(2)-P(2)	103.2(5)	P(2)-Pt(2)-Pt(1)	50.26(7)
C(1)-Pt(1)-Pt(2)	153.7(4)	P(1)-Pt(2)-Pt(1)	103.1(1)
P(2)-Pt(2)-Pt(2)	106.88(7)	P(1)-Pt(2)-Pt(2)	46.51(9)
Pt(1)-Pt(2)-Pt(2)	56.62(2)	C(1)-Pt(2)-Pt(2)	149.7(4)
P(1)-Pt(2)-P(2)	153.3(1)	Pt(1)-P(2)-Pt(2)	78.66(8)
Pt(2)-P(1)-Pt(2)	87.0(1)	Pt(2)-C(1)-O(1)	180.0(1)
C(3)-C(2)-Pt(1)	178.0(1)	C(2)-C(3)-C(4)	179.0(2)

Finally, the Pt(1)–C(2) [1.93(2) Å] and C(2)–C(3) [1.22(2) Å] bond lengths fall in the range commonly found for terminal phenylacetylide ligands bonded to platinum.[105] These data, with the *ca.* linear Pt(1)-C(2)-C(3) angle [178.0(1)°], confirm the σ,η^1 coordination of the alkynyl ligand.

2.2.2.2 Preparation and spectroscopic characterization of {Pt$_3$}CC(Ph)C$_2$H$_3$N(C$_8$H$_{17}$)C$_{60}$ (16).

The C_{60} derivative of the trinuclear cluster **16** was prepared by 1,3-dipolar cycloaddition of an azomethine ylide. The reaction was performed, under inert atmosphere, by dissolving in chlorobenzene $\{Pt_3\}CCC_6H_4CHO$ (**13**), C_{60} (**14**) and *N*-octylglycine (**15**, prepared according to the literature procedure)[108] in 1:1:3 ratio, (Scheme 13).

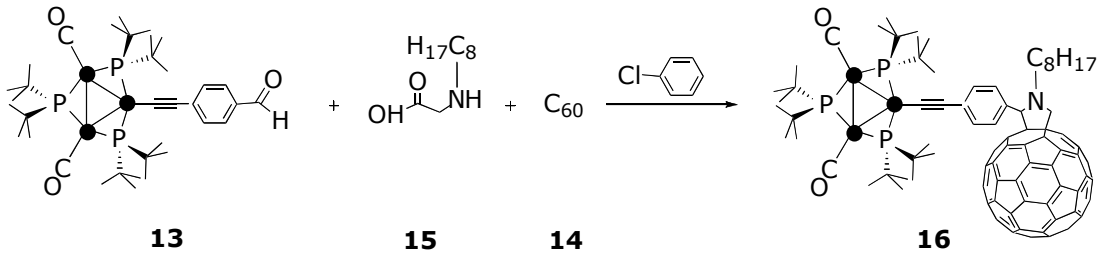

Scheme 13. Preparation of **16**.

The reaction mixture was stirred under reflux for 9 hours. After this period, the solvent was evaporated under vacuum and the crude product first was washed with water and ethanol, in order to remove the excess of *N*-octylglycine, and then was purified by column chromatography, using an ethyl acetate : *n*-hexane = 2 : 1 mixture as the eluent. The final product **16** was obtained in high purity as a brown solid (43% yield).

In spite of the presence of the alkyl chain, compound **16** has a low solubility in many organic solvents. However, it is enough soluble in chlorinated solvents as $CHCl_3$ and CH_2Cl_2 to allow a full spectroscopic characterization. Moreover, as fully reported in section 2.2.3, preliminary electrochemical and spectroelectrochemical studies were carried out, in order to start to the evaluate a possible "through-bond" electron transfer from the cluster to the [60]fullerene units.

Since the phosphorus and platinum nuclei have a chemical environment similar to that of the corresponding nuclei of the precursor, the $^{31}P\{^1H\}$ and $^{195}Pt\{^1H\}$ NMR ($CDCl_3$,

293K) spectra of **16** are very similar to the corresponding spectra discussed above for **13**. Thus, the $^{31}P\{^{1}H\}$ spectrum shows one doublet at 163.8 ppm (2 P) and a triplet at 99.1 ppm (1 P), both accompanied by ^{195}Pt satellites, and the $^{195}Pt\{^{1}H\}$ spectrum consists of two signals at −5727 (2 Pt) and −6068 (1 Pt) with the same multiplicity of the signals of **13**.

In the ^{1}H NMR ($CDCl_3$, 293K) spectrum, in addition to the signals due to the *t*-butyl protons of the phosphido ligands [a virtual triplet at 1.41 ppm, $^{3}J_{H\text{-}P} + {}^{5}J_{H\text{-}P} = 7.1$ Hz, 36 H, and a doublet at 1.33 ppm, $^{3}J_{H\text{-}P} = 14.3$ Hz, 18 H] and to the two doublets at 7.61 ppm ($^{3}J_{H\text{-}H} = 8.1$ Hz, 2H) and 7.32 ppm ($^{3}J_{H\text{-}H} = 8.1$ Hz, 2H) due to the four aromatic protons of the alkynyl ligand (H_1 and H_2, Figure 37), other signals are present. In particular, the spectrum shows four multiplets due to the alkyl protons of the octyl chain, at 3.40-3.18 (2 H), 2.56 (2 H), 2.12-1.60 (10 H) and 0.97 (3 H) ppm, and two doublets at 5.12 ($J = 9.2$ Hz, 1H) and 4.13 ppm ($J = 9.2$ Hz, 1 H) and one singlet at 5.02 ppm (1 H), respectively due to the H_4, H_5 and H_3 (Figure 37) nuclei of the substituted pyrrolidinic ring, that suggest the structure given in Figure 37 for **16**.

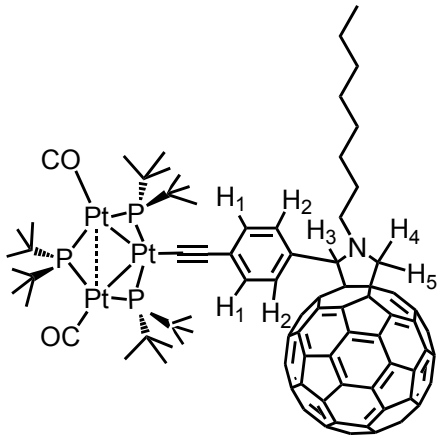

Figure 37. Supposed structure for **16**.

The $^{13}C\{^{1}H\}$ NMR ($CDCl_3$, 293K) spectrum shows an high number of signals with the expected frequencies and intensities (Figure 37). In particular, one singlet at 175.2 ppm, due to the C nuclei of the carbonyl ligands, four signals at 133.76, 131.39, 129.52, 129.38 ppm, due to the six aromatic carbons of the disubsituted benzene ring, two singlets for the two quaternary alkynyl C nuclei, at 121.3 ppm (Pt–*C*≡C) and at 82.20 ppm (Pt–C≡*C*), two singlets at 69.06, 66.87, due to the carbon nuclei of the pyrrolidinic ring, two signals at 38.93 and 33.51 ppm, due to the *t*-butyl carbons and eight signals (at

53.08, 32.03, 29.79, 29.42, 28.41, 27.56, 22.79, 14.27 ppm) due the C nuclei of the octyl chain are present. In addition, the spectrum shows 28 singlets between 156.83 and 135.79 ppm, attributable to the C nuclei of the C_{60}; similar signals are found in other fulleropyrrolidine derivatives, already known in literature.[83a,b,84]

The IR spectrum of a CH_2Cl_2 solution of **16** shows one broad signal centered at 2024 cm^{-1} (ν_{CO}), and two weak signals at 2102 ($\nu_{C\equiv C}$) and 1602 cm^{-1}, the latter due to the stretching of the C=C bonds of the aromatic ring.

Finally, compound **16** was analyzed by flow injection analysis - mass spectrometry (FIA-MS). The spectrum shows the molecular ion at m/z = 2052.7 amu, in full agreement with the molecular formula of the final cluster ($C_{104}H_{78}NO_2P_3Pt_3$, calculated molecular weight = 2051.8 amu).

2.2.2.3 Preparation and characterization of {Pt₆}(CCC₆H₄CHO)₂ (17).

Similarly to the procedure described above for the preparation of **16**, the synthesis of the symmetrical cluster $\{Pt_6\}(CCC_6H_4CHO)_2$ (**17**) is the first step for the preparation of the corresponding fullerene derivative. The reaction was performed by reacting the chloro-derivative $\{Pt_6\}Cl_2$ (**4**) with 4-ethynyl-benzaldehyde (Scheme 14) under Sonogashira-type conditions.

After stirring 24 hours at room temperature, the solvent was evaporated under vacuum, the residue was suspended in toluene and a colorless solid (Et_3NHCl) was filtered off. From the filtrate, cluster **17** was obtained as an air and moisture stable (both in solution and in solid state) dark orange solid, in a high purity and yield (80%).

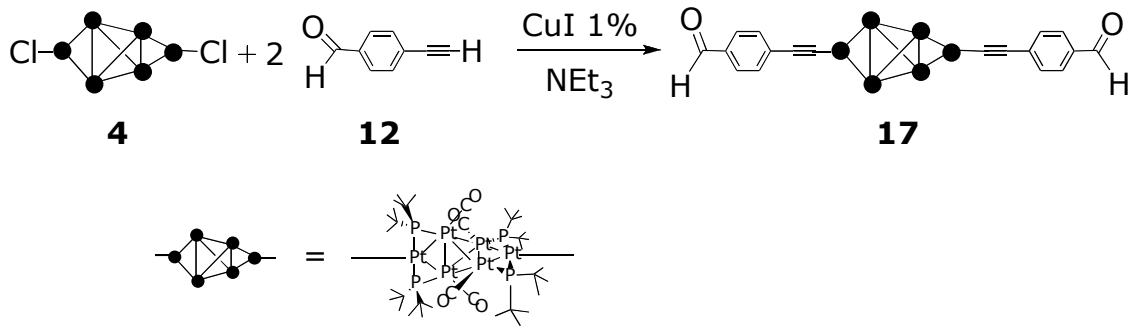

Scheme 14. Preparation of **17**.

The high solubility of **17** in both chlorinated and non-polar solvents, allowed its full spectroscopical (IR and ^{1}H, ^{13}C, ^{31}P, ^{195}Pt NMR) characterization.

The IR (solid state) spectrum shows strong bands at 2101 ($\nu_{C\equiv C}$) and 2010 ($\nu_{C\equiv O}$) cm^{-1}; similar spectral features are reported for $\{Pt_6\}(CCPh)_2$ (ν_{CC} = 2100 and ν_{CO} = 2010 cm^{-1}).[54] The absence of the ν_{CCH} absorption at *ca*. 3000 cm^{-1} confirms the coordination of the alkynyl ligand to the cluster.[109] In addition, the spectrum contains two absorptions at 1591 and 1552 cm^{-1} ($\nu_{C=C}$, aromatic ring) and one band at 1693 cm^{-1}, due to the aldehydic C=O stretching (ν = 1590 and 1680 cm^{-1} in **12**).[104]

The $^{31}P\{^{1}H\}$ NMR (C_6D_6, 293K) spectrum shows one singlet, centered at 336.2 ppm [δ_P = 335.7 ppm in $\{Pt_6\}(CCPh)_2$],[54] with the usual shape observed for symmetrically substituted hexanuclear clusters (see Appendix A, Figure 38).

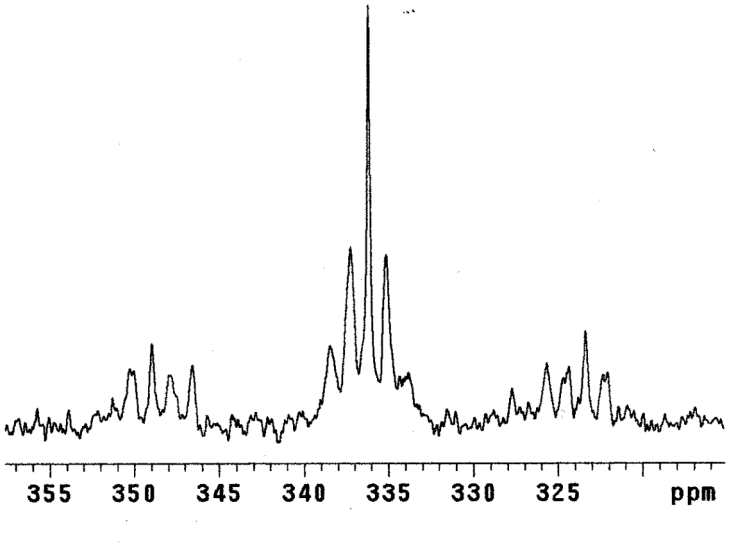

Figure 38. $^{31}P\{^{1}H\}$ NMR (C_6D_6, 293K) spectrum of **17**.

The ^{1}H NMR (C_6D_6, 293K) spectrum is in full agreement with structure **17** [virtual triplet, see Appendix A, at 1.48 ppm ($^{3}J_{H\text{-}P} + {}^{5}J_{H\text{-}P}$ = 7.1 Hz, 72 H, PCC*H*$_3$), and signals at 7.59 (d, $^{3}J_{H\text{-}H}$ = 7.5 Hz, 4 H, Ar-*H*), 7.53 (d, $^{3}J_{H\text{-}H}$ = 7.5 Hz, 4 H, Ar-H) and 9.66 ppm (s, C*H*O)]. The $^{195}Pt\{^{1}H\}$ NMR (C_6D_6, 293K) spectrum shows two multiplets at –2998 and –4664 ppm, respectively assigned to the four inner and to the two apical platinum atoms (δ_{Pt} = –3000 and –4675 ppm in $\{Pt_6\}(CCPh)_2$).[54]

The $^{13}C\{^1H\}$ NMR (C_6D_6, 293K) spectrum shows signals with the expected frequencies and intensities (see Experimental part for more details).

2.2.2.4 Preparation and characterization of {Pt$_6$}[CCC$_6$H$_4$-C$_2$H$_3$N(C$_8$H$_{17}$)C$_{60}$]$_2$ (18).

Compound **18** was synthesized similarly to its analogue **16**: a chlorobenzene solution of *N*-octylglycine (**15**), C_{60} (**14**) and $\{Pt_6\}[CC\text{-}C_6H_4\text{-}CHO]_2$ (**17**), in 6:2:1 ratio, was stirred for 9 h under reflux (Scheme 15).

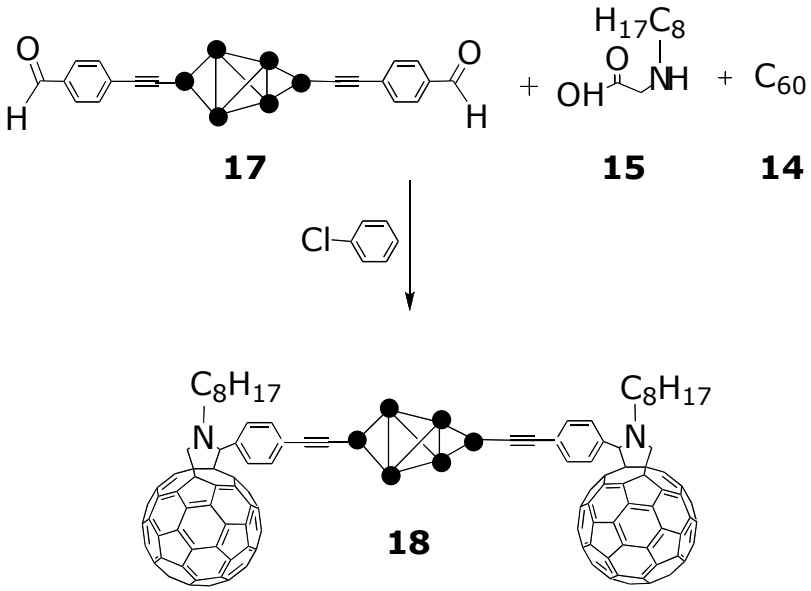

Scheme 15. Synthesis of **18**.

After this period, the solvent was evaporated under vacuum and the crude product was washed with water, ethanol and then purified by column chromatography (toluene : CH_2Cl_2 = 1:5 mixture as eluent). The final product **18** was obtained as a brown solid in good purity (39% yield).

The compound is air and moisture stable in solution and in solid state, but, unfortunately, in spite of the presence of the alkyl chains, it is insoluble in most of the organic solvents. It has a low solubility only in the chlorinated solvent CH_3Cl and CH_2Cl_2, which allowed the collection of significant NMR spectra of only the most sensitive nuclei (^1H and ^{31}P).

As expected, the $^{31}P\{^{1}H\}$ NMR ($CDCl_3$, 293K) spectrum of **18** is very similar to the one of its precursor **17**: a singlet at 336.0 ppm, flanked by the ^{195}Pt satellites, which confirms that the two apical ligands are identical.

The ^{1}H NMR ($CDCl_3$, 293K) spectrum shows the signals expected for structure **18** (as reference see Figure 37): two doublets at 7.62 ($^{3}J_{H\text{-}H}$ = 8.3 Hz, 4 H, Ar-*H*) and 7.31 ppm ($^{3}J_{H\text{-}H}$ = 8.3 Hz, 4 H, *Ar*-H), and two doublets at 5.09 ppm (*J* = 9.5 Hz, 2 H) and 4.10 ppm (*J* = 9.5 Hz, 2 H) and one singlet at 5.00 ppm (2 H) for the pyrrolidinic protons. The octyl chains give four multiplets at 3.78-3.62, 2.52, 2.13-1.74, 0.93 ppm, and the *t*-butyl protons of the phosphido ligands give a virtual triplet (see Appendix A) at 1.49 ppm ($^{3}J_{H\text{-}P} + {}^{5}J_{H\text{-}P}$ = 6.5 Hz, 72 H).

2.2.3 Electrochemical and spectroelectrochemical studies of 13 and 16.

As reported in section 2.1.6 and discussed in more detail in the Appendix B, electrochemical and spectroelectrochemical studies give information about the redox behavior and may be useful to evaluate the presence of an intramolecular electron transfer process. We carried out a preliminary electrochemical and spectroelectrochemical analysis on the trinuclear derivatives **13** and **16** whose results are presented in the following paragraph.

2.2.3.1 Cyclic voltammetry.

The cyclovoltammetric profile of several trinuclear clusters containing the $\{Pt_3\}$ unit is well known.[49] In CH_2Cl_2 solution, all clusters undergo two sequential monoelectronic oxidations. For cation $[\{Pt_3\}CO]^+$ (**2**$^+$), only the first oxidation process is reversible on the time scale of the cyclic voltammetry, whereas the second oxidation is complicated by subsequent chemical reactions. Moreover, one irreversible reduction process is present in the cathodic region.

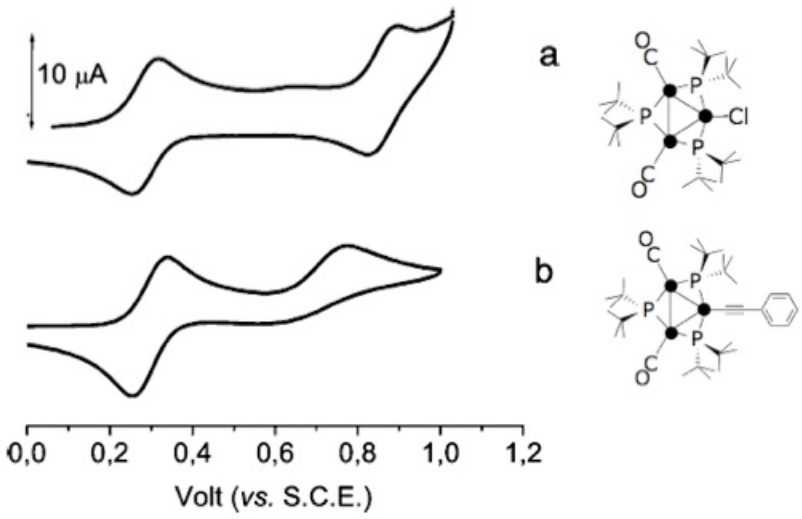

Figure 39. Cyclic voltammograms recorded at a platinum electrode in CH_2Cl_2 solutions of a) $\{Pt_3\}Cl$ (**4**) and b) $\{Pt_3\}CCPh$, using NBu_4PF_6 0.2 M as supporting electrolyte.

The voltammogram of the neutral trinuclear clusters $\{Pt_3\}X$ also shows two monoelectronic oxidation processes, but cathodically shifted with respect to the oxidations of $\mathbf{2}^+$. The first oxidation is chemically reversible on the CV time scale, and the second is coupled to chemical complications, the rate of which depends upon the nature of the ligand X (Figure 39). Halo-derivatives [X = Cl (**11**), Br, I] also possess one irreversible monoelectronic reduction at very negative potentials, which is also followed by chemical complications.

The cyclovoltammetric analyses on **13** and **16** were carried out in CH_2Cl_2, using NBu_4PF_6 0.2 M as the supporting electrolyte. Their redox potentials and, for reference, those of **11**,[49] $\{Pt_3\}CCPh$,[49] and C_{60}, the latter measured in similar conditions by Zanello and co-workers,[110] are summarized in Table 6.

Table 6: Formal electrode potentials (V *vs* SCE) and peak-to-peak separations (mV) for the redox processes exhibited in CH_2Cl_2 solution by compound **13** and **16** and, for comparison, by the trinuclear platinum clusters **11**,[49] $\{Pt_3\}CCPh$,[49] and by C_{60}.[110]

Compound	Solvent	Oxidations	Reductions
		$E^{0\prime}$ [a] (ΔE_p)[b]	$E^{0\prime}$ [a] (ΔE_p)[b]
$\{Pt_3\}$-Cl	CH_2Cl_2	+ 0.31 (60); +0.91 (70)	-1.91[c]
$\{Pt_3\}$-CCPh	CH_2Cl_2	+ 0.30 (85); +0.75[c]	/
13	CH_2Cl_2	+0.32 (90); +0.79[d]	-2.01[c]
16	CH_2Cl_2	+0.29 (80); +0.72[d]	-0.71 (80); -1.09 (81); -1.70[c]
C_{60}	CH_2Cl_2	/	-0.63 (59); -1.00 (60); -1.45 (64); -1.9[e]

[a,b] Measured at 0.1 $V \cdot s^{-1}$. [a] Measured in V, vs SCE. [b] Measured in mV. [c] Peak potential value for irreversible processes. [d] Coupled with fast chemical reactions. [e] Difficult to be appreciated because of the partial overlapping with subsequent processes.

As expected, the voltammogram of **13** (Figure 40, potential values reported *vs*. SCE) is very similar to the one of the analogous alkynyl derivative $\{Pt_3\}CCPh$ (Figure 39b) and shows two mono-electronic oxidation processes at + 0.32 and + 0.79 V, the former is reversible in the time scale of the cyclic voltammetry (i_{pc}/i_{pa} = 1 at 0.2 V s^{-1}), while the latter is coupled to chemical complications. Furthermore, a multielectronic irreversible reduction process was observed in the cathodic region at very negative potentials (–2.01 V).

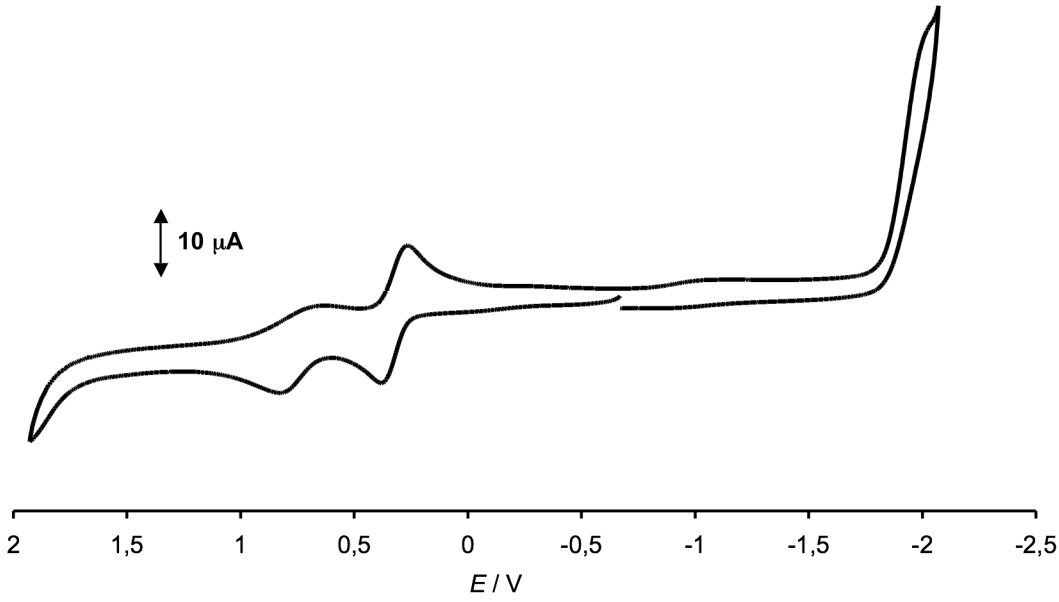

Figure 40. Cyclic voltammograms of **13** measured at 0.1 Vs^{-1}.

The voltammogram of **16** shows an high number of redox processes, due to both the cluster and the [60]fullerene units (Figure 41).

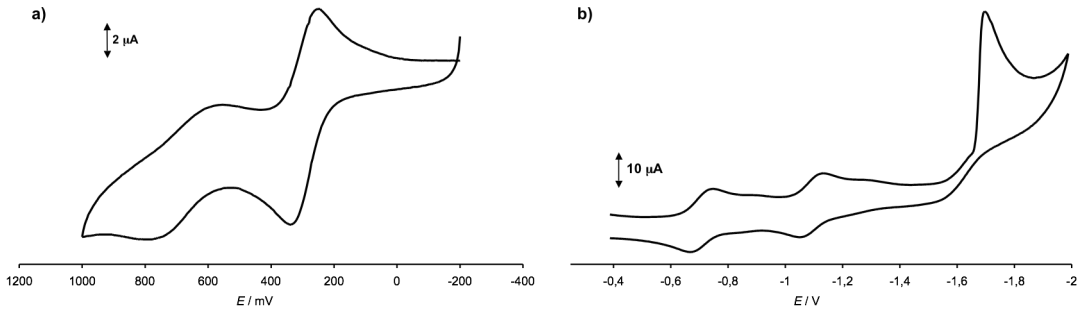

Figure 41. a) Oxidation and b) reduction processes of **16** measured at 0.1 Vs^{-1}.

The anodic region exhibits two monoelectronic oxidation processes, centered on the cluster. Also in this case, the former (+0.29 V) is chemically reversible and the second (+0.72 V) is partially reversible. Moreover, three processes, all assignable to the C_{60} unit, were observed in the cathodic region. The reductions at −0.71 and −1.09 V are monoelectronic and reversible in the time scale of the cyclic voltammetry, conversely, the process at higher potentials (−1.70 V) is multielectronic and irreversible. Comparing the cathodic region of the voltammogram of C_{60} and **16** (Table 6), in the latter the

reduction processes are cathodically shifted due to the saturation of the double bond, which raises the LUMO energy,[111] as reported in the literature for other fulleropyrrolidine derivatives. [83b, 86]

2.2.3.2 IR spectroelectrochemistry.

The IR spectroelectrochemical experiments carried out on CH_2Cl_2 solution of **13** and **16** (NBu_4PF_6 0.2 M as the supporting electrolyte) allowed the characterization of the products of their monoelectronic oxidation, $\mathbf{13}^+$ and $\mathbf{16}^+$, and of the bi-oxidized product $\mathbf{13}^{2+}$ (Table 7).

Table 7. CO stretching absorptions of **13** and **16** and their oxidation products.

Compound	Solvent	ν_{CO}/cm^{-1} Initial	ν_{CO}/cm^{-1} Mono-oxidized	ν_{CO}/cm^{-1} Bi-oxidized
13	CH_2Cl_2	2024; 2035	2068; 2077	2083
16	CH_2Cl_2	2024; 2034	2067; 2077	/

The IR spectrum of **13** shows a broad ν_{CO} absorption at 2024 cm^{-1} with a shoulder at 2035 cm^{-1}. Upon oxidation, these bands are gradually replaced by two new peaks at higher frequencies (2068 and 2077 cm^{-1}). The appearance of well-defined and withstanding isosbestic points and the quantitative restoration of the IR bands of the starting **13** observed in the reverse cycle confirm the remarkable stability of the oxidized cluster (Figure 42a). Going to the second oxidation potential, a new very broad band, that may be assigned to $\mathbf{13}^{2+}$, grows up at 2083 cm^{-1} (Figure 42c). On the time scale of the IR experiments, the oxidation is followed by partial decomposition in an unidentified product (proved by the presence of a weak absorption at 2051 cm^{-1}, which remains unchanged after the reverse cycle) that did not allow the complete recovery of the starting compound **13**.

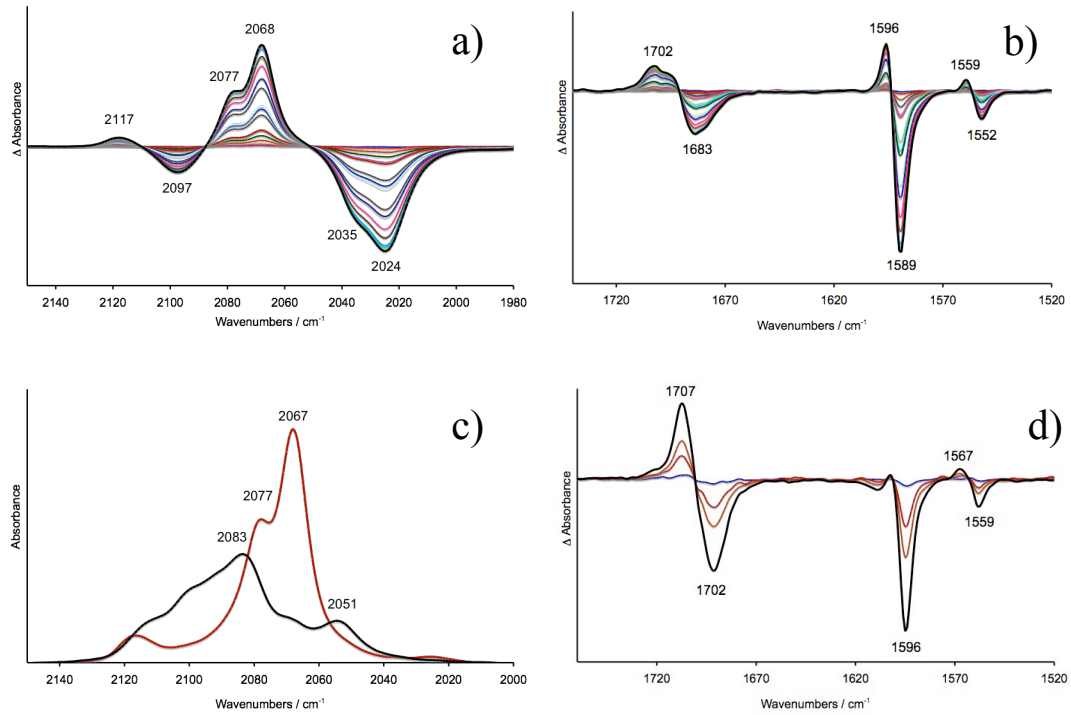

Figure 42. IR spectral changes recorded in a OTTLE cell during the progressive a) and b) one-electron and c), d) and e) two-electrons oxidation of **13** in CH_2Cl_2 solution. A reference spectrum, collected before the application of an oxidation potential, is used to calculate the differential absorbance spectra of a) and b). The final spectrum b) has been used to calculate the differential absorbance spectra of d). Due to the partial overlap of the CO bands in $\mathbf{13}^+$ and $\mathbf{13}^{2+}$, only the spectrum of the mono-oxidized product and the final spectrum of the di-oxidized species are shown (c).

The IR spectrum of **13** also shows absorptions due to the C≡C (2097 cm^{-1}), to the aldehydic C=O (1683 cm^{-1}) and to the C=C ring (1589 and 1552 cm^{-1}) vibrations of the alkynyl ligand (see section 2.2.2.1). During the stepwise oxidation also these bands shift at higher frequencies, due to the increase of the formal positive charge of the cluster. After the first oxidation, well-defined isosbestic points are present in all the spectral changes (Figure 42b). Unfortunately, after the second oxidation, the C≡C and one of the C=C stretching are no more detectable, probably due to symmetry changes of the cluster (Figure 42d). The collected data are summarized in Table 8.

Table 8. Absorption bands of the alkynyl ligand in **13** and its oxidation products.

	13	**13**$^{+}$	**13**$^{2+}$
$\nu_{C\equiv C}$/cm^{-1}	2097	2117	/
$\nu_{C=O}$/cm^{-1}	1683	1702	1707
$\nu_{C=C}$/cm^{-1}	1589; 1552	1596; 1559	1567

The oxidation products of **16** are less stable than those of **13**, for this reason only the IR spectrum of the mono-oxidized **16**$^{+}$ was recorded (Figure 43). In this case, only the spectral changes of the absorption bands due to the CO stretching are detectable.

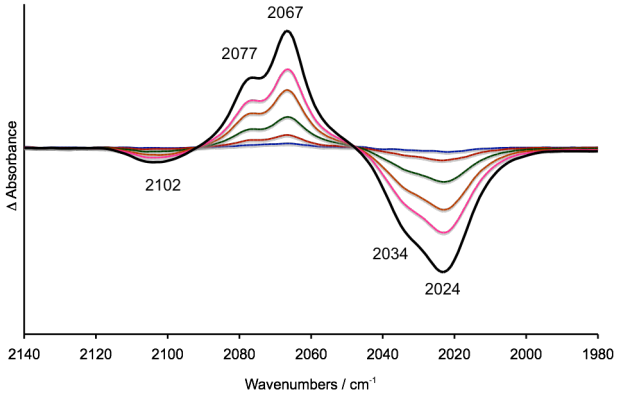

Figure 43. IR spectral changes recorded in an OTTLE cell during the progressive one-electron oxidation of **16** in CH_2Cl_2 solution. A reference spectrum, collected before the application of an oxidation potential, is used to calculate the differential absorbance spectra.

The IR spectral changes of **16** during the progressive one-electron oxidation are very similar to those of its precursor **13**: the initial spectrum shows one broad band at 2024 cm^{-1}, with a shoulder at 2034 cm^{-1} (ν_{CO}), which, during the oxidation, are gradually replaced by two bands at 2067 and 2077 cm^{-1}. The IR spectrum of **16** shows also one band at 2102 cm^{-1} ($\nu_{C\equiv C}$), which decreases during the oxidation.

IR spectra were also recorded during the reduction of compound **16**. In this case, the processes are centered on the [60]fullerene unit. During the electrolysis, no spectral changes of the CO absorption band at 2024 cm^{-1} were detected, as if the carbonyl ligands coordinated to the cluster weren't affected by the electronic changes on the C_{60}

unit. This, together with the similarity of the spectral changes during the oxidation with its precursor **13**, prefigures the absence of any significant electronic communication between C_{60} and the $\{Pt_3\}$ unit in **16**.

2.2.3.3 UV-Vis and NIR spectroelectrochemistry.

UV-Vis spectroelectrochemical experiments were executed on CH_2Cl_2 solution of **13** and **16**, using NBu_4PF_6 0.2 M as the supporting electrolyte. The UV-Vis spectral changes are shown in Figure 44 for **13** and in Figure 45 for **16**. Spectral data are summarized in Table 9.

Table 9. UV-Vis absorption bands of **13**, **16** and theirs mono-oxidized product.

Compound	λ_{max}/nm initial	λ_{max}/nm mono-oxidized
13	222; 242; 357; 400	229; 304; 400; 496
16	233; 290; 317; 349; 393; 430	233; 290; 317; 430

The UV-Vis spectrum of **13** (Figure 44, green line) shows two absorptions at λ_{max} = 357 and 400 nm assignable to the cluster unit (the UV-Vis spectrum of $\{Pt_3\}Cl$ (**11**) shows two peaks at 357 and 396 nm) and two overlapped bands at 222 and 242 nm, probably due to metal-ligand-charge-transfer (MLCT) and to the acetylide-based intraligand transitions (similar absorptions were found in Pt(phenantroline)(CC-C_6H_4-CHO)$_2$ by Wadas *et al.*).[112]

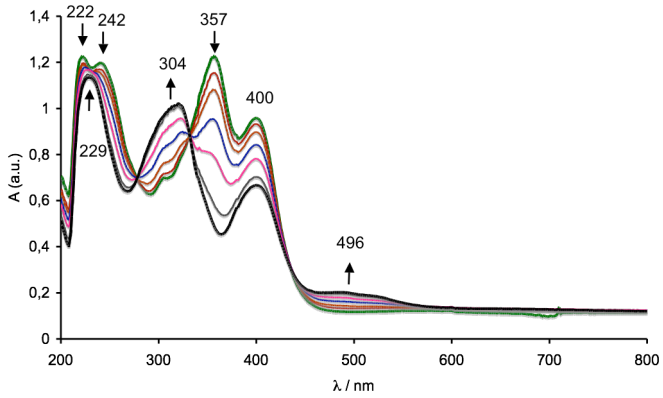

Figure 44. UV-Vis spectra of **13** in CH_2Cl_2 solution containing NBu_4PF_6 (0.2 M) as supporting electrolyte recorded in a OTTLE cell during the stepwise one electron oxidation.

During the oxidation at the first oxidation potential, the peak at 357 nm decreases and is replaced by new bands at 304 and 500 nm which were assigned to the mono-oxidized $\{Pt_3\}$ unit. Spectral changes involve also the ligand-centered absorptions, in fact the bands at 222 and 242 nm are replaced by a new peak at 229 nm (Figure 44). Quantitative restoration of the UV-Vis bands of the starting **13** was observed in the reverse cycle. Unfortunately, the two-electron oxidation product, $\mathbf{13}^{2+}$, is not stable in the time scale of the UV-Vis experiments and it was not possible to record its spectrum.

The UV-Vis spectrum of **16** (Figure 45, green line) is more complex than the one of its precursor **13**. In fact, the region between 500 and 200 nm shows an high number of overlapped absorptions. For comparison with the spectra of **13**, we may tentatively assign the peaks at 349 and 393 nm to the cluster unit. The other absorptions, especially the one at 430 nm, might be assigned to the fulleropyrrolidine unit, in fact similar bands were found in other fulleropyrrolidine derivatives known in literature.[83a,d;86] However, the assignment of the bands with $\lambda_{max} < 330$ nm is difficult because also the MLCT and acetylide intraligand transitions fall in this region.

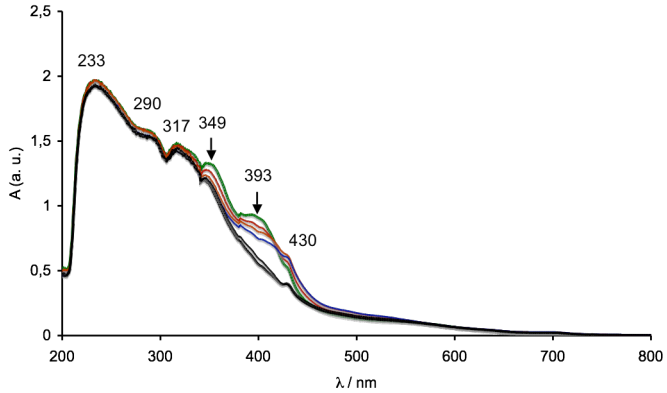

Figure 45. UV-Vis spectra of **16** in CH_2Cl_2 solution, containing NBu_4PF_6 (0.2 M) as the supporting electrolyte, recorded in an OTTLE cell during the stepwise one-electron oxidation.

During the stepwise one-electron oxidation, we observed spectral changes of only the absorptions due to the cluster unit: the bands at 349 and 393 nm decrease, but no new peak appears. In this case, it was not possible to detect clearly the absorptions of the cluster unit in $\mathbf{16}^+$ because, probably, they fall in a spectral region occupied by other transitions.

The absence of spectral changes of the bands attributable to the alkynyl ligand during the oxidation, supports the lack of electronic communication between the C_{60} and $\{Pt_3\}$ units, as already found in the IR spectroelectrochemical experiments.

Furthermore, NIR spectroelectrochemical measurements were made on a CH_2Cl_2 solution of **16**, using NBu_4PF_6 0.2 M as the supporting electrolyte. The spectral changes during the first reduction process are shown in Figure 46. In this part of the spectral region the singly reduced fullerene has a characteristic absorption around 1080 nm; in the fulleropyrrolidine derivatives, this maximum is shifted to higher energies, at *ca.* 1010 nm.[86]

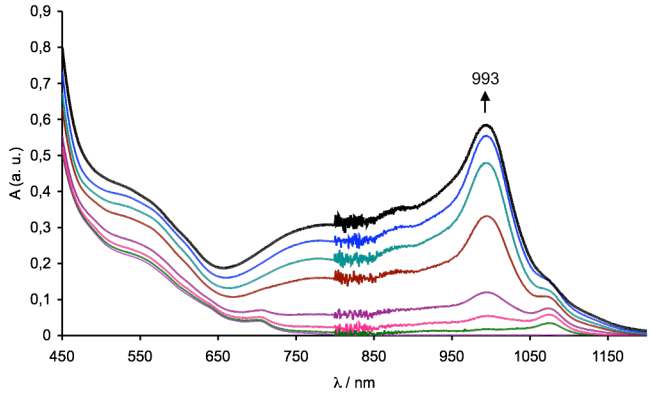

Figure 46. NIR spectra of **16** in CH_2Cl_2 solution containing NBu_4PF_6 (0.2 M) as supporting electrolyte recorded in an OTTLE cell during the stepwise one electron reduction.

As expected, the initial spectrum does not show absorptions in the NIR region (750-2500 nm). During the electrolysis a broad peak increases at λ_{max} = 993 nm, reaching its maximum intensity at the first reduction potential; the position of this absorption is thus very close to those previously attributed to monoreduced fulleropyrrolidine-derivatives.[86] The band decreases until complete disappearance in the reverse cycle, confirming the reversibility of the reduction process in the time scale of NIR spectroelectrochemistry. Conversely, no spectral changes were observed during the oxidation of **16**.

2.2.4 Conclusion and future works.

In conclusion, the electrochemical and spectroelectrochemical analyses are in agreement with a lack of electronic communication between the cluster and the fullerene units of these derivatives. A similar result was observed by Guldi and co-workers[83b] in dumbbell-type architectures in which two C_{60} stoppers are bridged by π-conjugated oligophenyleneethynylenes (OPEs) of various lengths, covalently connected to the fullerene units through pyrrolidine rings (Figure 47). Also in this case, the cyclovoltammetric analysis certifies the lack of electronic communication between the bridge and the C_{60} moieties, which behave as two independent units in the ground state.

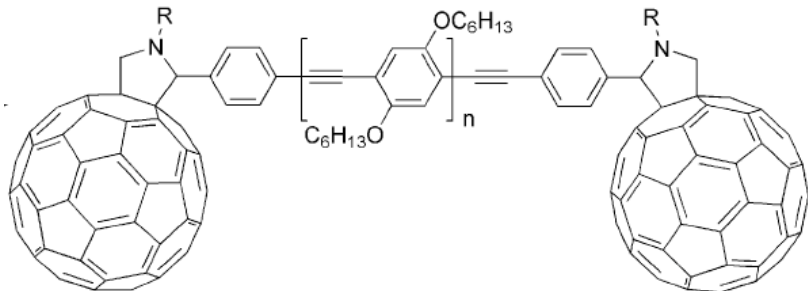

Figure 47. C_{60}-oligomer-C_{60} triads.

The authors suggest that this failure can be accounted for by the interruption of conjugation caused by the interposition of two sp^3 carbon atoms of the pyrrolidinic ring between the C_{60} moieties and the conjugated oligomeric bridge. Actually, it is worth noting that spectroscopic and electrochemical studies on the alkynyl derivatives shown in Figure 48, in which *only one* sp^3 carbon is interposed between C_{60} and the spacer, revealed also in this case the lack of any detectable electronic communication in the ground state.[113]

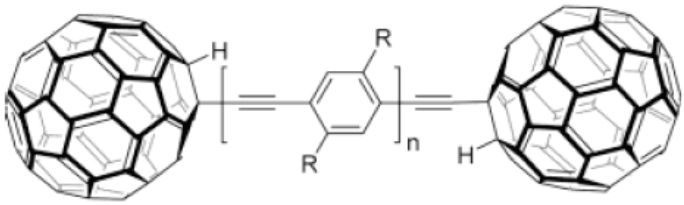

Figure 48. Fullerene-terminated oligo(phenylene ethynylene)s (OPE)s.

On the other hand, in a large number of C_{60}-based donor-acceptor systems, the charge transfer is studied after exciting the fullerene or the donor unit by light irradiation.[114,115] This leads (directly, or after energy transfer from the singlet excited state of the donor) to the population of the singlet excited state of the fullerene moiety, which has a short lifetime (nanoseconds) and, generally, converts rapidly to the longer-lived triplet excited state, after a spin-forbidden intersystem crossing. Population of the excited states [whose energies are *ca* 1.9 eV (singlet) and 1.5 eV (triplet)][86] renders the fullerene both a better electron acceptor and an electron donor compared to the ground state. These electron transfer processes may occur with two possible pathways: "through-bond" and "through-space". In the case of rigid conjugated spacers (such as

the one used in compounds **16** and **18**) the lack of freedom of conformational changes allows only the through-bond pathway; on the contrary, the presence of flexible unconjugated spacers (such as alkyl chains) makes the first pathway unfavorable, but allows the acceptor and donor units to come in close proximity, thus facilitating the through-space pathway.

The tri- and hexanuclear clusters prepared in our laboratories may be respectively considered as donor or acceptor units, due to their electrochemical responses; thus it would be interesting to reinvestigate the electron-transfer capabilities of these systems after photoexcitation of the fullerene or of the spacer units. It will also be interesting to introduce flexible, not-necessarily conjugated, spacers in order to test possible through-space electron transfer. In any case, it will be of great help to carry out theoretical studies in order to understand if the molecular orbital geometry and energy of the C_{60} and of the donor or acceptor cluster units, in their ground or excited states, may assist a charge transfer.

2.3 Tris-Phosphido Bridged triangular clusters of palladium.

As briefly introduced in section 1.2, one of the targets of my PhD Thesis was to prepare new clusters in order to use them as synthons for the synthesis of ordered macromolecular assemblies. For this type of utilization, these new compounds should posses a remarkable stability under the reaction conditions needed to build the final structures and should contain only a few reactive sites, well positioned to give the expected shape to the final structures. Since the tri- and hexanuclear platinum clusters prepared in our laboratories, and fully described in the previous parts of this Thesis, have these features, we thought to prepare similar palladium compounds. While platinum mixed-valence tris-phosphido-bridged triangulo clusters of this type are well known, we found out that the analogous palladium compounds of general formula $[Pd_3(\mu\text{-}PR_2)_3(L)_3]^+$ or $Pd_3(\mu\text{-}PR_2)_3(L)_2X$ were virtually unknown. Actually, only the chloro derivative $Pd_3(\mu\text{-}PBu^t_2)_3(CO)_2Cl$, obtained in very low yields (12%) as a by-product in a reaction conceived for other purposes, has been described by Jones and co-workers in 1987.[116] Other loosely related derivatives reported meanwhile are: the bis(dialkylamino)phosphide derivatives of Pd(II), $Pd_3(\mu\text{-}PR_2)_3Cl_3$ [R = NPr^i_2, N(c-

Hex)$_2$], prepared by Dyer and co-workers,[117] the Pd(0) phosphinine cluster $Pd_3(\mu$-PC_5H_2-2,4,6-$Ph_3)_3(PEt_3)_3$, prepared by Reetz, Thiel and co-workers,[118] and the primary phosphido derivative of Pd(II), $Pd_3(\mu$-$PHCH_2Fc)_3(PPh_3)_3Cl_3$, prepared by Mastrorilli and co-workers.[119] In the latter, however, the Pd centres are not bonded to each other, but the three [$Pd(PPh_3)Cl$] subunits are held together by the bridging μ-$PHCH_2Fc$ groups.

2.3.1 Synthesis and spectroscopical characterization of $Pd_3(\mu$-$PBu^t_2)_3(CO)_2Br$ (20) and $Pd_3(\mu$-$PBu^t_2)_3(CO)_2I$ (21).

In order to plan the synthesis of the tris-phosphido bridged triangular palladium clusters, we inspired to the preparation of their analogous trinuclear platinum compounds prepared in our laboratories.[48,49] As shown in section 1.2, the precursor of all the phosphido bridged trinuclear platinum clusters is the hydride derivative $Pt_3(\mu$-$PBu^t_2)_3(CO)_2H$ (**1**).[48] This is synthesized by heating at 100 °C a toluene suspension of the dinuclear Pt(II) complex $[Pt(PBu^t_2H)(H)(\mu$-$PBu^t_2)]_2$,[120] under an atmosphere of CO (1 atm, Scheme 16).

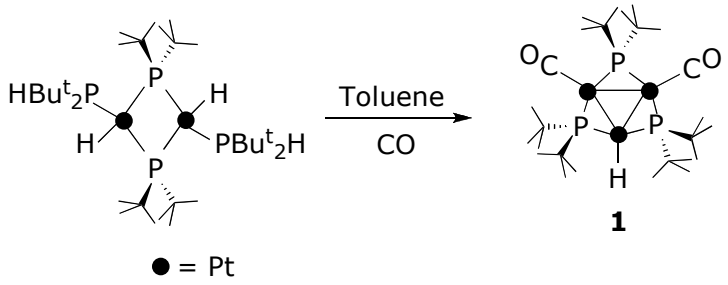

Scheme 16. Synthesis of {Pt_3}H (**1**).

In the palladium case, it was not possible to repeat the reaction using the same conditions shown in Scheme 16, because the analogous dinuclear compound of Pd(II), $[Pd(PBu^t_2H)(H)(\mu$-$PBu^t_2)]_2$, is unstable and immediately undergoes a reductive elimination, releasing H_2 and giving the more stable Pd(I) dinuclear complex $[Pd(PBu^t_2H)(\mu$-$PBu^t_2)]_2$, (**19**).[121] In fact, by heating compound **19** under an atmosphere of CO we did not achieve the desired compound but we obtained the monosubstitution product $[Pd_2(\mu$-$PBu^t_2)_2(PBu^t_2H)(CO)]$, together with other unidentified compounds. The

$^{31}P\{^{1}H\}$ NMR spectrum, recorded on a portion of the reaction mixture, shows two main signals (together with other several weak and unassigned singlets in the region between 0 and 250 ppm), one doublet at 305.2 ppm ($^{2}J_{P\text{-}P}$ = 28 Hz) and a triplet at 58.2 ppm ($^{2}J_{P\text{-}P}$ = 28 Hz). Similar parameters (295.8 ppm, d, $^{2}J_{P\text{-}P}$ = 38 Hz; 60.7 ppm, t, $^{2}J_{P\text{-}P}$ = 28 Hz) were found for $[Pt_2(\mu\text{-}PBu^t_2)_2(PBu^t_2H)(CO)]$.[122]

Due to the lack of hydride ligands in **19**, its reaction with CO was also performed in the presence of a reagent that may release H^- ($NaBH_4$). Unfortunately, under these conditions we did not achieve the desired trinuclear product but only a mixture of unidentified compounds. Probably in these conditions the palladium compounds present in solution may be reduced; otherwise, the hydride derivative of an hypothetic trinuclear cluster may be unstable and, hence, may decompose before isolating.

We then attempted the reaction in presence of an halide ion, since we knew that halide derivatives of phosphido-bridged trinuclear palladium clusters are stable (as reported above, $Pd_3(\mu\text{-}PBu^t_2)_3(CO)_2Cl$ is known in literature[116]). The reaction was performed by heating a toluene suspension of the dinuclear complex **19** under 1 atmosphere of CO in presence of a stoichiometric amount of NBu_4X (X = Br, I, Scheme 17).

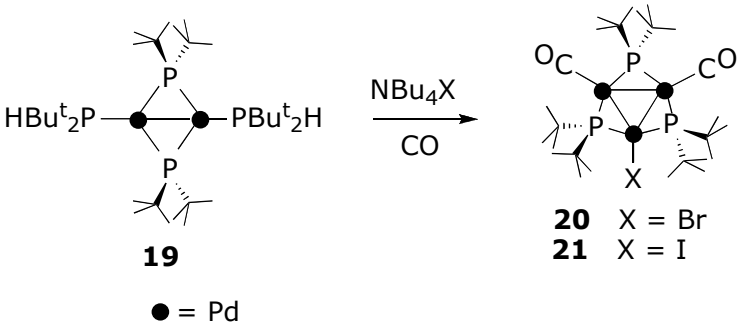

Scheme 17. Synthesis of $\{Pd_3\}Br$ (**20**) and $\{Pd_3\}I$ (**21**).

After stirring three days at 100°C, the reaction mixture was cooled to room temperature and the solid residue was filtered off. The remaining red solution was evaporated under vacuum and the crude product was purified by column chromatography on neutral alumina. The desired products $\{Pd_3\}X$ [hereafter $Pd_3(\mu\text{-}PBu^t_2)_3(CO)_2$ = $\{Pd_3\}$; X = Br (**20**), I (**21**)] were isolated in satisfactory to good yields (**20**: 63%, **21**: 85%) as dark red microcrystalline solids. The attempted reaction between **19** and NBu_4Cl was unsuccessful, giving only complex mixtures of unidentified products (this cluster was

obtained in high yields using a different synthetic method, which will be fully described below). The stability of the $\{Pd_3\}X$ halo derivatives increases going from the chloro to the iodo-derivative, and $\{Pd_3\}Cl$ (**22**) decomposes under the reaction conditions. This stability scale is supported also by the fact that $\{Pd_3\}I$, (**21**) is air stable both in the solid state and in solution, whereas $\{Pd_3\}Br$, (**20**) is air stable only in the solid state and decomposes in solution after a few days, giving a mixture of unidentified complexes.

The high solubility of both the clusters in the most common organic solvents allowed their full spectroscopic characterization (IR and ^{1}H, ^{13}C and ^{31}P NMR); moreover, the solid state structure of **20** was determined by X-ray diffractometric studies (see *infra*).

Differently from the trinuclear platinum clusters, in which the presence of the satellites due to the coupling with the ^{195}Pt nucleus complicates the shape of the signals, the $^{31}P\{^{1}H\}$ NMR (C_6D_6, 293K) spectra of **20** and **21** show simpler signals. In particular, one doublet at *ca.* 280-290 ppm, due to the two equivalent P_2 nuclei, and a triplet at *ca.* 210 ppm, due to the P_1 nucleus bridged to the Pd–Pd bond opposite to the halide ligand ($^{2}J_{P\text{-}P}$ *ca.* 115-116 Hz); the spectrum of $\{Pd_3\}I$ (**21**) is reported in Figure 49, and the NMR parameters for **20** and **21** are summarized in Table 11.

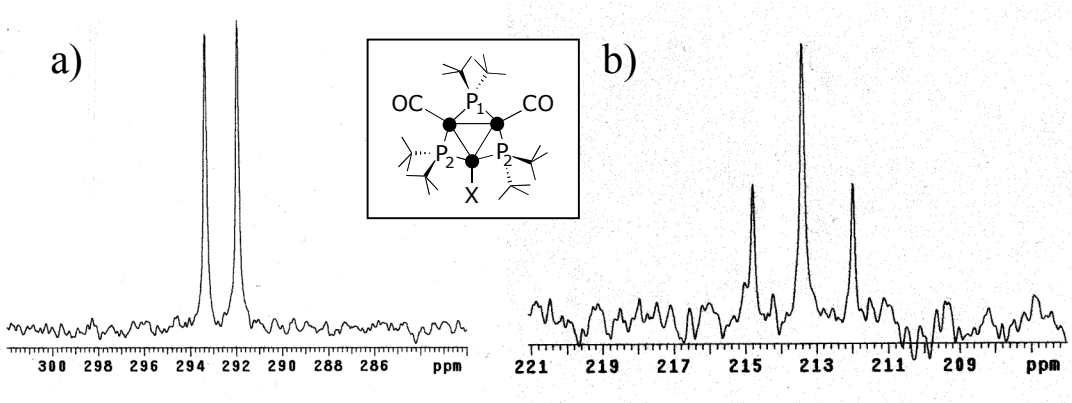

Figure 49. $^{31}P\{^{1}H\}$ NMR (C_6D_6, 293K) of **21**.

The multiplicity of the $^{31}P\{^{1}H\}$ NMR signals is in full agreement with the structure suggested for these compounds; moreover, similar signals were found by Jones and co-workes in $\{Pd_3\}Cl$ (δ_{P2} = 280.1 ppm, δ_{P1} = 207.5 ppm and $^{2}J_{P\text{-}P}$ = 119 Hz).[116]

As expected, the ^{1}H NMR (C_6D_6, 293K) spectrum of both clusters shows only two signals due to the protons of the *t*-butyl phosphido ligands: one virtual triplet (see

Appendix A) at *ca.* 1.50 ppm ($^3J_{H-P} + {}^5J_{H-P}$ *ca.* 7.0 Hz, 36 H) and one doublet at *ca.* 1.13 ppm ($^3J_{H-P}$ *ca.* 14.5 Hz, 18 H). The signals of {Pd_3}Br (**20**) are shown in Figure 50.

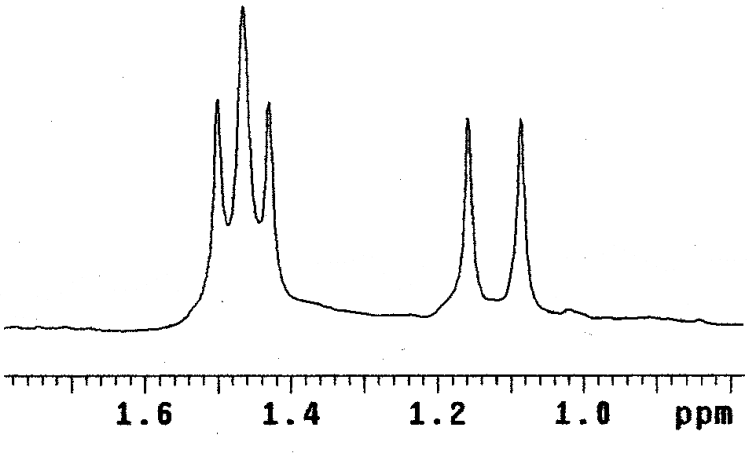

Figure 50. ^{1}H NMR (C_6D_6, 293K) spectrum of **20**.

Again, the signals are similar to those found in {Pd_3}Cl (δ_H = 1.45 and 1.11 ppm; $^3J_{H-P}$ = 15 Hz).[116] The $^{13}C\{^1H\}$ NMR (C_6D_6, 293K) spectra of **20** and **21** show the expected signals: one singlet at *ca.* 188 ppm due the C nuclei of the carbonyl ligands and four singlets, two at *ca.* 41-39 ppm and two at *ca.* 34-29 ppm, respectively, due to the quaternary and the *C*H_3 carbon nuclei of the three *t*-butyl phosphido ligands, two of which are chemically equivalent.

The IR spectrum (solid state) of both clusters shows one absorption at *ca.* 2040 cm^{-1} (Table 11), due to the CO stretching. The found ν_{CO} values are higher compared to the analogous ones in the corresponding platinum clusters (ν_{CO} = 2027 cm^{-1} in {Pt_3}Br and ν_{CO} = 2024 cm^{-1} in {Pt_3}I);[49] the difference may be assigned to the greater π-basicity of platinum.

2.3.1.1 Crystal and molecular structure of {Pd$_3$}Br (20).

Single crystals of **20** suitable for crystallographic studies were obtained by slow evaporation from hexane solution. The molecular structure is shown in Figure 51 and its more significant geometrical parameters are summarized in Table 10.

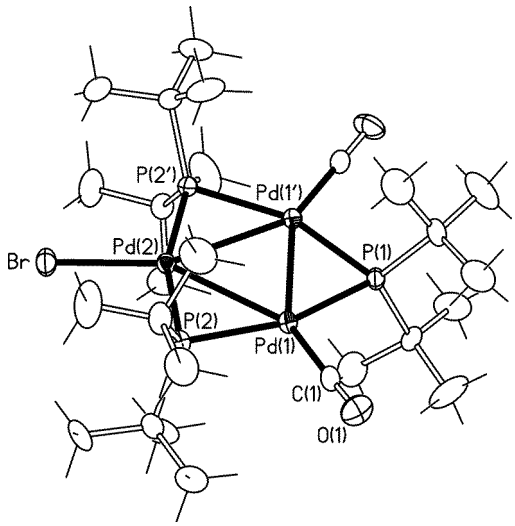

Figure 51. ORTEP view of the molecular structure of $[Pd_3(\mu\text{-}PBu^t_2)_3(CNBu^t)_3]^+$ (**26**$^+$). Thermal ellipsoids are at 20% probability.

The molecule belongs to the Pnma space group and its structure is similar to that of the isotypic chloro derivative.[116] The coordination neighbourhood of palladium is planar. Each pair of *t*-butyl groups lie on either side of the Pd_3 plane, thus offering steric protection to the inner $Pd_3(\mu\text{-}P_3)$ core. The asymmetric unit is half molecule for the mirror plane passing through Br, Pd(2), P(1) and the two carbon atoms connected to P(1). The Pd_3 triangle is isosceles with two Pd(1)–Pd(2) distances [2.9474(10) Å] slightly shorter than the Pd(1)–Pd(1') [2.9960(13) Å] distance, opposing the bromine ligand. The P(1) atom, bridging the longer Pd–Pd bond, shows Pd–P distances [Pd(1)–P(1) = 2.314(2) Å] slightly longer than the other Pd–P distances [Pd(1)–P(2) = 2.298(2) Å and Pd(2)–P(2) = 2.273(2) Å]. These data confirm the flexibility of the phosphido ligands, which can bridge two bonded or non-bonded metals. Thus, the short Pd–Pd distances in **20** are not imposed by the ligand but may be attributed to a real Pd–Pd bond. The Cambridge Crystallographic Data Base[123] also shows that the observed Pd(2)–Br distance [2.4601(16) Å] is almost coincident with the average calculated [2.456 Å] on the result of 180 Pd–Br distances in structures with terminal Br. Finally, the two carbonyl ligands are terminally coordinated, with Pd(1)–C(1)–O(1) angle [177.5(9)°] and Pd(1)–C(1) distance [1.874(10) Å] similar to those found in $\{Pd_3\}Cl$. The C(1)–O(1) distance [1.124(11) Å] is slightly shorter than in $\{Pt_3\}Cl$

[1.16(2) Å],[49] confirming, together with the IR data, the minor π-backbonding of palladium.

Table 10. Significant Bond lenghts [Å] and angles [°] in **20**.

Pd(1)–Pd(2)	2.9474(10)	Pd(1)–P(2)	2.298(2)
Pd(1)–Pd(1')	2.9960(13)	Pd(2)–P(2)	2.273(2)
Pd(1)–P(1)	2.314(2)	Pd(2)–Br	2.4601(16)
Pd(1)–C(1)	1.874(10)	C(1)-O(1)	1.124(11)
Pd(2)–Pd(1)–Pd(1')	59.452(15)	P(2)–Pd(1)–Pd(2)	49.49(6)
Pd(1)–Pd(2)–Pd(1')	61.10(3)	P(2)–Pd(2)–Pd(1)	50.22(6)
P(1)–Pd(1)–Pd(1')	49.66(5)	Pd(2)–P(2)–Pd(1)	80.30(7)
Pd(1)–P(1)–Pd(1')	80.69(10)	P(2)–Pd(2)–Br	99.24(6)
C(1)–Pd(1)–P(1)	101.1(3)	C(1)–Pd(1)–P(2)	100.4(3)
Pd(1)-C(1)-O(1)	177.5(9)		

2.3.2 Reactivity of {Pd$_3$}I (21).

After obtaining the trinuclear palladium clusters **20** and **21**, we started the study of their reactivity, in particular of the iodo derivative {Pd$_3$}I (**21**). This cluster proved to be an excellent precursor for other trinuclear palladium clusters for its air stability both in the solid state and in solution, and its high solubility in polar and non-polar organic solvents. Until now, four substitution reactions, involving only the iodo ligand or the whole set of terminal ligands, were studied and are summarized in Scheme 18.

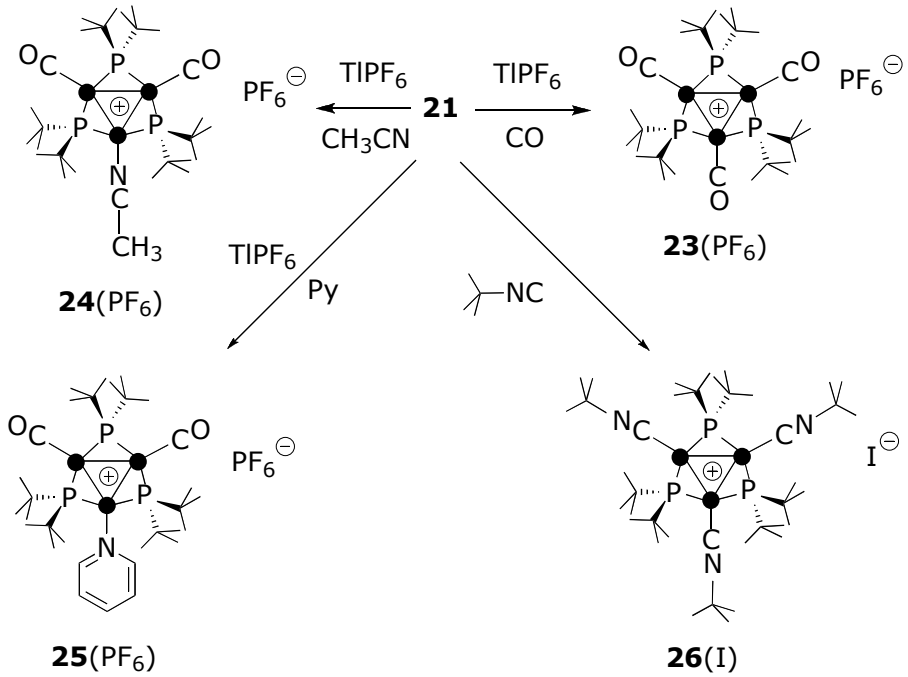

Scheme 18: Reactivity of **21** with neutral ligands.

2.3.2.1 Substitution of the iodo ligand.

The iodo ligand may be quantitatively removed by reacting {Pd_3}I (**21**) with an excess of $TlPF_6$ in acetonitrile or pyridine, which gives, respectively, [Pd_3(μ-PBu^t_2)$_3$(CO)$_2$($NCCH_3$)] [PF_6] **24**(PF_6) and [Pd_3(μ-PBu^t_2)$_3$(CO)$_2$(py)][PF_6] **25**(PF_6), (Scheme 18). In fact, the reaction between **21** and $TlPF_6$ leads to the formation of the insoluble salt (TlI), which precipitates out in the reaction mixture, and, probably, of an unstable intermediate palladium cluster, where one metal atom is coordinatively unsaturated, which coordinates a solvent molecule (CH_3CN or pyridine). After stirring overnight at room temperature, filtering off TlI and washing with hexane, the monosubstitution products **24**(PF_6) and **25**(PF_6) were obtained as dark red solid in high purity and in good yields (74 and 86%).

Moreover, by treating a dry THF solution of **21** with a 2-fold excess of $TlPF_6$ under 1 atm of carbon monoxide we obtained the substitution of the iodide by a carbonyl ligand (Scheme 18). After stirring overnight at room temperature, filtering off the TlI and washing with hexane, the symmetrical cationic cluster [Pd_3(μ-PBu^t_2)$_3$(CO)$_3$][PF_6] **23**(PF_6) was achieved as red solid in a good yield (77%).

The monocationic clusters **23**(PF_6), **24**(PF_6) and **25**(PF_6) are air stable for a few days in the solid state and decompose in a few hours in solution. However, their stability in solution under an inert atmosphere and their solubility in polar organic solvents, allowed their full spectroscopic characterization (IR and ^{1}H, ^{13}C and ^{31}P NMR, see *infra*).

2.3.2.1.1 Synthesis of {Pd$_3$}Cl (22).

Previously, we reported that the reaction between the dinuclear complex **19** and NBu_4Cl under 1 atm of CO (Scheme 17) didn't lead to the chloro derivative {Pd_3}Cl (**22**). In order to conceive a better synthetic method for this cluster, compared to the one reported in the literature,[116] we inspired to the synthesis of its analogous {Pt_3}Cl (**11**), prepared by reacting the monocationic [{Pt_3}CO]$^+$ (**2**$^+$) with NBu_4Cl, in acetone.[55]

Thus, we tried the reaction by adding an equimolar amount of $[(PPh_3)_2N]Cl$, to a solution of [{Pd_3}CO](PF_6), **23**(PF_6) in dry acetone (Scheme 19).

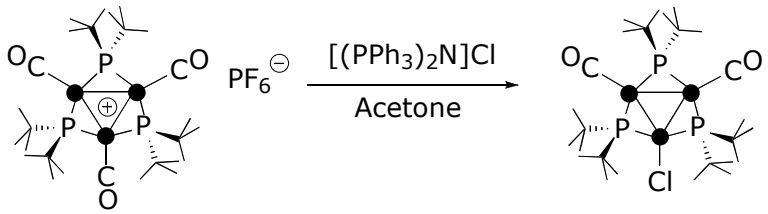

23(PF_6) **22**

Scheme 19: Synthesis of **22**.

Under these conditions, we obtained the desired product {Pd_3}Cl (**22**) as a red solid in high purity and yield (77%). Cluster **22** is slightly less stable compared to the bromo-derivative **20**: in fact, it is air stable, both in the solid state and in solution, only for a few days.

2.3.2.2 Reaction with isocyanides.

The reaction of **21** with the alkylisocyanide $CNBu^t$ leads to the substitution of all the terminal ligands affording the symmetrical cationic cluster $[Pd_3(\mu\text{-}PBu^t_2)_3(CNBu^t)_3]I$,

26(I) (Scheme 18). The reaction was performed by treating a toluene solution of **21** with a 3-fold excess of $CNBu^t$; after stirring the mixture for 1 hour, cluster **26**(I) precipitated out and was isolated as an orange solid in good yield (87%, Scheme 18). The final product is air stable both in solid state and in solution and it is soluble in polar organic solvents. Furthermore, the iodide anion, which complicates the cyclic voltammetric profile of the cation (see below), was exchanged by treating **26**(I) with a stoichiometric amount of $AgPF_6$. After filtering off AgI, which precipitated out during the reaction, the methathesis product **26**(PF_6) was obtained in quantitative yields. Moreover, **26**(CF_3SO_3) was obtained by adding a stoichiometric amount of $AgCF_3SO_3$ to a CH_2Cl_2 solution of **26**(I). After filtering off AgI, the final product, **26**(CF_3SO_3), was isolated as an orange microcrystalline solid in high yield (90%). The solid state structure of **26**(CF_3SO_3) was determined by diffractometric studies (see *infra*). Unfortunately, the stepwise substitution of the terminal ligands yielding $[Pd_3(\mu\text{-}PBu^t_2)_3(CO)_2(CNBu^t)]I$ or $[Pd_3(\mu\text{-}PBu^t_2)_3(CNBu^t)_2I]$, which was attempted by reacting **21** with an equimolar or a 2-fold excess of $CNBu^t$, was unsuccessful, and gave only minor amounts of the persubstituted cluster **26**(I), in mixture with the starting material **21**.

2.3.2.3 Spectroscopic characterization of trinuclear palladium derivatives 22-26(I).

Significant IR and NMR parameters for clusters **22**-**26**(I), together with those of the bromo- and iodo-derivatives, **20** and **21**, are shown in Table 11.

The IR (solid state) spectrum of the neutral chloro-derivative **22** shows one ν_{CO} absorption band at 2038 cm^{-1}, which is in the frequency range of the other halo-derivatives **20** and **21** (2030-2040 cm^{-1}). The CO stretching absorptions of cation $\mathbf{23}^+$ were found at 2094 and 2053 cm^{-1}, which, in comparison with the corresponding bands of the halo derivatives, are shifted as expected after the substitution of a σ–donor halide with a π-acceptor carbonyl ligand and the resulting charge increase. Also the ν_{CO} absorptions of the monocations $\mathbf{24}^+$ and $\mathbf{25}^+$ are shifted to higher frequencies (*ca.* 2045-2070 cm^{-1}) compared to the corresponding bands of the neutral compounds **20**-**22**, due to the increase of the total charge of the compounds. The IR (solid state) spectrum of cation $\mathbf{26}^+$ shows one absorption at 2156 cm^{-1} for the CN stretching of the terminal isocyanide ligands, which is higher than in the free $CNBu^t$ molecule (2136 cm^{-1});

similar frequencies were found in other trinuclear palladium clusters with terminal isocyanide ligands [ν_{CN} = 2175 and 2148 cm^{-1} in $[Pd_3(\mu\text{-}SO_2)_2(CNBu^t)_2(PBz_3)_3]$[124] and 2138 cm^{-1} in $[Pd_3(\mu\text{-}PBu^t_2)_2(CN\text{-}C_6H_4\text{-}p\text{-}Me)_5](CF_3SO_3)_2]$.[125] The $^{31}P\{^1H\}$ NMR (C_6D_6, 293K) spectrum of the chloro derivative **22**, similarly to those of the bromo and iodo-derivatives, shows a doublet at 277.4 ppm (P_2, $^2J_{P\text{-}P}$ = 115.4 Hz) well separated from a triplet at 204.8 ppm (P_1, $^2J_{P\text{-}P}$ = 115.4 Hz).

Table 11: Significant IR ν[cm^{-1}] (solid state) and NMR δ[ppm] parameters for **20**-**26**(I).

	Cluster	X	Y	*n*	ν [a]	$\delta_{P1}(J_{P1P2}/Hz)$	$\delta_{P2}(J_{P1P2}/Hz)$
	20	Br	CO	0	2040	206.4 t (115.8)	282.7 d (115.8)
	21	I	CO	0	2034	213.4 t (116.4)	292.5 d (116.4)
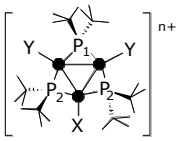	**22**	Cl	CO	0	2038	204.8 t (115.4)	277.4 d (115.4)
	23(PF_6)	CO	CO	1	2094, 2053	295.6 s	
	24(PF_6)	CH_3CN	CO	1	2058, 2044	245.4 t (128.0)	275.8 d (128.0)
	25(PF_6)	Py	CO	1	2066	250.8 t (121.3)	258.9 d (121.3)
	26(I)	CN^tBu	CN^tBu	1	2156	257.2 s	

[a] ν(CO) in **20**-**22**, **23**(PF_6), **24**(PF_6) and **25**(PF_6); ν(CN) in **26**(I).

Similar spectra were observed for the cationic derivatives **24**(PF_6) and **25**(PF_6), with a small high-field shift of the doublet (δ_{P2} = 275.8 and 258.9 ppm) and a low-field shift of the triplet (δ_{P1} = 245.4 and 250.8 ppm, $^2J_{P\text{-}P}$ *ca.* 120-130 Hz). The symmetrical cationic clusters **23**(PF_6) and **26**(I) show only a singlet in the low-field region (δ_P = 295.6 and 257.2 ppm, respectively) due to the three equivalent phosphorus nuclei. The spectra of **26**(PF_6) and **26**(CF_3SO_3), obtained from **26**(I) by exchanging the counterion, show one singlet at the same chemical shift of their precursor **26**(I). In addition, the spectrum of **26**(PF_6) shows an heptet at −142.5 ppm ($^1J_{P\text{-}F}$ = 709.9 Hz, 1 P) due to the PF_6^- anion. A similar signal, at *ca* −140 ppm ($^1J_{PF}$ = *ca* 700 Hz), is also present in the spectra of all the ionic compounds containing PF_6^- as counterion.

The ^{1}H-NMR spectra of all clusters show signals in good agreement with the structures proposed in Table 11; the chloro-derivative and the asymmetrical cationic clusters give a doublet at 1.12–1.41 ppm ($^{3}J_{H\text{-}P}$ *ca.* 15 Hz, 18 H) for the protons of the *t*-butyl substituents of P_1 and a virtual triplet (see Appendix A) at 1.29 –1.50 ppm ($^{3}J_{H\text{-}P} + {}^{5}J_{H\text{-}P}$ *ca.* 7 Hz, 36 H) for the equivalent *t*-butyls of the P_2 nuclei. The symmetrical cationic complexes show only a virtual triplet at 1.32–1.42 ppm ($^{3}J_{H\text{-}P} + {}^{5}J_{H\text{-}P}$ *ca.* 7 Hz, 54 H) due to the *t*-butyl groups bonded to the three equivalent P nuclei. The spectra of **24**(PF_6), **25**(PF_6) and **26**(I) show additional signals due to the protons of the terminal ligands, respectively one singlet at 2.90 ppm (NCCH_3), three multiplet at 7.63, 7.87 and 8.21 ppm (NC_5H_5) and one singlet at 1.72 ppm [CNC(CH_3)].

The ^{13}C{^{1}H} NMR spectra show signals with the expected frequencies and intensities (see the Experimental part for more details).

2.3.2.4 Crystal and molecular structure of [Pd$_3$(μ-PBu$^t_2$)$_3$(CNBu^t)$_3$](CF$_3$SO$_3$), 26(CF$_3$SO$_3$).

Single crystals of **26**(CF_3SO_3) suitable for a crystallographic study were obtained by stratifying *n*-hexane on a CH_2Cl_2 solution of the cluster. The molecular structure is shown in Figure 51 and its more significant geometrical parameters summarized Table 10.

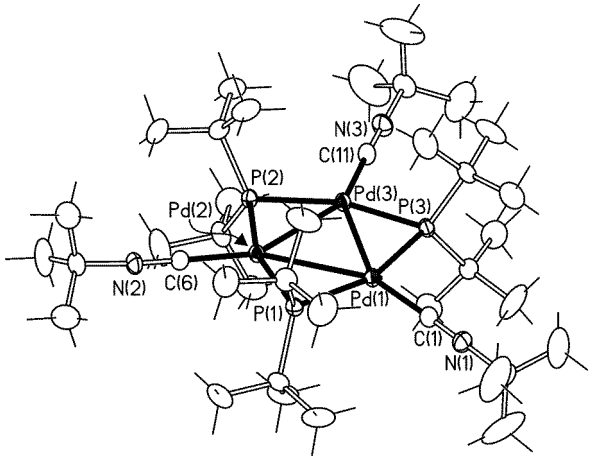

Figure 52: ORTEP view of the molecular structure of $[Pd_3(\mu\text{-}PBu^t_2)_3(CNBu^t)_3]^+$ (**26**$^+$). Thermal ellipsoids are at 20% probability.

Table 12: Significant Bond lenghts [Å] and angles [°] in $\mathbf{26}^{+}$.

Pd(1)–Pd(2)	2.9525(6)	Pd(2)–P(2)	2.2933(14)
Pd(1)–Pd(3)	3.0055(6)	Pd(3)–P(2)	2.2965(14)
Pd(2)–Pd(3)	2.9686(6)	Pd(3)–P(3)	2.2954(15)
Pd(1)–P(1)	2.2947(15)	Pd(1)–C(1)	1.947(6)
Pd(1)–P(3)	2.2949(16)	Pd(2)–C(6)	1.936(6)
Pd(2)–P(1)	2.2990(15)	Pd(3)–C(11)	1.948(7)
Pd(1)–Pd(2)–Pd(3)	61.005(14)	P(3)–Pd(3)–Pd(1)	49.09(4)
Pd(2)–Pd(1)–Pd(3)	59.763(14)	P(3)–Pd(1)–Pd(3)	49.11(4)
Pd(2)–Pd(3)–Pd(1)	59.232(14)	Pd(3)–P(3)–Pd(1)	81.80(5)
P(1)–Pd(2)–Pd(1)	49.94(4)	C(1)–Pd(1)–P(3)	99.54(19)
P(1)–Pd(1)–Pd(2)	50.07(4)	C(1)–Pd(1)–P(1)	101.72(19)
Pd(1)–P(1)–Pd(2)	79.99(5)	C(6)–Pd(2)–P(1)	100.35(18)
P(2)–Pd(2)–Pd(3)	49.75(4)	C(6)–Pd(2)–P(2)	99.08(18)
P(2)–Pd(3)–Pd(2)	49.65(4)	C(11)–Pd(3)–P(2)	102.48(18)
Pd(2)–P(2)–Pd(3)	80.60(5)	C(11)–Pd(3)–P(3)	99.63(18)
N(1)-C(1)-Pd(1)	176.4(7)	C(1)-N(1)-C(2)	176.8(8)
N(2)-C(6)-Pd(2)	179.0(7)	C(6)-N(2)-C(7)	175.7(8)
N(3)-C(11)-Pd(3)	177.7(6)	C(11)-N(3)-C(12)	175.3(8)

Differently to $\{Pd_3\}Br$ (**20**), the cation $[Pd_3(\mu\text{-}PBu^t_2)_3(CNBu^t)_3]^+$ ($\mathbf{26}^{+}$) belongs entirely to the asymmetric unit and do not show any symmetry operation rigorously valid. Locally, however, it approaches to the 3*m* symmetry, C_{3v} in the Schönflies notation, which is not completely satisfied due to slight rotations of the *t*-butyl groups of the isocyanide ligands. The molecule exhibits a scalene Pd_3 triangle core with two shorter and slightly different Pd(1)–Pd(2) and Pd(2)–Pd(3) bonds [respectively 2.9525(6) and

2.9686(6) Å] and one long Pd(1)-Pd(3) [3.0055(6) Å] distances. These distances are almost the same of those of compound **20**. The Pd–P distances, between 2.293 and 2.299 Å, are similar to those found in $\{Pd_3\}Br$ (**20**). The three isocyanide ligands are terminally coordinated (N–Pd–C angles of *ca.* 177°), in an approximately linear fashion (C–N–C angles of *ca.* 176°). The Pd–C [Pd(1)–C(1) = 1.947(6) Å, Pd(2)–C(6) = 1.936(6) Å and Pd(3)–C(11) = 1.948(7) Å] distances from the isocyanide carbons are longer than those from the carbonyl carbons found in **20** [Pd–C = 1.874(10) Å] but are similar to Pd–C distances found in other trinuclear palladium clusters with terminal isocyanide ligands (*i.e.* Pd–C *ca.* 2.0 Å in $[Pd_3(\mu\text{-}SO_2)_2(CNBu^t)_2(PBz_3)_3]$[124] and Pd–C 1.94-2.06 Å in $[Pd_3(\mu\text{-}PBu^t_2)_2(CN\text{–}C_6H_4\text{-}p\text{-}Me)_5](CF_3SO_3)_2$[125]).

2.3.3 Cyclo-voltammetric measurements on 20-26(PF_6).

In order to start the study of the redox behavior of the trinuclear palladium clusters, the electrochemical properties of compounds **20-26**(PF_6) were studied by cyclic voltammetry in CH_2Cl_2 solutions containing NBu_4PF_6 (0.2 M) as the supporting electrolyte.

Two sequential monoelectronic oxidations, typifying the redox fingerprint of the analogous 44e$^-$ $[\{Pt_3\}L_{3-n}X_n]^{(1-n)+}$ clusters,[49] were observed also in the cyclic voltammograms of the palladium clusters described here. The former is reversible in the CV time scale, while the second oxidation is complicated by a subsequent chemical reaction in all but one case (cation **26**$^+$, see below). In the cathodic region, only one irreversible reduction is observed for several compounds. The formal electrode potentials for the observed electron transfers are summarized in Table 13, and the CV profiles of **21**, **23**$^+$ and **26**$^+$ are shown in Figure 53.

The neutral monohalide clusters **20-22** are oxidized at *ca* 0.40 and 0.85 V, only the first oxidation being reversible on the CV time scale (i_{pc}/i_{pa} = 1 at 0.2 V s^{-1}) while the second one is complicated by a subsequent chemical reaction, which appears faster in the order **22** ≅ **20** > **21**.

Table 13. Formal electrode potentials (V *vs* SCE) and peak-to-peak separations (mV) for the redox processes exhibited in CH_2Cl_2 solution by $[\{Pd_3\}L_{3-n}X_n]^{(1-n)+}$ and, for comparison, by the corresponding platinum clusters $[\{Pt_3\}L_{3-n}X_n]^{(1-n)+}$ (values in round brackets from reference 49).

Compounds	Oxidation processes			Reduction processes	
	$E°'$	ΔEp^a	$E°'$	ΔEp^a	$E°'$
22	0.83[b] (0.91)	90 (70)	0.41 (0.31)	76 (60)	−1.84[c,a] (−1.91)[c]
20	0.90[c,a] (0.88)	(70)	0.41 (0.29)	80 (60)	(−1.91)[c]
21	0.85 (0.86)	74 (70)	0.38 (0.28)	70 (70)	−1.73[c,a] (−1.91)[c]
23(PF_6)	1.75[c,a] (1.56[c])	/	1.14 (1.13)	64 (90)	−1.27[c,a] (−1.29)[c]
26(PF_6)	1.14 (0.82)[d]	65 (65)[d]	0.35 (0.26)[d]	65 (65)[d]	/
24(PF_6)	1.50[c,a]	/	0.79	70	−1.35[c,a]
25(PF_6)	1.54[c,a]	/	0.80	80	−1.36[c,a]

[a] Measured at 0.1 V s^{-1}. [b] Coupled to relatively fast chemical reactions. [c] Peak potential value for irreversible processes. [d] Unpublished results for $[Pt_3(\mu\text{-}PBu^t_2)_3(CNBu^t)_3]PF_6$.

The two oxidations occur at higher potentials (+1.14 and +1.75 V) for the cationic tricarbonyl derivative (**23**)PF_6, as expected for the presence of the positive charge and for the substitution of a σ-donor halide with a π-acid carbonyl ligand.

The substitution of one of the CO ligands in $\mathbf{23}^+$ with a good σ-donor as acetonitrile or pyridine makes easier the removal of either the first (0.79 for $\mathbf{24}^+$ and 0.80 V for $\mathbf{25}^+$) and the second electron (1.50 for $\mathbf{24}^+$ and 1.54 V for $\mathbf{25}^+$). Again, for either $\mathbf{23}^+$, $\mathbf{24}^+$ and $\mathbf{25}^+$, the first oxidation is reversible on the CV time scale (i_{pc}/i_{pa} = 1 at 0.2 V s^{-1}) and the second oxidation is followed by fast chemical reactions. Moreover, cations $\mathbf{24}^+$ and $\mathbf{25}^+$ slowly decompose in CH_2Cl_2 solution and, on standing, redox processes attributable to decomposition products become evident in the CV profile.

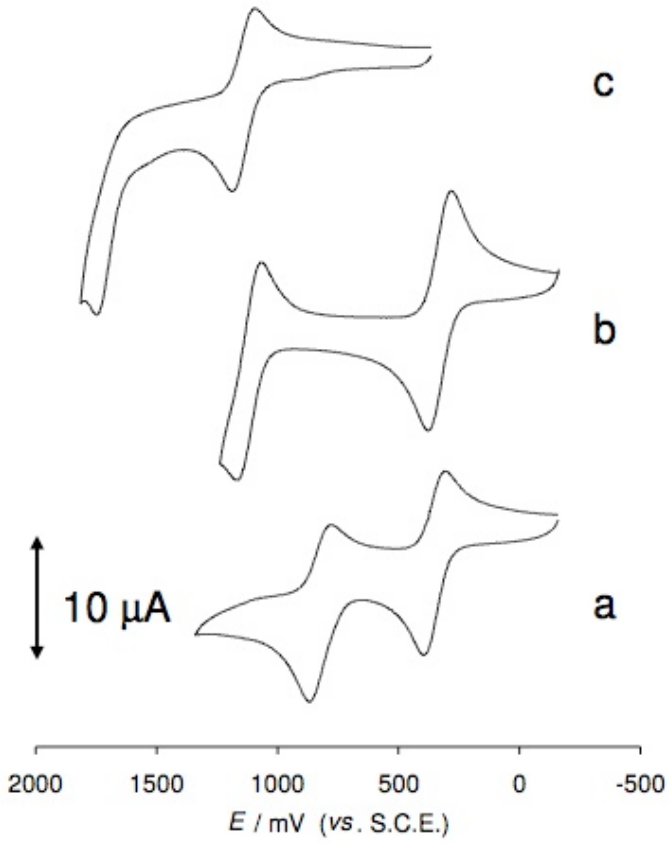

Figure 53. Cyclic voltammograms recorded at a platinum electrode in CH_2Cl_2 solutions of (a) **21**, (b) **26**$^+$, (c) **23**$^+$; using NBu_4PF_6 (0.2 M) as supporting electrolyte. Scan rates: 0.2 V s^{-1}.

Finally the cationic cluster **26**(PF_6), with three good σ-donor and relatively poor π-acid isocyanide ligands, as well as its oxidation products, distinguish themselves for their remarkable stability. In spite of the positive charge, compared to all the clusters analyzed in this study, the removal of the first electron occurs at the lowest potential (+0.35 V). The potential of the second oxidation (+1.14 V) is lower than those of the other cations but is higher in comparison to those of the neutral derivatives **20-22**. Both oxidation processes (among which **26**$^+$ exhibits the largest gap, 0.79 V) possess features of chemical reversibility in the CV time scale. [†]

[†] **26**(I) behaves as **26**(PF_6) showing two reversibile oxidations, but the first process is superimposed to the wave due to the oxidation of I^-.

2.3.4 IR and UV-Vis spectroelectrochemical analysis on 22, 23(PF_6) and 26(PF_6).

Further investigations on the redox behavior of the trinuclear palladium clusters prepared during this Thesis, were made on the neutral $\{Pd_3\}I$, (**21**) and on the monocationic derivatives $[\{Pd_3\}CO]PF_6$, **23**(PF_6) and $[Pd_3(\mu\text{-}PBu^t_2)_3(CNBu^t)_3]PF_6$, **26**($PF_6$), which are the most stable among all the trinuclear derivatives of palladium prepared up to now.

The IR and UV-Vis spectroelectrochemical experiments were executed on CH_2Cl_2 solutions of **21**, **23**(PF_6) and **26**(PF_6), using NBu_4PF_6 (0.2 M) as the supporting electrolyte. As fully explained below, all their mono-oxidized products $\mathbf{21}^+$, $\mathbf{23}^{2+}$ and $\mathbf{26}^{2+}$, as well as the di-oxidized product of the isocyanide derivative, $\mathbf{26}^{3+}$, were characterized; the obtained data are summarized in Table 14.

Table 14: IR and UV-Vis data of **21**, $\mathbf{23}^+$ and $\mathbf{26}^+$ and theirs oxidation products.

	21	$\mathbf{21}^+$	$\mathbf{23}^+$	$\mathbf{23}^{2+}$	$\mathbf{26}^+$	$\mathbf{26}^{2+}$	$\mathbf{26}^{3+}$
ν/cm^{-1}	2049[a]	2089[a,c]	2079[a]	2115[a]	2164[b]	2188[b]	2212[b]
λ_{max}/nm	464	555[c], 592[c], 643[c]	441	521, 555, 710	421	524, 690	/

[a] ν_{CO}, [b] ν_{CN}, [c] disappear after the end of the electrolysis.

2.3.4.1 IR and UV-Vis spectroelectrochemical experiments on 21.

Even though the first monoelectronic oxidation of **21** is reversible in the CV time scale, the lability of the electrogenerated species $\mathbf{21}^+$ becomes evident in the longer times of the macroelectrolysis experiments (E_w = +0.5 V). The UV-Vis and IR spectroelectrochemical changes following the oxidation of **21** in correspondence of the first oxidation process show the presence of well-defined isosbestic points for the time required for the quasi complete oxidation of **21**, suggesting the initial formation of a metastable cation $\mathbf{21}^+$ that is then consumed by a subsequent reaction. As illustrated in Figure 54a, upon oxidation the CO stretching absorption exhibited by **21** at 2049 cm^{-1} vanishes rapidly while a new absorption, assigned to $\mathbf{21}^+$**,** grows at 2089 cm^{-1}; this is

then slowly replaced (Figure 54b) by a band at 2079 cm^{-1}, that can be assigned to the tricarbonyl cation **23**$^+$, and by an elusive band at 2097 cm^{-1}, that we tentatively assign (Scheme 20) to a 42 e^- cluster $[Pd_3(\mu\text{-}PBu^t_2)_3(CO)I_2]^+$, **27**$^+$. The latter may be formed, together with **23**$^+$, from a disproportionation reaction of the metastable oxidized species **21**$^+$ accompanied by a CO/I^- ligand exchange. As highlighted in Scheme 20, a linear upshift in the ν_{CO} of 9 cm^{-1} *per* removed electron is observed for the clusters **23**$^+$, **21**$^+$, **27**$^+$ when the substitution of a neutral CO ligand with I^- leaves unchanged the total charge of these compounds in spite of the oxidation. Unfortunately, the characterization of **27**$^+$ was prevented by its fast decomposition (Figure 54c), which proceeds by forming a further amount of **23**$^+$, the only carbonyl species detectable in solution after long times, and other unidentified non-carbonyl derivatives (the $^{31}P\{^1H\}$ NMR spectra of the final solution contain an intense singlet at 295.6 ppm, due to **23**$^+$, and several weak and unassigned singlets in the region between 0 and 200 ppm).

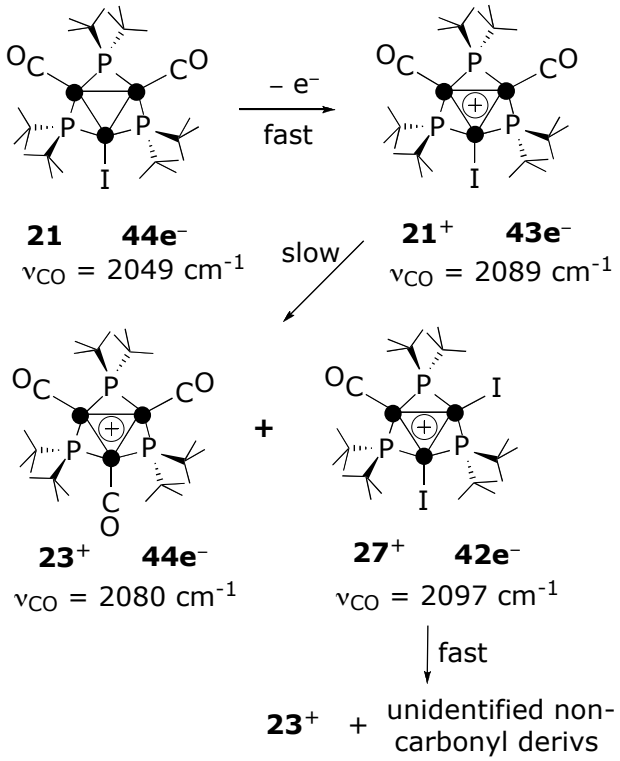

Scheme 20: Plausible decomposition mechanism of **21**$^+$.

The UV-vis spectroelectrochemistry (Figure 55) agrees with this picture: the broad absorption at 464 nm observed in the original sample of **21** decreases during electrolysis

at +0.5 V, while three new bands at 555, 592 and 643 nm, assigned to $\mathbf{21}^{+}$, keep growing; their intensity increases until cluster **21** has nearly disappeared at the end of current flow in the cell. The absorbance changes observed after this step confirm the decay of $\mathbf{21}^{+}$: the three absorptions at 555, 592 and 643 nm are replaced by two bands at 441 and 635 nm, the former of which is consistent with the formation of cluster $\mathbf{23}^{+}$ while the second may be assigned to unidentified decomposition compounds.

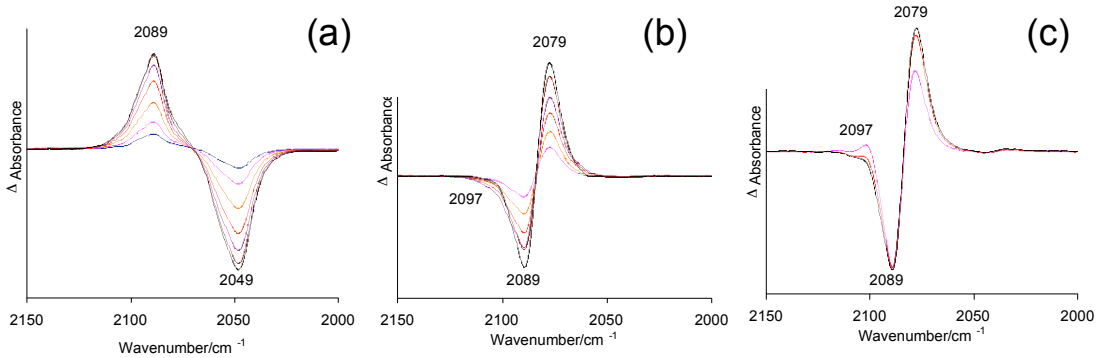

Figure 54. : IR spectral changes recorded in an OTTLE cell (a) during and (b), (c) after the progressive one electron oxidation of **21** in CH_2Cl_2 (NBu_4PF_6 (0.2 M) as the supporting electrolyte). A reference spectrum, collected before the application of an oxidation potential, is used to calculate the differential absorbance spectra of (a). The final spectrum of (a) is used to calculate the differential absorbance spectra of (b) and (c).

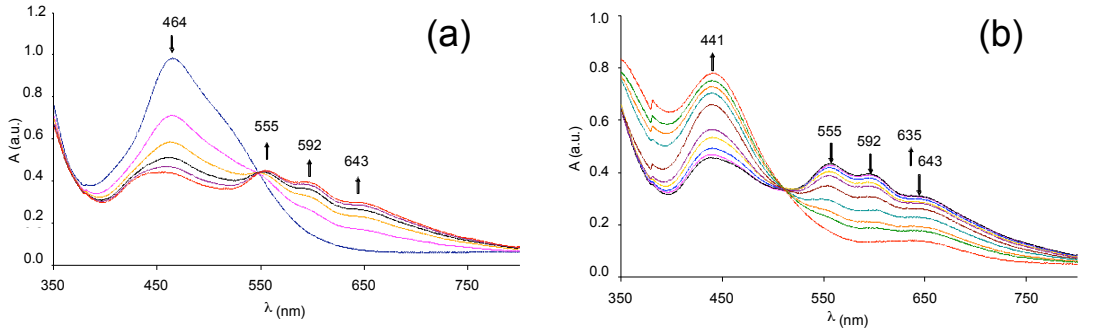

Figure 55. UV-vis spectra of **21** in CH_2Cl_2 solution containing NBu_4PF_6 (0.2 M) as the supporting electrolyte recorded in an OTTLE cell (a) during and (b) after the stepwise one-electron oxidation.

2.3.4.2 IR and UV-Vis spectroelectrochemical experiments on 23(PF_6).

IR and UV-vis *in situ* spectroelectrochemical experiments on CH_2Cl_2 solutions of $\mathbf{23}^{+}$ allowed the characterization of the product of its monoelectronic oxidation $\mathbf{23}^{2+}$. Upon

oxidation, the CO stretching vibration of $\mathbf{23}^{+}$ at 2079 cm^{-1} is gradually replaced by a new absorption at 2115 cm^{-1} (Figure 56). On the timescale of the IR experiment, however, the oxidation is followed by a partial decomposition that did not allow the complete recovery of the starting compound in the backward reduction of $\mathbf{23}^{2+}$.

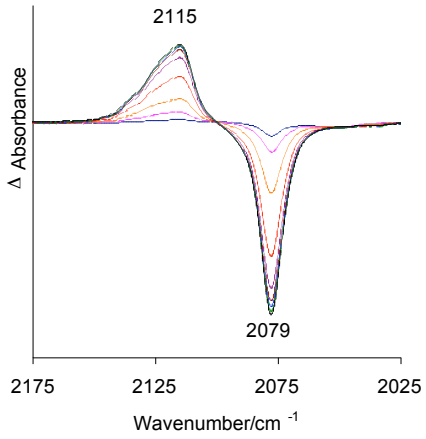

Figure 56. IR spectral changes recorded in an OTTLE cell during the progressive one-electron oxidation of $\mathbf{23}^{+}$ in CH_2Cl_2 solution, in the presence of NBu_4PF_6 (0.2 M) as the supporting electrolyte. A reference spectrum, collected before the application of an oxidation potential is used to calculate the differential absorbance spectra.

In the UV-Vis experiments, the removal of one electron by $\mathbf{23}^{+}$ produces a pattern of absorption bands in the visible region of the electronic spectrum (Figure 57). The 441 nm band of the starting cluster is substituted, during the course of the spectroelectrochemical oxidation, by three new absorptions at 521, 555 and 710 nm.

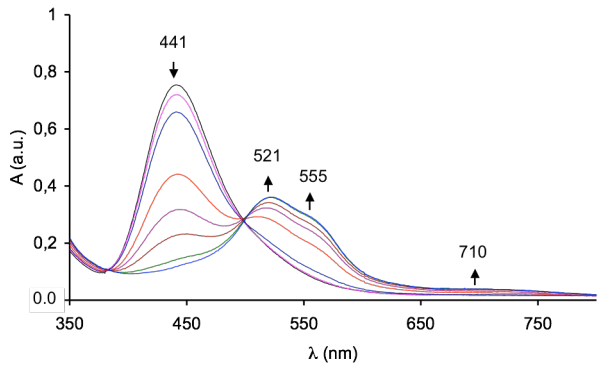

Figure 57. UV-vis spectra of $\mathbf{23}^{+}$ in CH_2Cl_2 solution containing NBu_4PF_6 (0.2 M) as the supporting electrolyte recorded in an OTTLE cell during the stepwise one electron oxidation.

2.3.4.3 IR and UV-Vis experiments on 26(PF$_6$).

The IR spectroelectrochemical changes following the stepwise two-electron oxidation of cation **26**$^+$, shown in Figure 58, put in evidence the appearance of well-defined and withstanding isosbestic points confirming a remarkable stability of the oxidized clusters **26**$^{2+}$ and **26**$^{3+}$. The ν_{CN} absorptions exhibit a linear upshift of 24 cm^{-1} *per* removed electron: the original absorption found at 2164 cm^{-1} in **26**$^+$ moves to 2188 cm^{-1} upon one electron oxidation (the same ν_{CN} absorption was found after chemical oxidation of **26**(I) with $AgPF_6$, see paragraph 2.3.5), and to 2212 cm^{-1} after removal of the second electron. Quantitative restoration of the IR band of the starting **26**$^+$ was observed in the reverse potential cycle, which indicates the stability of all the oxidized species.

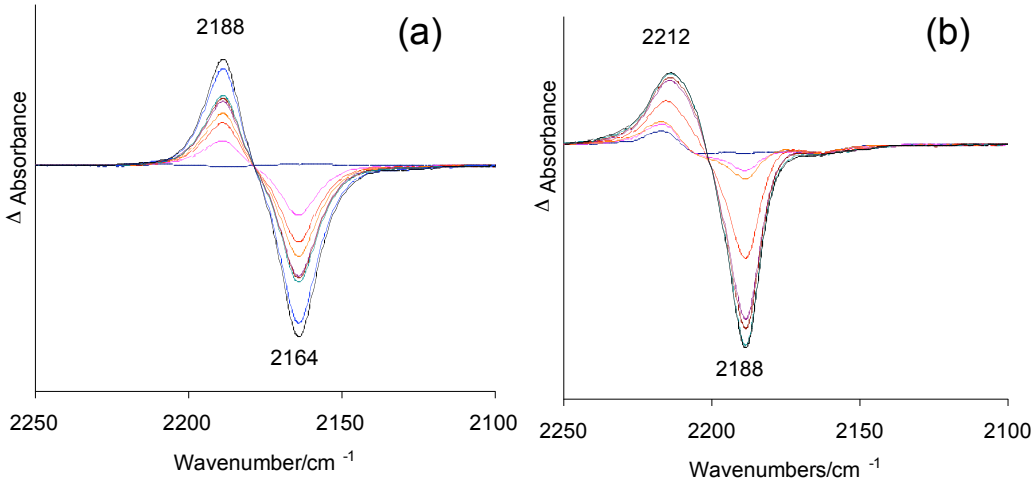

Figure 58. IR spectral changes recorded in an OTTLE cell during the first (a) and the second (b) monoelectronic oxidation of **26**$^+$ in CH_2Cl_2 solution; NBu_4PF_6 (0.2 M) as the supporting electrolyte. A reference spectrum, collected before the application of an oxidation potential, was used to calculate the differential absorbance spectra of (a). The final spectrum of (a) was used to calculate the differential absorbance spectra of (b).

The step-wise oxidation of **26**$^+$ in a UV-Vis spectroelectrochemical experiment is shown in Figure 59. In the UV-Vis spectroelectrochemical experiments time scale, only the removal of the first electron gives rise to evident spectral changes: the disappearance of the 421 nm band due to **26**$^+$ is accompanied by the growth of an absorption at 524 nm together with a weak band at 690 nm.

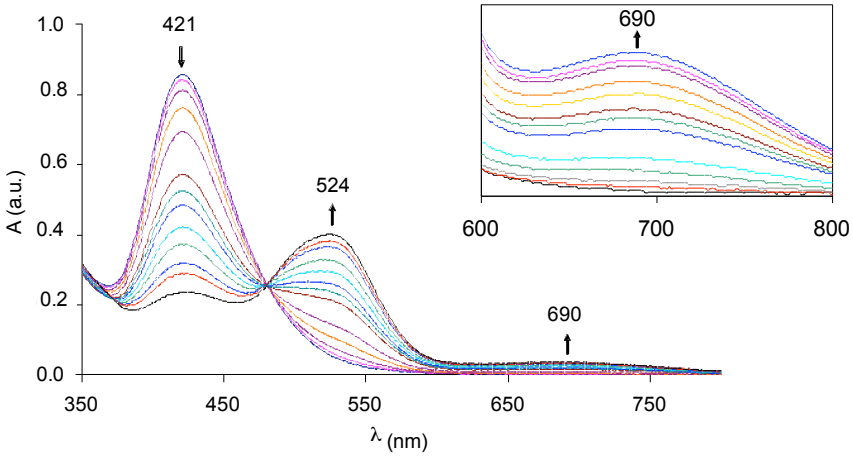

Figure 59. UV-Vis spectra of $\mathbf{26}^{+}$ in CH_2Cl_2 solution, containing NBu_4PF_6 (0.2 M) as the supporting electrolyte, recorded in an OTTLE cell during the stepwise one-electron oxidation.

2.3.5 Chemical oxidation of $[Pd_3(\mu\text{-}PBu^t_2)_3(CNBu^t)_3]I$, 26(I).

The redox couple Ag^{+}/Ag^{0} has a reduction potential of +1.11 V *vs.* SCE[126] in CH_2Cl_2 solution and it is able to oxidize cation $\mathbf{26}^{+}$ ($E°'$ = 0.35 V *vs.* SCE) by one electron. As described above, the addition of a stoichiometric amount of $AgPF_6$ to a dry CH_2Cl_2 solution of **26**(I) leads the methathesis product **26**(PF_6), without involving redox reactions. On the contrary, by adding 2-fold excess of $AgPF_6$ to a dry CH_2Cl_2 solution of **26**(I), we noticed that, in addition to the formation of an insoluble white salt (AgI) due to the counterion exchange, the initial orange solution turned to dark pink and a dark solid (Ag^{o}) precipitated out. After filtering off the insoluble solids, the solvent was evaporated and a dark pink solid, the mono-oxidized dicationic product **26**$(PF_6)_2$, was isolated in nearly quantitative yield. The starting cluster **26**(I) has $44e^{-}$, thus the removal of one electron leads to a paramagnetic $43e^{-}$ cluster. This compound is soluble in polar and chlorinated organic solvents; it is air unstable both in the solid state (it decomposes in few hours) and in solution. Under inert atmosphere, it is stable in the solid state but it decomposes to unidentified products after a few days if in solution. The IR spectra on the solid state and on a CH_2Cl_2 solution of **26**$(PF_6)_2$ were recorded; both show one absorption band, due to the CN stretching, shifted to higher frequencies compared to the monocationic **26**(I), as a consequence of the increase of the total charge of the molecule

(ν_{CN} respectively at 2193 and 2188 cm^{-1}). Identical data where found for the dicationic **26**$^{2+}$ obtained after electrolysis during the IR spectroelectrochemical experiments. Due to its paramagnetism, the $^{31}P\{^{1}H\}$ NMR (acetone-d_6, 293K) spectrum do not show signals, and the ^{1}H NMR (acetone-d_6, 293K) spectrum contains only a very broad signal, due to the *t*-butyl protons at 16.00 ppm, shifted to a lower-field region in comparison to its precursor.

2.3.6 Conclusions and future works.

In conclusion, during my Thesis, new tris-phosphido bridged palladium clusters of general formula $Pd_3(\mu\text{-}PBu^t_2)_3(CO)_2X$ [X = Cl, Br, I] and $[Pd_3(\mu\text{-}PBu^t_2)_3(L)_2L']^+$ (L = CO, L' = CO, MeCN, Py; L = L' = $CNBu^t$) were prepared and fully characterized. The results obtained up to now are promising for our purposes; in fact, the synthesized derivatives have a stable inner Pd_3P_3 core and three the reactive positions, mutually directed at 120°. These features may allow to use these clusters as synthons for macromolecular compounds with expected final structures, in which the different units may be connected by appropriate bifunctional spacers, such as N-, S- or alkynyl ligands. Before planning the synthesis of compounds containing more than one cluster units, further investigations about the reactivity and the stability of the trinuclear palladium clusters will be necessary. Currently, we are attempting the preparation of sulfide and alkynyl derivatives. For example, we reacted the halide derivatives **20**-**22** with a stoichiometric amount or with an excess of a thiol (1-butanethiol, thiophenol) in diethylamine (Scheme 21); the latter was employed because it is able to deprotonate the thiol and capture halide, forming the NH_2Et_2X ammonium salt. The synthesis of an alkynyl derivative we attempted by reacting between terminal alkynes **21** or **22**, under Sonogashira-type conditions (Scheme 21). Until now, the desired products have been obtained only in very low yields, and the improvement of the synthetic protocols is under investigation.

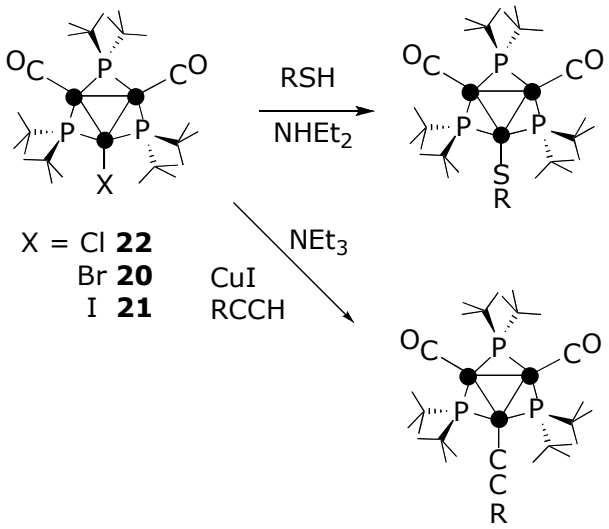

Scheme 21. Plausible synthetic methods of sulfide and alkynyl derivatives of the $\{Pd_3\}$ unit.

Furthermore, the electrochemical and spectroelectrochemical studies have shown an interesting redox behavior of the trinuclear derivatives and in particular of the monocationic isocyanide derivative, $\mathbf{26}^+$, which undergoes two reversible oxidation processes (among which the first occurs at low potential value) and whose oxidation products are remarkably stable. Thus, it will be interesting to prepare "polycluster" assemblies in which the $Pd_3(\mu\text{-}PBu^t_2)_3$ units are linked by bis-isocyanide ligands and to study their redox behavior.

3 Conclusion.

The studies carried out in this Thesis are part of a research project addressed to apply the knowledge of the fundamental reactivity of molecular clusters to their utilization as synthons for organometallic and macromolecular synthesis, an issue up to now poorly developed but with considerable potential in the chemistry of new materials. In this framework, we have recently shown that the tri- and hexanuclear clusters $[Pt_3(\mu\text{-}PBu^t_2)_3(CO)_3](CF_3SO_3)$, **2**$(CF_3SO_3)$, and $[Pt_6(\mu\text{-}PBu^t_2)_4(CO)_6](CF_3SO_3)_2$, **3**$(CF_3SO_3)_2$, can be functionalized with a great variety of ligands which occupy three coplanar positions, mutually directed at 120°, in functional derivatives of **2**(CF_3SO_3), or two colinear positions, mutually directed at 180°, in functional derivatives of **3**$(CF_3SO_3)_2$. The functionalization leaves unchanged the central core of the starting cluster due to the presence of sterically encumbering di-*t*-butylphosphides, which grants a high thermal stability and a chemical inertness of the internal core (Figure 60).

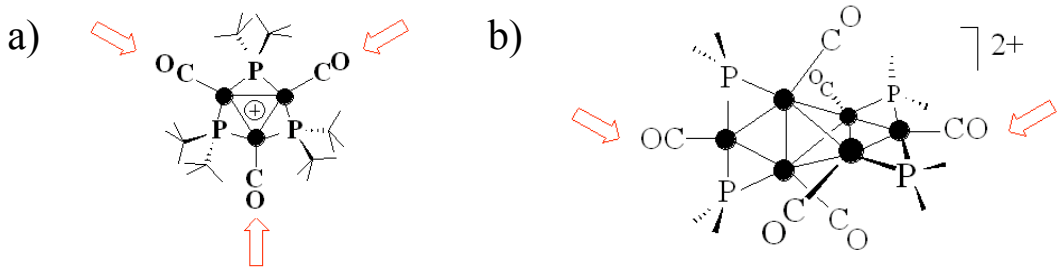

Figure 60. Reactive positions in a) $[Pt_3(\mu\text{-}PBu^t_2)_3(CO)_3](CF_3SO_3)$, **2**$(CF_3SO_3)$ and b) $[Pt_6(\mu\text{-}PBu^t_2)_4(CO)_6](CF_3SO_3)_2$, **3**$(CF_3SO_3)_2$; counterions are omitted for clarity.

Thanks to these remarkable features and starting from the knowledge acquired during the last years about the general reactivity of the precursors, well-tested synthetic protocols had been settled affording linear or branched oligomers containing $\{Pt_3\}$ units as stoppers or up to 16 $\{Pt_6\}$ units embedded in the main chain and connected by bis-alkynyl spacers –CC–Ar–CC–, in which the Ar group may be selected in a broad library of aromatic fragments (phenyls, biphenyls, anthranyls, thienyls or polythienyls, ferrocenyls or diferrocenyls).

The targets we set for this work were to find new synthetic procedures for similar oligomers and models by changing the structure of either the spacer or the cluster units.

Moreover, since we were particularly interested in the construction of structures with conductive features, we were interested in achieving information on the electron delocalization within the new structures. Along these lines we have prepared and fully characterized dicationic model compounds containing two hexanuclear units $[\{Pt_6\}(H)]_2(\mu\text{-}Y)(CF_3SO_3)_2$ [**9**$(CF_3SO_3)_2$, Y = 4,4′-bipyridine; **10**$(CF_3SO_3)_2$, Y = 1,4-dicyanobenzene]. Preliminary cyclovoltammetric analysis on these compounds evidenced the presence of an higher number of reduction processes than in the reference compounds containing a "single" hexanuclear cluster. Although this may suggest a possible electronic communication, an unambiguous interpretation of the results is made difficult by the presence of the redox active organic spacers; the IR spectroelectrochemical analysis of **9**$(CF_3SO_3)_2$ and **10**$(CF_3SO_3)_2$ allowed the characterization of their reduction products but not a clear evaluation about the presence of electronic communication between the two clusters.

The reaction of [60]fullerene with *N*-octylglycine and the alkynyl derivative $[\{Pt_3\}CCC_6H_4CHO]$ (**13**) or $[\{Pt_6\}(CCC_6H_4CHO)_2]$ (**17**) afforded, respectively, the neutral compounds $[\{Pt_3\}CCC_6H_4C_2H_3N(C_8H_{17})C_{60}]$ (**16**) or $[\{Pt_6\}(CCC_6H_4C_2H_3N(C_8H_{17})C_{60})_2]$ (**18**), in which the cluster units are coordinated to one or two C_{60} molecules. Preliminary cyclovoltammetric and spectroelectrochemical (IR, UV-Vis and NIR) analyses on **16**, much easier to handle than **18**, and on its precursor **13**, show that in **16** an electron transfer is probably absent; in fact, for example, its CV profile is similar to the one of its precursor **13** and the CO stretching absorptions remain unchanged during its stepwise reduction, which involves only the fullerene unit.

Finally, we prepared and fully characterized the 44 e^- tris-phosphido bridged palladium triangular clusters, $Pd_3(\mu\text{-}PBu^t_2)_3(CO)_2X$ [(**20**), X = Br; (**21**), X = I] by reacting the dinuclear complex $[Pd(PBu^t_2H)(\mu\text{-}PBu^t_2)]_2$, (**19**) with NBu_4X (X = Br, I) under 1 atmosphere of CO. Furthermore, starting from the iodo-derivative **21**, which is more stable than **20**, we prepared the monocationic derivatives, $[Pd_3(\mu\text{-}PBu^t_2)_3(L)_2L']^+$ [L = CO, L' = CO (**23**$^+$), MeCN (**24**$^+$), Py (**25**$^+$); L = L' = $CNBu^t$ (**26**$^+$)], arising from the substitution of only the iodide ligand or of all the three terminal ligands; $[Pd_3(\mu\text{-}PBu^t_2)_3(CO)_2Cl]$, (**22**) was prepared by reacting cation **23**$^+$ with PPNCl. The strict

similarity of these derivatives to the trinuclear platinum clusters described previously, suggest that they also will be useful as synthons for ordered macromolecular structures.

Electrochemical studies performed on the palladium derivatives have shown that all these compounds undergo two oxidation processes and in some case also a reduction process. Moreover, the oxidation products of **21**, $\mathbf{23}^{+}$ and $\mathbf{26}^{+}$ were characterized by spectroelectrochemical (IR, UV-Vis) analysis and the mono-oxidized product $[Pd_3(\mu\text{-}PBu^t_2)_3(CNBu^t)_3]^{2+}$, ($\mathbf{26}^{2+}$), was also obtained by chemical oxidation of $\mathbf{26}^{+}$ with a stoichiometric amount of an Ag^{+} salt.

The work performed up to now may be the starting point for new studies; from the synthetic point of view, we demonstrated that it is possible to prepare systems containing two hexanuclear platinum clusters or containing the tri- and hexanuclear clusters and, respectively, one or two fullerene units, connected by organic spacers, and that these compounds are stable during electrochemical and spectroelectrochemical analysis. It will be interesting to enhance the knowledge of the properties of these systems with further electrochemical analysis and with theoretical studies, focalized on the study of the symmetry and energy of the molecular orbitals in both the ground and excited states, which is fundamental for the evaluation of intramolecular charge delocalization.

4 Experimental part

4.1 General remarks.

All operations were carried out using standard Schlenk-tube technique, under an atmosphere of prepurified nitrogen. The reaction vessels were oven dried at 150 °C prior to use.

4.2 Solvents and reagents.

Commercial grade solvents were purified by employing conventional procedures,[127] distilled as explained below and stored over activated molecular sieves under nitrogen atmosphere prior to their use.

- Acetonitrile (Carlo Erba, RPE) and pyridine (J. T. Baker) were dried by refluxing for 12 hours over CaH_2 and then distilled.
- Acetone (Carlo Erba, RPE) was dried by refluxing for 12 hours over Na_2CO_3 and then distilled.
- Dichloromethane (Carlo Erba, RPE) was dried by refluxing for 12 hours over P_2O_5 and then distilled.
- Diethyl Ether (Carlo Erba, RPE) and THF (Carlo Erba, RPE) were refluxed over Na/K for 12 hours, transferred by distillation over $LiAlH_4$, refluxed for further 12 hours and finally distilled.
- *n*-Hexane (Carlo Erba, RPE), *n*-pentane (Carlo Erba, RPE) and toluene (Carlo Erba, RPE) were dried by refluxing for 12 hours over Na/K and then distilled.
- Triethylamine (Merck) was dried by refluxing for 12 hours over $Ca(OH)_2$ and then distilled.

Chlorobenzene (Sigma Aldrich), ethyl acetate (Carlo Erba, RPE) and ethanol (Fluka) were used without further purification.

The following reagents were commercially available and used without further purification:

- CuI (Alfa Aesar).
- $TlPF_6$ (Apollo Scientific).
- CO (Rivoira).
- C_{60} (**14**) (MER Corporation).
- NBu_4PF_6 (Fluka)
- 4-ethynyl-benzaldehyde (**12**), 4,4′-bipyridine (**7**), 1,4-dicyanobenzene (**8**), CF_3SO_3H, NBu_4Br, NBu_4I, $AgCF_3SO_3$, $AgPF_6$, $[(PPh_3)_2N]Cl$, $CNBu^t$ (Sigma Aldrich).

The following reagents were prepared according to the literature: $\{Pt_3\}Cl$ (**11**),[55] $\{Pt_6\}Cl_2$ (**4**),[55] $\{Pt_6\}H_2$ (**5**),[53] decamethylferrocene,[128] *N*-octylglycine (**15**),[129] $[Pd(PBu^t_2H)(\mu\text{-}PBu^t_2)]_2$, (**19**). [121]

4.3 Analytical and physico-chemical measurements.

Infrared spectra were recorded on a Perkin-Elmer Spectrum 100 FT-IR or with a Perkin Elmer Spectrum one FT-IR spectrometer equipped with a UATR sampling accessory.

UV-VIS spectra were recorded on a Perkin Elmer Lamba EZ201 spectrophotometer.

UV-Vis-NIR spectra were recorded on a Cary 500 Scan Varian spectrophotometer.

NMR spectra were recorded on a Varian Gemini 200 BB instrument; frequencies are referred to the residual resonances of the deuterated solvent (^1H, ^{13}C), 85% H_3PO_4 (^{31}P) and H_2PtCl_6 (^{195}Pt). For spectral interpretation the symbols used are: s = singlet, bs = broad singlet, d = doublet, t = triplet, vt = virtual triplet, hept = heptet, m = multiplet, Pt_{tetr} = inner platinum atoms and Pt_{ap} = apical platinum centres.

Mass spectra were recorded on an Applied Biosystem-MDS Sciex API 4000 triple quadrupole mass spectrometer equipped with HPLC Perkin Elmer Serie 200 Micro system.

Single crystal X-ray diffraction experiments were performed either with a Bruker P4 diffractometer or with a Bruker Smart Breeze CCD diffractometer, both operating with a graphite-monochromated Mo-K_α radiation.

Electrochemical measurements were recorded on a Princeton Applied Research (PAR) 273A Potentiostat/Galvanostat and were performed in dichloromethane solutions containing NBu_4PF_6 (0.2 M) as the supporting electrolyte. Cyclic voltammetry was performed in a three-electrode cell, having a platinum reference electrode, a platinum-spiral counter electrode and a platinum-disc working electrode, and containing a $5\cdot10^{-4}$ M analyte solution. After recording a sufficient number of voltammograms, a small amount of decamethylferrocene was added to the solution and a further voltammogram was recorded. Compounds' potential values were determined placing the redox couple decamethylferrocenium/decamethylferrocene [E_{redox} calculated as $(E_{pc} + E_{pa})/2$] at –0.16 V *vs* SCE. Controlled potential coulometry was performed in an H-shaped cell with anodic and cathodic compartments separated by a sintered-glass disk. The working macroelectrode was a platinum gauze; a platinum-spiral was used as the counter electrode. UV-Vis, UV-Vis-NIR and infrared (IR) spectroelectrochemical measurements were carried out using an optically transparent thin-layer electrochemical (OTTLE) cell equipped with CaF_2 windows, platinum minigrid working and auxiliary electrodes and silver wire pseudoreference electrode.[130] Controlled-potential electrolysis were carried out with a BAS CV-27 electrochemical analyser. Argon-saturated CH_2Cl_2 solutions of the compounds (10^{-3} M or 10^{-2} M for UV-Vis or IR analysis, respectively) under study, containing NBu_4PF_6 0.2 M as the supporting electrolyte, were used. The *in situ* spectroelectrochemistry has been performed by collecting spectra during the stepwise reduction or oxidation.

4.4 Experimental procedures.

4.4.1 Preparation of $\{Pt_6\}(H)(OSO_2CF_3)$ (6).

CF_3SO_3H (10 μL, 0.11 mmol) was added to a solution of $\{Pt_6\}H_2$ (**5**) (135 mg, 0.080 mmol) in 5 mL of Et_2O. The red solution was stirred for 1 hour. During this period, a red solid precipitated out. Subsequently, the precipitate was filtered off, washed with Et_2O (3 x 3 mL) and dried under vacuum. 117 mg of $\{Pt_6\}(H)(OSO_2CF_3)$ (**6**) (0.058 mmol, yield 73%) were obtained as red solid.

^{1}H NMR (CD_2Cl_2, 293K): δ (ppm) = 1.50 (vt, $^3J_{H\text{-}P} + {}^5J_{H\text{-}P}$ = 7.6 Hz, PBu^t, 36 H); 1.37 (vt, $^3J_{H\text{-}P} + {}^5J_{H\text{-}P}$ = 7.3 Hz, PBu^t, 36 H); -0.27 (bs, $^1J_{H\text{-}Pt}$ = 1154 Hz, *H*-Pt, 1 H).

$^{31}P\{^1H\}$ NMR (CD_2Cl_2, 293K): δ (ppm) = 352.2 (s, 2 P); 320.8 (s, 2 P).

IR (solid state): ν (cm^{-1}) = 2006 (C≡O); 1322, 1228, 1169, 999 (CF_3SO_3).

UV-Vis (CH_2Cl_2, 293K): λ (nm) = 445, 304.

Elemental analysis: Calculated for $C_{37}H_{73}F_3O_7P_4Pt_6S$: C 22.1%; H 3.65%. Found C 21.9%; H 3.71%.

4.4.2 Preparation of $[\{Pt_6\}(H)]_2(\mu\text{-}Y)(CF_3SO_3)_2$ [$9(CF_3SO_3)_2$, Y = 4,4′-bipyridine; $10(CF_3SO_3)_2$, Y = 1,4-dicyanobenzene].

4.4.2.1 General procedure.

$\{Pt_6\}(H)(OSO_2CF_3)$ (**6**) and the appropriate ligand, in 2:1 ratio, were dissolved in 2 ml of CH_2Cl_2. The solution was stirred for 2 hours at room temperature. After this period, the solvent was evaporated. The obtained brown solid was dissolved in 2 mL of acetone and a red solid (the unreacted **6**) precipitated out. This solid was filtered off. Removal of the solvent under vacuum gave the desired product.

4.4.2.2 Preparation of $[\{Pt_6\}(H)]_2(\mu\text{-}NC_5H_4\text{-}C_5H_4N)(CF_3SO_3)_2$, $9(CF_3SO_3)_2$.

Used reagents: $\{Pt_6\}(H)(OSO_2CF_3)$ (**6**) (18 mg, $8.94\bullet10^{-3}$ mmol); 4,4′-bipyridine (**7**) (0.69 mg, $4.47\bullet10^{-3}$ mmol).

Product: brown solid, 22 mg ($5.72\bullet10^{-3}$ mmoli), yield 64%.

^1H NMR (Acetone-d_6, 293K): δ (ppm) = 9.68 (d, $^3J_{H\text{-}H}$ = 5.3 Hz, NC_5H_4-C_5H_4N, 4 H); 8.67 (d, $^3J_{H\text{-}H}$ = 5.3 Hz, NC_5H_4-C_5H_4N, 4 H); 1.50 (vt, $^3J_{H\text{-}P} + {}^5J_{H\text{-}P}$ = 7.3 Hz, PBu^t, 72 H), 1.45 (vt, $^3J_{H\text{-}P} + {}^5J_{H\text{-}P}$ = 7.3 Hz, PBu^t, 72 H); -0.37 (bs, $^1J_{H\text{-}Pt}$ = 1209 Hz, *H*-Pt, 2 H).

$^{13}C\{^1H\}$ NMR (Acetone-d_6, 293K): δ (ppm) = 204.1 (s, Pt-*C*O); 156.8, 146.5, 126.3 (s, NC_5H_4-C_5H_4N); 45.4 (m, P*C*-CH_3); 32.1 (s, PC-*C*H_3).

$^{31}P\{^1H\}$ NMR (Acetone-d_6, 293K): δ (ppm) = 356.6 (s, 4 P); 316.2 (s, 4 P).

$^{195}Pt\{^1H\}$ NMR (Acetone-d_6, 293K): δ (ppm) = -2953 (m, 4 Pt_{tetr}); -3327 (m, 4 Pt_{tetr}); -4361 (m, 2 Pt_{ap}); -5080 (m, 2 Pt_{ap}).

IR (solid state): ν (cm^{-1}) = 2024, 2005 (C≡O); 1259, 1171, 1029 (CF_3SO_3).

UV-Vis (CH_2Cl_2, 293K): λ (nm) = 447, 304.

Elemental analysis: Calculated for $C_{84}H_{154}F_6N_2O_{14}P_8Pt_{12}S_2$: C 24.2%; H 3.71%; N 0.67%. Found C 24.7%; H 3.78%; N 0.65%.

4.4.2.3 Preparation of [{Pt₆}(H)]₂(μ-NC-C₆H₄-CN)(CF₃SO₃)₂, 10(CF₃SO₃)₂.

Used reagents: $\{Pt_6\}(H)(OSO_2CF_3)$ (**6**) (31 mg, 0.015 mmol); 1,4-dicyanobenzene (**8**) (0.98 mg, $7.70 \bullet 10^{-3}$ mmol).

Product: brown solid, 40 mg (0.01 mmol), yield 67%.

^{1}H NMR(Acetone-d_6, 293K): δ (ppm) = 8.54 (s, C_6H_4, 4 H); 1.58 (vt, $^3J_{P\text{-}H} + {}^5J_{P\text{-}H}$ = 7.6 Hz, PBu^t, 72 H); 1.43 (vt, $^3J_{P\text{-}H} + {}^5J_{P\text{-}H}$ = 7.1 Hz, PBu^t, 72 H); -0.52 (bs, $^1J_{H\text{-}Pt}$ = 1148 Hz, *H*-Pt, 2 H).

^{13}C{^{1}H} NMR (Acetone-d_6, 293K): δ (ppm) = 204.2 (s, Pt-*C*O); 135.2 (s, *C*H of NC-C_6H_4-CN); 117.0 (s, N*C*-C_6H_4-*C*N) 116.5 (s, quaternary *C* of NC-C_6H_4-CN); 44.3 (m, P*C*-CH_3); 31.9 (s, PC-*C*H_3).

^{31}P{^{1}H} NMR (Acetone-d_6, 293K): δ (ppm) = 362.6 (s, 4 P); 334.5 (s, 4 P).

^{195}Pt{^{1}H} NMR (Acetone-d_6, 293K): δ (ppm) = -2971 (m, 4 Pt_{tetr}); 3413 (m, 4 Pt_{tetr}); -4431 (m, 2 Pt_{ap}); -5066 (m, 2 Pt_{ap}).

IR (solid state): ν (cm^{-1}) = 2166 (C≡N); 2022, 2000 (C≡O); 1258, 1172, 1030 (CF_3SO_3).

UV-Vis (CH_2Cl_2, 293K): λ (nm) = 443, 302.

Elemental analysis: Calculated for $C_{82}H_{150}F_6N_2O_{14}P_8Pt_{12}S_2$: C 23.7%; H 3.64%; N 0.67%. Found C 23.4%; H 3.61%; N 0.69%.

4.4.3 Preparation of [{Pt₃}CCC₆H₄CHO] (13).

To a stirred solution of **11** (100 mg, 0.089 mmol) in NEt_3 (20 mL), 4-ethynyl-benzaldehyde (12 mg, 0.092 mmol) and CuI (0.017 mg, $0.089 \bullet 10^{-3}$ mmol) were added. The brown solution was stirred at room temperature for 24 hours and after this period the solvent was evaporated under vacuum. Then, toluene was added to the crude product in order to separate the final product from the insoluble salt (NEt_3HCl) formed

during the reaction. The compound **13** was obtained as brown microcrystalline solid after solvent evaporation (89 mg, 0.074 mmol, yield 83%).

^{1}H NMR (C_6D_6, 293K): δ (ppm) = 9.69 (s, CO*H*, 1 H); 7.76 (d, $^{3}J_{H\text{-}H}$ = 8.0 Hz, C_6H_4, 2 H); 7.46 (d, $^{3}J_{H\text{-}H}$ = 8.0 Hz, C_6H_4, 2 H); 1.47 (vt, $^{3}J_{H\text{-}P} + {}^{5}J_{H\text{-}P}$ = 7.6 Hz, CCH_3, 36 H); 1.19 (d, $^{3}J_{H\text{-}P}$ = 15.2 Hz, CCH_3, 18 H).

^{13}C{^{1}H} NMR (C_6D_6, 293K): δ (ppm) = 190.4 (s, C-*C*OH); 175.5 (s, Pt-*C*O); 136.0, 133.7, 131.2, 129.9, 128.3 (s, C_6H_4); 124.6 (Pt- *C*≡C); 95.7 (s, Pt-C≡*C*); 39.2, 38.9 (s, P*C*-CH_3); 33.6, 33.4 (s, PC-*C*H_3).

^{31}P{^{1}H} NMR (C_6D_6, 293K): δ (ppm) = 164.8 (d, $^{2}J_{P\text{-}P}$ = 128.0 Hz, 2 P); 98.4 (t, $^{2}J_{P\text{-}P}$ = 128.0 Hz, 1 P).

^{195}Pt{^{1}H} NMR (C_6D_6, 293K): δ (ppm) = -5715 (m, 2 Pt); -6089 (m, 1 Pt).

IR (CH_2Cl_2): ν cm^{-1} = 2097 (C≡C); 2024, 2035 (C≡O); 1683 (C=O); 1589, 1552 (C=C).

Elemental analysis: Anal. calcd for $C_{35}H_{59}O_3P_3Pt_3$: C, 34.9%; H, 4.93%. Found: C, 34.7%; H, 4.90%.

4.4.4 Preparation of [{Pt_3}$CCC_6H_4C_2H_3N(C_8H_{17})C_{60}$] (16).

Complex **13** (50 mg, 0.041 mmol) and *N*-octylglycine (23 mg, 0.12 mmol) were added to a solution of C_{60} (30 mg, 0.041 mmol) in chlorobenzene (15 mL). The mixture was heated under reflux for 9 hours. After evaporation of the solvent under vacuum, the residue was washed with water (5 mL), ethanol (5 mL) and purified by column chromatography on silica gel (ethyl acetate : *n*-hexane = 2 : 1 as eluent). The final product **16** was obtained as brown solid (37 mg, 0.018 mmol, yield 43%).

^{1}H NMR ($CDCl_3$, 293K): δ (ppm) = 7.61 (d, $^{3}J_{H\text{-}H}$ = 8.1 Hz, C_6H_4, 2 H); 7.32 (d, $^{3}J_{H\text{-}H}$ = 8.1 Hz, C_6H_4, 2 H); 5.12 (d, *J* = 9.2 Hz, NCH_2CC_{60}, 1 H); 5.02 (s, $NCHCC_{60}$, 1 H); 4.13 (d, *J* = 9.2 Hz, NCH_2CC_{60}, 1 H); 3.40-3.18 (m, NCH_2-CH_2, 2 H); 2.56 (m, NCH_2-CH_2, 2 H); 2.12-1.60 (m, NC_2H_4-C_5H_{10}-CH_3, 10 H); 1.41 (vt, $^{3}J_{H\text{-}P} + {}^{5}J_{H\text{-}P}$ = 7.1 Hz, CCH_3, 36 H); 1.33 (d, $^{3}J_{H\text{-}P}$ = 14.3 Hz, CCH_3, 18 H); 0.97 (m, NC_7H_{14}-CH_3, 3 H).

^{13}C{^{1}H} NMR ($CDCl_3$, 293K): δ (ppm) = 175.2 (s, Pt-*C*O); 156.83, 154.54, 154.02, 153.95, 147.31, 147.07, 146.63, 146.32, 146.19, 145.92, 145.54, 145.28, 144.76, 144.47, 144.42, 143.15, 142.98, 142.56, 142.40, 142.16, 141.66, 141.58, 140.15,

140.08, 139.93, 136.85, 136.72, 135.79 (C_{60}); 133.76, 131.39, 129.52, 129.38 (s, C_6H_4); 121.13 (Pt- *C*≡C); 82.80 (s, Pt-C≡*C*); 69.06, 66.87 (s, *C*H-N-*C*H_2); 53.08 (s, N*C*H_2-C_7H_{15}); 38.93 (s, P*C*-CH_3); 33.51 (s, PC-*C*H_3); 32.03, 29.79, 29.42, 28.41, 27.56, 22.79, 14.27 (s, NCH_2-*C*$_7H_{15}$).

^{31}P{^{1}H} NMR ($CDCl_3$, 293K): δ (ppm) = 163.2 (d, $^2J_{P\text{-}P}$ = 127.4 Hz, 2 P); 99.1 (t, $^2J_{P\text{-}P}$ = 127.4 Hz, 1 P).

^{195}Pt{^{1}H} NMR ($CDCl_3$, 293K): δ (ppm) = -5727 (m, 2 Pt); -6068 (m, 1 Pt).

IR (solid state): ν cm^{-1} = 2017 (C≡O).

IR (CH_2Cl_2): ν cm^{-1} = 2102 (C≡C); 2024 (C≡O); 1602 (C=C).

FIA-MS: *m/z* = calcd for $C_{104}H_{78}NO_2P_3Pt_3$ $[M]^+$: 2051.8 amu. Found: 2052.7 amu.

Elemental analysis: Anal. calcd for $C_{104}H_{78}NO_2P_3Pt_3$: C, 60.9%; H, 3.83%. Found: C, 60.3%; H, 3.85%.

4.4.5 Preparation of [{Pt$_6$}(CCC$_6$H$_4$CHO)$_2$] (17).

4-ethynyl-benzaldehyde (11.4 mg, 0.088 mmol) and CuI (0.0167 mg, 0.088 x 10^{-3} mmol) were added to a solution of complex **4** (85 mg, 0.044 mmol) in NEt_3 (20 mL). The brown solution was stirred at room temperature for 24 hours. Then, the solvent was evaporated under vacuum. The salt formed during the reaction was removed by filtration after dissolving **17** in toluene. 78 mg of **17** (0.038 mmol, yield 86%) as dark orange solid were obtained.

^{1}H NMR (C_6D_6, 293K): δ (ppm) = 9.66 (s, CO*H*, 2 H); 7.59 (d, $^3J_{H\text{-}H}$ = 7.5 Hz, C_6H_4, 4 H); 7.53 (d, $^3J_{H\text{-}H}$ = 7.5 Hz, C_6H_4, 4 H); 1.48 (vt, $^3J_{H\text{-}P}$ + $^5J_{H\text{-}P}$ = 7.1 Hz, PBu^t, 72 H).

^{13}C{^{1}H} NMR (C_6D_6, 293K): δ (ppm) = 217.2 (s, Pt-*C*O); 190.3 (s, C-*C*OH); 133.7, 130.9, 129.7, 129.1 (s, C_6H_4); 124.1 (Pt- *C*≡C); 94.8 (s, Pt-C≡*C*); 39.2, 44.0 (m, P-*C*-CH_3); 31.3 (s, PC-*C*H_3).

^{31}P{^{1}H} NMR (C_6D_6, 293K): δ (ppm) = 336.2 (s, 4 P).

^{195}Pt{^{1}H} NMR (C_6D_6, 293K): δ (ppm) = -2998 (m, 4 Pt_{tetr}); - 4664 (m, 2 Pt_{ap}).

IR (solid state): ν cm^{-1} = 2101 (C≡C); 2010 (C≡O); 1693 (C=O); 1591, 1552 (C=C).

Elemental analysis: Anal. calcd for $C_{54}H_{82}O_6P_4Pt_6$: C, 30.6%; H, 3.89%. Found: C, 31.2%; H, 3.85%.

4.4.6 Preparation of [{Pt$_6$}{CCC$_6$H$_4$C$_2$H$_3$N(C$_8$H$_{17}$)C$_{60}$}$_2$] (18).

To a solution of C_{60} (30 mg, 0.042 mmol) in chlorobenzene (15 mL), 45 mg of **17** (0.021 mmol) and 24 mg of *N*-octylglycine (0.13 mmol) were added. The reaction mixture was heated under reflux for 9 hours. After this period the solvent was evaporated under vacuum. The crude product was washed with water (5 mL), ethanol (5 mL) and purified by column chromatography, using the solvents mixture toluene : CH_2Cl_2 = 1:5 as eluent. **18** was obtained as brown solid (31 mg, 0.008 mmol, yield 39%).

^{1}H NMR ($CDCl_3$, 293K): δ (ppm) = 7.62 (d, $^3J_{H\text{-}H}$ = 8.3 Hz, C_6H_4, 4 H); 7.31 (d, $^3J_{H\text{-}H}$ = 8.3 Hz, C_6H_4, 4 H); 5.09 (d, *J* = 9.5 Hz, NCH_2CC_{60}, 2 H); 5.00 (s, $NCHCC_{60}$, 2 H); 4.10 (d, *J* = 9.5 Hz, NCH_2CC_{60}, 2 H); 3.78-3.62 (m, NCH_2-CH_2, 4 H); 2.52 (m, NCH_2-CH_2, 4 H); 2.13-1.74 (m, NC_2H_4-C_5H_{10}-CH_3, 20 H); 1.49 (vt, $^3J_{H\text{-}P}$ + $^5J_{H\text{-}P}$ = 6.5 Hz, PBu^t, 72 H); 0.93 (m, NC_7H_{14}-CH_3, 6 H).

^{31}P{^{1}H} NMR ($CDCl_3$, 293K): δ (ppm) = 336.0 (s, 4 P).

Elemental analysis: Anal. calcd for $C_{192}H_{120}N_2O_4P_4Pt_6$: C, 60.5%; H, 3.17%. Found: C, 59.5%; H, 3.24%.

4.4.7 Preparation of {Pd$_3$}Br (20).

NBu_4Br (39 mg, 0.12 mmol) and $[Pd(PBu^t_2H)(\mu\text{-}PBu^t_2)]_2$, (**19**) (145 mg, 0.18 mmol) were suspended in toluene (10 mL) under 1 atm of carbon monoxide. The suspension was stirred for 3 days at 100 °C. The solid residue was filtered off and the remaining red solution was evaporated under vacumm. The residue was purified by column chromatography on neutral alumina (hexane-acetone 20:1 as eluent). Complex **20** was obtained as red solid (67 mg, 0.076 mmol, yield 63%).

^{1}H NMR (C_6D_6, 293K): δ (ppm) = 1.47 (vt, $^3J_{H\text{-}P}$ + $^5J_{H\text{-}P}$ = 7.1 Hz, CCH_3, 36 H); 1.13 (d, $^3J_{H\text{-}P}$ = 14.6 Hz, CCH_3, 18 H).

$^{13}C\{^1H\}$ NMR (C_6D_6, 293K): δ (ppm) = 188.6 (s, Pd-*C*O); 40.8, 38.9 (s, P*C*-CH_3); 33.3, 29.9 (s, PC-*C*H_3).

$^{31}P\{^1H\}$ NMR (C_6D_6, 293K): δ (ppm) = 282.7 (d, $^2J_{P\text{-}P}$ = 115.8 Hz, 2 P); 206.4 (t, $^2J_{P\text{-}P}$ = 115.8 Hz, 1 P).

IR (solid state): ν cm^{-1} = 2040 (C≡O) cm^{-1}.

Elemental analysis: Anal. calcd for $C_{26}H_{54}O_2P_3Pd_3Br$: C, 35.1%; H, 6.11%. Found: C, 34.9%; H, 6.13%.

4.4.8 Preparation of {Pd_3}I (21).

NBu_4I (51 mg, 0.139 mmol) and complex **19** (166 mg, 0.208 mmol) were suspended in toluene (15 mL) under 1 atm of carbon monoxide. The suspension was stirred for 3 days at 100 °C. The solid residue was filtered off and the remaining red solution was evaporated. The residue was purified by column chromatography on neutral alumina (hexane-acetone 20:1), achieving **21** as red solid (110 mg, 0.118 mmol, yield 85%).

^1H NMR (C_6D_6, 293K): δ (ppm) = 1.50 (vt, $^3J_{H\text{-}P}$ + $^5J_{H\text{-}P}$ = 7.0 Hz, CC*H*$_3$, 36 H); 1.13 (d, $^3J_{H\text{-}P}$ = 14.5 Hz, CC*H*$_3$, 18 H).

$^{13}C\{^1H\}$ NMR (C_6D_6, 293K): δ (ppm) = 188.4 (s, Pd-*C*O); 41.1, 39.1 (s, P*C*-CH_3); 34.2, 33.3 (s, PC-*C*H_3).

$^{31}P\{^1H\}$ NMR (C_6D_6, 293K): δ (ppm) = 292.5 (d, $^2J_{P\text{-}P}$ = 116.4 Hz, 2 P); 213.4 (t, $^2J_{P\text{-}P}$ = 116.4 Hz, 1 P).

IR (CH_2Cl_2): ν cm^{-1} = 2049 (C≡O) cm^{-1}.

IR (solid state): ν cm^{-1} = 2034 C≡O) cm^{-1}.

Elemental analysis: Anal. calcd for $C_{26}H_{54}O_2P_3Pd_3I$: C, 33.3%; H, 5.80%. Found: C, 33.1%; H, 5.85%.

4.4.9 Preparation of [{Pd_3}(CO)]PF_6, 23(PF_6).

$TlPF_6$ (67 mg, 0.19 mmol) was added to a solution of **21** (90 mg, 0.096 mmol) in 25 mL of THF. The red solution was stirred overnight under 1 atm of carbon monoxide. TlI was filtered off and the solvent was evaporated. The crude residue was washed with

hexane and vacuum-dried. 73 mg of **23**(PF_6) (0.074 mmol) were obtained as a reddish solid, yield 77%.

^{1}H NMR (acetone-d_6, 293K): δ (ppm) = 1.42 (vt, $^3J_{H\text{-}P}$ + $^5J_{H\text{-}P}$ = 7.5 Hz, CCH_3, 54 H). **^{13}C{^{1}H} NMR** (acetone-d_6, 293K): δ (ppm) = 185.8 (s, Pd-*C*O); 42.4 (s, P*C*-CH_3); 33.5 (s, PC-*C*H_3).

^{31}P{^{1}H} NMR (acetone-d_6, 293K): δ (ppm) = 295.6 (s, 3 P); –142.2 (hept, $^1J_{P\text{-}F}$ = 707.9 Hz, *P*F_6, 1 P).

IR (CH_2Cl_2): ν cm^{-1} = 2079 (C≡O) cm^{-1}

IR (solid state): ν cm^{-1} = 2094, 2053 (C≡O) cm^{-1}.

Elemental analysis: Anal. calcd for $C_{27}H_{54}F_6O_3P_4Pd_3$: C, 33.0%; H, 5.53%. Found: C, 32.8%; H, 5.49%.

4.4.10 Preparation of {Pd_3}Cl, (22).

[(PPh_3)$_2$N]Cl (40 mg, 0.070 mmol) was added to a red solution of **23**(PF_6) (69 mg, 0.070 mmol) in 5 mL of dry acetone and the mixture was stirred for 1 hour at room temperature. After this period, the solvent was evaporated and the residue was dissolved in 5 mL of *n*-pentane. A colourless solid was filtered off and **22** was collected as a red solid after solvent evaporation (46 mg, 0.054 mmol, yield 77%).

^{1}H NMR (C_6D_6, 293K): δ (ppm) = 1.46 (vt, $^3J_{H\text{-}P}$ + $^5J_{H\text{-}P}$ = 7.1 Hz, CCH_3, 36 H); 1.12 (d, $^3J_{H\text{-}P}$ = 14.6 Hz, CCH_3, 18 H).

^{13}C{^{1}H} NMR (C_6D_6, 293K): δ (ppm) = 188.4 (s, Pd-*C*O); 40.6, 38.9 (s, P*C*-CH_3); 33.3, 32.9 (s, PC-*C*H_3).

^{31}P{^{1}H} NMR (C_6D_6, 293K): δ (ppm) = 277.4 (d, $^2J_{P\text{-}P}$ = 115.4 Hz, 2 P); 204.8 (t, $^2J_{P\text{-}P}$ = 115.4 Hz, 1 P).

IR (solid state): ν cm^{-1} = 2038 (C≡O) cm^{-1}.

Elemental analysis: Anal. calcd for $C_{26}H_{54}O_2P_3Pd_3Cl$: C, 36.9%; H, 6.43%. Found: C, 37.2%; H, 6.39%.

4.4.11 Preparation of $[Pd_3(\mu\text{-}PBu^t_2)_3(CNBu^t)_3]I$, 26(I).

$CNBu^t$ (32 μL, 0.288 mmol) and complex **21** (90 mg, 0.096 mmol) were dissolved in 5 mL of toluene. Immediately an orange solid precipitated out. The mixture was stirred for further 1 hour and the orange solid was filtered, washed with toluene (3 x 5 mL) and vacumm-dried (94 mg, 0.083 mmol, yield 87%).

^{1}H NMR (acetone-d_6, 293K): δ (ppm) = 1.32 (vt, $^3J_{H\text{-}P} + {}^5J_{H\text{-}P}$ = 7.0 Hz, PCCH_3, 54 H); 1.72 (s, CNCCH_3, 27 H).

^{13}C{^{1}H} NMR (acetone-d_6, 293K): δ (ppm) = 137.4 (s, Pd-*C*N); 59.9 (s, N*C*-CH_3); 40.0 (s, P*C*-CH_3); 34.0 (s, PC-*C*H_3); 30.5 (s, NC-*C*H_3).

^{31}P{^{1}H} NMR (acetone-d_6, 293K): δ (ppm) = 257.2 (s, 3 P).

IR (CH_2Cl_2): ν cm^{-1} = 2164 (C≡N) cm^{-1}.

IR (solid state): ν cm^{-1} =2156 (C≡N) cm^{-1}.

Elemental analysis: Anal. calcd for $C_{39}H_{81}N_3P_3Pd_3I$: C, 41.4%; H, 7.22%; N, 3,71%. Found: C, 41.2%; H, 7.25%; N, 3.69%.

4.4.12 Preparation of $[Pd_3(\mu\text{-}PBu^t_2)_3(CNBu^t)_3]PF_6$, 26($PF_6$).

$AgPF_6$ (11 mg, 0.044 mmol) was added to a solution of **26**(I) (50 mg, 0.044 mmol) in CH_2Cl_2 (3 mL) and the reaction mixture was stirred for 1 hour at room temperature. After this period, AgI, which precipitated out during the reaction, was filtered off. **26**(PF_6) was obtained as an orange solid in a nearly quantitative yield (48 mg, 0.042 mmol) after solvent evaporation.

^{31}P{^{1}H} NMR (acetone-d_6, 293K): δ (ppm) = 251.7 (s, 3 P); –142.5 (hept, $^1J_{P\text{-}F}$ = 709.9 Hz, *P*F_6, 1 P).

4.4.13 Preparation of $[Pd_3(\mu\text{-}PBu^t_2)_3(CNBu^t)_3]CF_3SO_3$, 26($CF_3SO_3$).

To a solution of **26**(I) (60 mg, 0.053 mmol) in 4 mL of CH_2Cl_2, $AgCF_3SO_3$ (13.6 mg, 0.053 mmol) was added. The reaction mixture was stirred for 30 minutes at room temperature. During this period, a white salt (AgI) precipitated out. This solid was

filtered off and, after removal the solvent under vacuum, the final product **26**(CF_3SO_3) was obtained as an orange microcrystalline solid (55 mg, 0.048 mmol, yield = 90%).

4.4.14 Chemical oxidation of $[Pd_3(\mu\text{-}PBu^t_2)_3(CNBu^t)_3]I$, 26$(PF_6)_2$.

$AgPF_6$ (13.4 mg, 0.053 mmol) was added to a solution of **26**(I) (30 mg, 0.026 mmol) in 3 mL of CH_2Cl_2. Immediately, the orange solution turns to dark pink and a dark solid (Ag^0 and AgI) precipitated out. The precipitate was filtered off, and the solvent was evaporated under vacuum. The crude residue was then washed with diethyl ether (3 x 2 mL). **26**$(PF_6)_2$ was obtained as a dark pink solid in a nearly quantitative yield (31 mg, 0.024 mmol) after solvent evaporation.

^{1}H NMR (acetone-d_6, 293K): δ (ppm) = 16.00 (bs, PCCH_3, 54 H).

IR (CH_2Cl_2): ν cm^{-1} =2188 (C≡N) cm^{-1}.

IR (solid state): ν cm^{-1} = 2193 (C≡N) cm^{-1}.

4.4.15 Preparation of $[\{Pd_3\}(NCCH_3)]PF_6$, 24(PF_6).

$TlPF_6$ (52 mg, 0.149 mmol) was added to a solution of **21** (70 mg, 0.075 mmol) in acetonitrile (3 mL); the mixture was stirred overnight at room temperature. TlI was filtered off and the solvent was evaporated. The crude residue was washed with hexane and vacuum-dried. Complex **24**(PF_6) was obtained as a dark red solid (65 mg, 0.064 mmol, yield 86%).

^{1}H NMR (acetone-d_6, 293K): δ (ppm) = 2.90 (s, NCCH_3, 3 H); 1.40 (vt, $^3J_{H\text{-}P} + {}^5J_{H\text{-}P}$ = 7.4 Hz, CCH_3, 36 H); 1.38 (d, $^3J_{H\text{-}P}$ = 15.1 Hz, CCH_3, 18 H).

^{13}C{^{1}H} NMR (acetone-d_6, 293K): δ (ppm) = 185.2 (s, Pd-*C*O); 124.3 (s, N*C*CH_3); 41.7, 40.6 (s, P*C*-CH_3); 32.8, 32.3 (s, PC-*C*H_3); 2.6 (s, NC*C*H_3).

^{31}P{^{1}H} NMR (acetone-d_6, 293K): δ (ppm) = 275.8 (d, $^2J_{P\text{-}P}$ = 128.0 Hz, 2 P); 245.4 (t, $^2J_{P\text{-}P}$ = 128.0 Hz, 1 P); –137.1 (hept, $^1J_{P\text{-}F}$ = 697.4 Hz, *P*F_6, 1 P).

IR (solid state): ν cm^{-1} = 2058, 2044 (C≡O) cm^{-1}.

Elemental analysis: Anal. calcd for $C_{28}H_{57}NF_6O_3P_4Pd_3$: C, 33.7%; H, 5.76% N, 1.41%. Found: C, 33.9%; H, 5.78%; N, 1.39%.

4.4.16 Preparation of [{Pd_3}(NC_5H_5)]PF_6, 25(PF_6).

An excess of $TlPF_6$ (32 mg, 0.094 mmol) was added to a red solution of **21** (44 mg, 0.047 mmol) in pyridine (3 mL) and the mixture was stirred for 3 days at room temperature. After this period the solvent was evaporated under vacuum. The crude residue was washed with hexane, dissolved in acetone and TlI was filtered off. Complex **25**(PF_6) was obtained as a dark red solid (36 mg, 0.035 mmol, yield 74%) after evaporation of the solvent under vacuum.

^{1}H NMR (acetone-d_6, 293K): δ (ppm) = 8.21 (m, NC_5H_5, 2 H); 7.87 (m, NC_5H_5, 1 H); 7.63 (m, NC_5H_5, 2 H); 1.41 (d, $^3J_{H\text{-}P}$ = 15.0 Hz, CCH_3, 18 H), 1.29 (vt, $^3J_{H\text{-}P}$ + $^5J_{H\text{-}P}$ = 7.4 Hz, CCH_3, 36 H).

^{13}C{^{1}H} NMR (acetone-d_6, 293K): δ (ppm) = 186.2 (s, Pd-*C*O); 156.0 (s, N*C*$_5$H$_5$, 2 C); 140.2 (s, N*C*$_5$H$_5$, 1 C); 127.6 (s, N*C*$_5$H$_5$, 2 C); 41.5, 41.3 (s, P*C*-CH_3); 33.8, 33.4 (s, PC-*C*H_3).

^{31}P{^{1}H} NMR (acetone-d_6, 293K): δ (ppm) = 258.9 (d, $^2J_{P\text{-}P}$ = 121.3 Hz, 2 P); 250.8 (t, $^2J_{P\text{-}P}$ = 121.3 Hz, 1 P); –137.1 (hept, $^1J_{P\text{-}F}$ = 702.3 Hz, *P*F_6, 1 P).

IR (solid state): ν cm^{-1} = 2066 (C≡O) cm^{-1}.

Elemental analysis: Anal. calcd for $C_{31}H_{59}NF_6O_3P_4Pd_3$: C, 36.0%; H, 5.75%; N, 1.35%. Found: C, 35.8%; H, 5.73%; N, 1.36%.

4.5 Crystallographic Section.

Table 15. Crystal data and structure refinements of [{Pt_3}CC-C_6H_4-CHO] (**13**).

	13
Empirical formula	C_{35} H_{59} O_3 P_3 Pt_3
Formula weight	1206.03
Crystal system	Monoclinic
Temperature (K)	293(2)
Space group	C 2/m
a (Å)	19.025(3)
b (Å)	15.496(2)
c (Å)	13.934(2)
α (°)	90.00
β (°)	93.194(2)
γ (°)	90.00
U (Å^3)	4101.52
Z	4
R-Factor (%)	4.75

Table 16. Crystal data and structure refinements of $Pd_3(PBu^t_2)_3(CO)_2Br$ (**20**).

	20
Empirical formula	$C_{26}H_{52}BrO_2P_3Pd_3$
Formula weight	888.70
Crystal system	Orthorhombic
Space group	*Pnma* (No. 62)
a / Å	18.084(2)
b / Å	17.808(2)
c / Å	11.8374(14)
β / °	-
U / Å^3	3812.1(8)
Z	4
D_{calc} / Mg·m^{-3}	1.548
μ / mm^{-1}	2.592
No. measured	5080
No. unique [R_{int}]	4090 [0.0458]
No. parameters	170
R_1, wR_2 [$I>2\sigma(I)$] [a]	0.0565, 0.0979
R_1, wR_2 [all data] [a]	0.1277, 0.1205
Goodness of fit [a] on F^2	0.988

[a] $R(F_o) = \Sigma \big| \, |F_o| - |F_c| \, \big| \, / \, \Sigma |F_o|$; $Rw(F_o^2) = [\Sigma[w(F_o^2 - F_c^2)^2] / \Sigma[w(F_o^2)^2]]^{½}$; $w = 1 / [\sigma^2 (F_o^2) + (AQ)^2 + BQ]$ where $Q = [MAX(F_o^2,0) + 2F_c^2] / 3$; GOF = $[\Sigma [w(F_o^2 - F_c^2)^2]/(N-P)]^{½}$, where N, P are the numbers of observations and parameters, respectively.

Table 17. Crystal data and structure refinements of $[Pd_3(PBu^t_2)_3(CNBu^t)_3](CF_3SO_3)$, **26**$(CF_3SO_3)$.

	26(CF_3SO_3)
Empirical formula	$C_{40}H_{81}F_3N_3O_3P_3\ SPd_3$
Formula weight	1153.25
Crystal system	Monoclinic
Space group	$P2_1/n$ (No. 14)
a / Å	9.7168(6)
b / Å	19.8254(12)
c / Å	28.9139(17)
β / °	92.257(2)
U / Å^3	5565.6(6)
Z	4
D_{calc} / Mg·m^{-3}	1.376
μ / mm^{-1}	1.126
No. measured	46049
No. unique [R_{int}]	12117 [0.0392]
No. parameters	441
R_1, wR_2 [$I>2\sigma(I)$] [a]	0.0543, 0.1345
R_1, wR_2 [all data] [a]	0.0887, 0.1554
Goodness of fit [a] on F^2	1.047

[a] $R(F_o) = \Sigma \big| \, |F_o| - |F_c| \, \big| \, / \, \Sigma |F_o|$; $Rw(F_o^2) = [\Sigma[w(F_o^2 - F_c^2)^2] / \Sigma[w(F_o^2)^2]]^{½}$; $w = 1 / [\sigma^2 (F_o^2) + (AQ)^2 + BQ]$ where $Q = [MAX(F_o^2,0) + 2F_c^2] / 3$; GOF = $[\Sigma [w(F_o^2 - F_c^2)^2]/(N-P)]^{½}$, where N, P are the numbers of observations and parameters, respectively.

5 Appendix A

5.1 ^{1}H, ^{31}P and ^{195}Pt NMR characterization of platinum compounds containing terminal phosphine and bridging phosphides.

Besides ^{1}H and ^{13}C NMR, ^{31}P and ^{195}Pt NMR have provided a crucial support for the characterization of the new tri- and hexanuclear platinum cluster derivatives prepared in this Thesis.

The ^{31}P nucleus (I = ½, natural abundance = 100%) has a wide range of chemical shifts (550 ÷ −500 ppm, reference H_3PO_4) and, generally, gives sharp and well-defined peaks. Phosphine and phosphido ligands have signals that generally lie in different regions of the spectrum. The chemical shift values of coordinated aryl- or alkyl-phosphines are normally included in the range from +70 to −50 ppm and, generally, are shifted to lower field in comparison to the free phosphines (+10 ÷ −70 ppm), P^{III} shifts of ligands with electronegative substiuents (phosphites, halophosphines) move to still lower fields. Values of δ_P of bridging phosphides may be found at very low fields (450 ÷ 40 ppm),[131,132,121] typical of bridges on a metal-metal bonded edge, or at the opposite upfield region (50 ÷ −150 ppm),[132, 121] when the metal-metal bond is absent; some examples of compounds which follow this rule are reported in Figure 61.

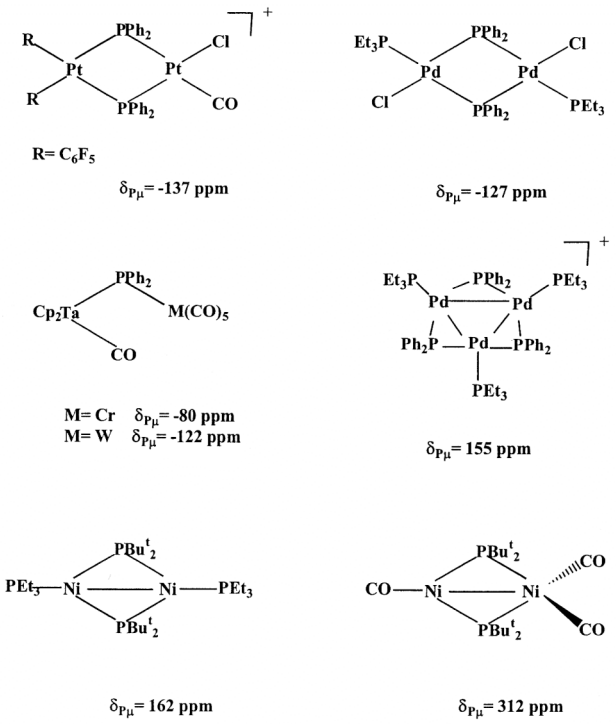

Figure 61. Example of δ_P values for bridging phosphides.

While the chemical shift gives qualitative information about the type of phosphorus nucleus and the multiplicity of the signals indicates the number of ^{31}P (or other NMR active) nuclei coupled with it, the coupling constants, which depends on dihedral bond angles, give information on the geometry of the complex, suggesting the relative positions of these nuclei.

In the compounds prepared in this Thesis, the ^{31}P NMR spectra are further complicated by the presence of platinum, only one isotope of which is NMR active (^{195}Pt, I = ½, natural abundance = 33.8%).[133]

In mononuclear complexes, the 33.8% of the species contains ^{195}Pt (isotopomer **A**) and the remaining 66.2% contains NMR inactive Pt isotopes (isotopomers **B**). Thus, the ^{31}P NMR spectrum is constituted by an intense central signal (isotopomers **B**, area 66.2%) flanked by a couple of weaker satellites, due to the coupling with ^{195}Pt (isotopomer **A**, total area 33.8%). In mononuclear complexes, the P–Pt coupling constants reach very high values [$^1J_{PPt}$= 1000 ÷ 5000 Hz, higher than J_{PP} (< 500 Hz)] when the two nuclei are

directly bonded to each other, in which case the satellites are well separated from the central signal.

In polynuclear complexes, the ^{31}P NMR spectra are more complex. In fact, due to the presence of more than one platinum center, the P nuclei may be directly bonded to a ^{195}Pt nucleus or may be separated from it by two or more bonds; in the latter case, the J_{PPt} values decrease rapidly ($^{2}J_{PPt}$ = 0 ÷ 300 Hz), and the central signal and the satellites may overlap. However, the complex shape of the spectra gives a lot of information; for example, in addition to the chemical shift values, the coupling constants J_{PPt} are useful to evaluate if the observed P nucleus is coordinated terminally to a single platinum atom or bridges two (or more) metal atoms.

As an example, Figure 62 shows how may be reconstructed the ^{31}P{^{1}H}NMR spectra of a dinuclear complex, in which only one phosphorus atom is coordinated in three alternative ways: a) bridging two chemically and magnetically equivalent platinum centers; b) bridging two unequivalent Pt atoms; c) terminally bonded to one of the two metal centers. The spectrum results from the sum of the subspectra due to the four different isotopomers **A-D** (isotopic composition and natural abundances shown in the first column).

Isotopomer **A**, has inactive Pt isotopes and gives the central singlet. The most intense satellites are due to isotopomers **B** and **C** which give two doublets with an identical and large coupling constant $^{1}J_{PPt1}$ in the case of structure a), two doublets with large, but different coupling constants $^{1}J_{PPt1} \neq {}^{1}J_{PPt2}$ for structure b), and two doublets, one with a large coupling $^{1}J_{PPt2}$ and one with a much smaller coupling $^{2}J_{PPt1}$ for structure c). The weak satellites due to istopomer **D** [triplet for a) and double doublets for b) and c)] complete the signal, which, as a whole, appears as a quintuplet (intensities ratio *ca.* 1:8:18:8:1, $J_{apparent} = {}^{1}J_{PPt}/2$) in case a), contains nine lines with an intensities ratio of *ca.* 1:4:4:1:16:1:4:4:1 in case b) or appears as a triple triplet with nine lines of relative intensity of *ca*. 1:4:1:4:16:4:1:4:1 in case c).

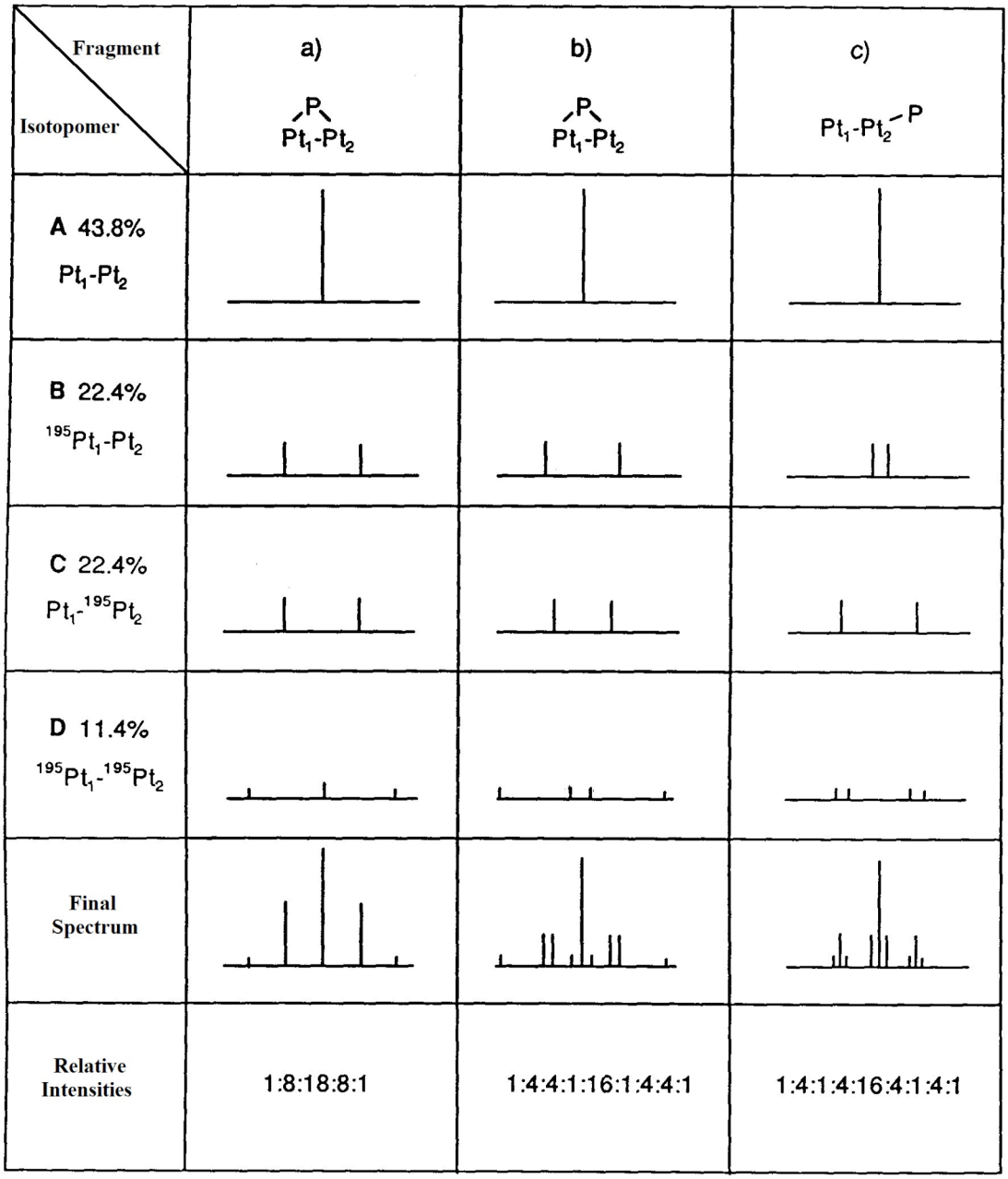

Figure 62. Subspectra due to the different isotopomers and final spectrum ($^{31}P\{^{1}H\}$NMR) of a dinuclear platinum complex with only one phosphorus ligand.

The ^{195}Pt NMR[134] spectra are, also, useful for the characterization of polynuclear compounds. Here, the chemical shift range is really huge (*ca*. 13000 ppm), and thus the signals are quite generally well separated. However, it is difficult to anticipate in which region of the spectrum the signals will fall; moreover, it is not possible to formulate general rules which correlate the chemical shift to the type of ligands coordinated to the

metal atom; only approximated indications may be provided by examining the data reported in literature for compounds with structures similar to those under investigation.

The coupling constants $^{1}J_{LPt}$ are useful for structural assignment: for examples, in Pt(II) approximately square planar systems, similar to those prepared in our laboratories and in this Thesis, we can find ^{1}J = 700 ÷ 1400 Hz when L = H (decreases for bridging hydrides), and ^{1}J = 1400 ÷ 5000 Hz when L = P. The Pt–Pt coupling constant values ($^{1}J_{PtPt}$) are, also, important because are often correlated to the M–M bond order: the general trend demonstrates that large $^{1}J_{PtPt}$ values (1000 ÷ 9000 Hz) are attributable to M–M bond interactions. On the other hand, this trend is not always observed, and the presence of M–M bond should be confirmed by using other methods (*i.e.* determining the solid state structure by crystallographic studies).

In this Thesis, both tri- and hexanuclear platinum clusters have been prepared. As previously described, the trinuclear compounds, with general formula [$Pt_3(\mu$-$PBu^t_2)_3(CO)_2X$], have an internal triangular core of platinum atoms and three bridging di-*t*-butylphosphido ligands. Due to the presence of the platinum atoms, the ^{31}P and ^{195}Pt NMR final spectra are obtained by the sum of the subspectra due to eight isotopomers with different ^{195}Pt content, whose composition and natural abundance are reported in Figure 63.

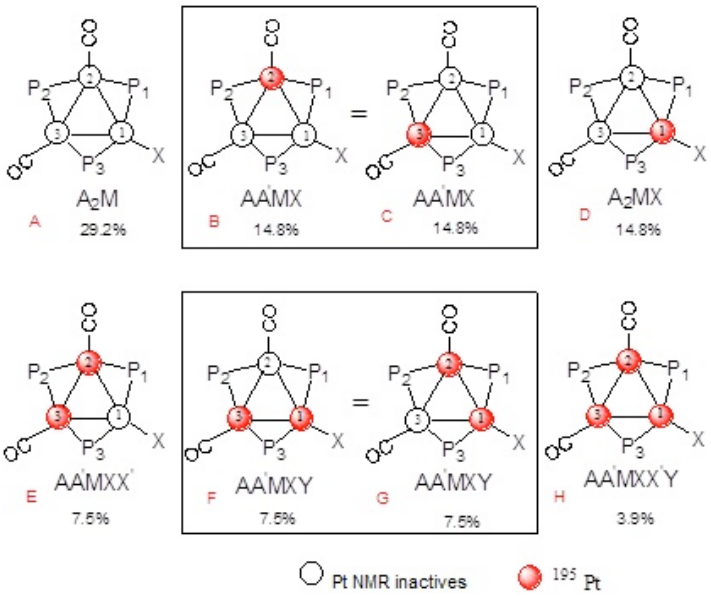

Figure 63. Trinuclear clusters isotopomers.

The signals observed in the $^{31}P\{^{1}H\}$ and $^{195}Pt\{^{1}H\}$ NMR spectra of the triangular clusters prepared in this Thesis, have a characteristic shape consistent with the expected spin system AA'MXX'Y (AA'= P_1P_3, M = P_2, XX' = Pt_2Pt_3, Y = Pt_1), defined by four chemical shift values and nine coupling constants.

The $^{31}P\{^{1}H\}$ NMR spectra show two signals whose central lines, due to isotopomer **A**, are a doublet and a triplet, in accord with the presence of two equivalent phosphides (P_1, P_3) coupled to a third one (P_2). Each signal is flanked by satellites due to the presence of isotopomers **B**-**H**. Isotopomers **B** and **C** (AA'MX spin system, A, A' = P_1, P_3; M = P_2; X = Pt_2 (in ***B***) or Pt_3 (in ***C***)] are equivalent and give the more intense satellites (total abundance 29.6%). The M part can be analyzed under first-order approximation and gives a doublet of triplets while the A part is not first order. The first order subspectrum due to isotopomer **D** (A_2MX, A = P_1, P_3; M = P_2; X = Pt_1; 14.8%) consists of a doublet of doublets (part A) and a doublet of triplets (part M). Finally, the signal is completed by the presence of weak satellites due to the isotopomers **E**-**H**.

The $^{195}Pt\{^{1}H\}$ NMR spectra show two signals respectively assigned to the two equivalent Pt_2 and Pt_3 nuclei and to the Pt_1 nucleus bonded to the X ligand. The first signal is a doublet of doublet of doublets, due to isotopomers **B** and **C**; the second is a doublet of triplets due to isotopomer **D**; moreover, each signal is complicated by the presence of weaker lines due to the less abundant isotopomers **E-H**. Generally, the values of δ_P and δ_{Pt} and many of the nine coupling constants which determine the shape of both the $^{31}P\{^{1}H\}$ and the $^{195}Pt\{^{1}H\}$ NMR spectra can be obtained directly from the spectra and the remaining ones are quite easily obtained by spectral simulation.

Together with the ^{31}P and ^{195}Pt, the ^{1}H NMR spectra may provide important structural information, in particular, when two P nuclei, with alkyl substituents which have protons bonded to the α or β carbon atoms (*i. e.* R = Me, Bu^t), are coordinated to the same platinum center (both in mononuclear and polynuclear systems).

When the two P nuclei are in cis or pseudo-cis position (PMP angle *ca*. 90°, Figure 64), the ^{1}H NMR spectrum appears as a doublet, due to the coupling between the alkyl protons with the P nucleus to which the alkyl chain is directly bonded ($^{2}J_{HP}$ when R = Me and $^{3}J_{HP}$ when R = Bu^t).

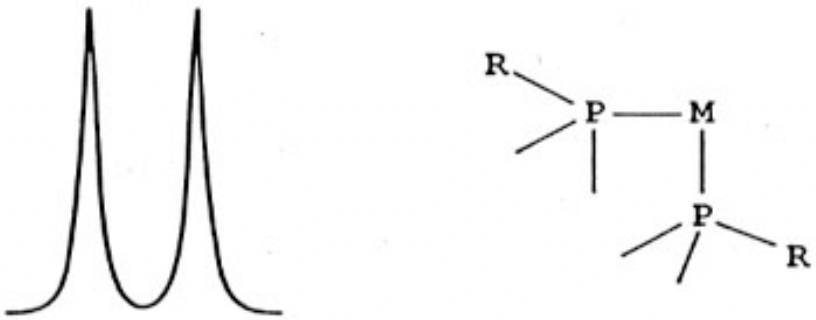

Figure 64. Alkyl protons signal in the ^{1}H NMR spectrum for cis or pseudo-cis systems.

When the two nuclei are in trans or pseudo-trans position (PMP angle *ca*. 180°, Figure 65), the P-P coupling constant becomes enough large to affect the ^{1}H NMR spectrum of the alkyl protons. In this case, the spectrum appears as a triplet, called *virtual triplet*, and the gap between the triplet lines gives the sum of the couplings between the alkyl protons and both the P nuclei ($^{2}J_{HP} + {}^{4}J_{HP}$ when R = Me and $^{3}J_{HP} + {}^{5}J_{HP}$ when R = Bu^{t}).

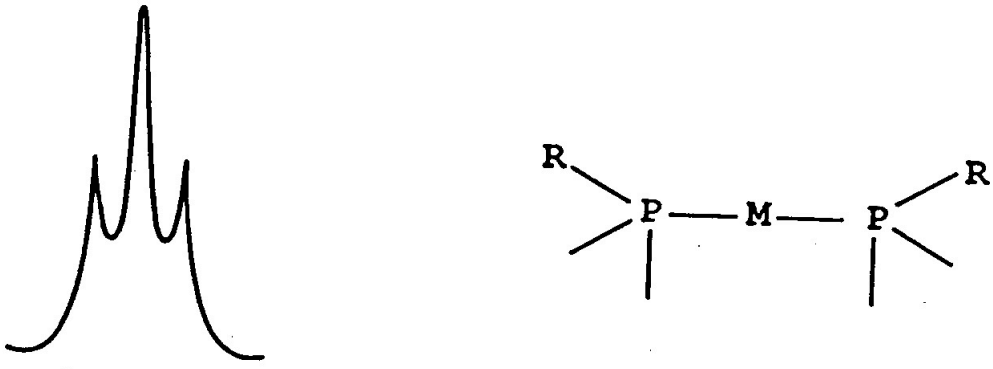

Figure 65. Alkyl protons signal ^{1}H NMR spectrum for trans or pseudo-trans systems.

Finally, intermediate values of the P-P coupling constants correspond to a spatial arrangement of the two phosphorus nuclei with PMP angle between 90° and 180° (Figure 66). In this case, the spectrum shows signals intermediate between a doublet and a virtual triplet (Figure 66); the gap between the lines is due to the sum of the coupling between the alkyl protons and both the P nuclei, as observed in the trans and pseudo-trans systems).

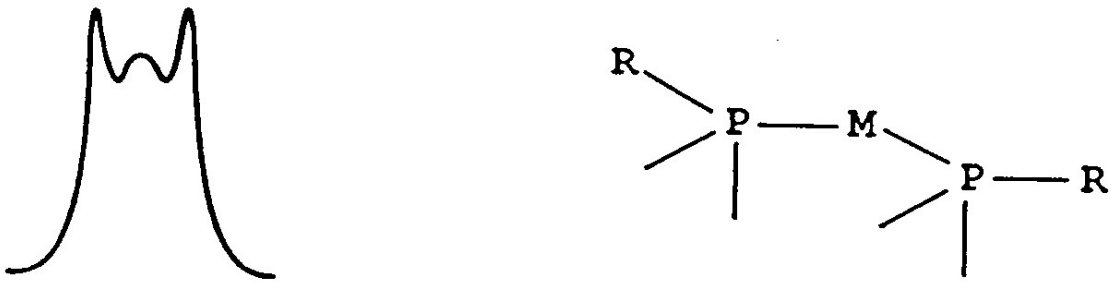

Figure 66. Alkyl protons signal ^{1}H NMR spectrum for intermediate systems.

The ^{1}H NMR spectra of the hexanuclear clusters prepared in this Thesis [general structure $[Pt_6(\mu\text{-}PBu^t_2)_4(CO)_4L_2]^{n+}$ (n = 0, 2; Figure 67)] show one signal due to the *t*-butyl protons of the phosphido ligands similar to the one illustrated in Figure 66, where the peak separation is attributed to the sum of the two coupling constants $^{3}J_{HP} + {}^{5}J_{HP}$.

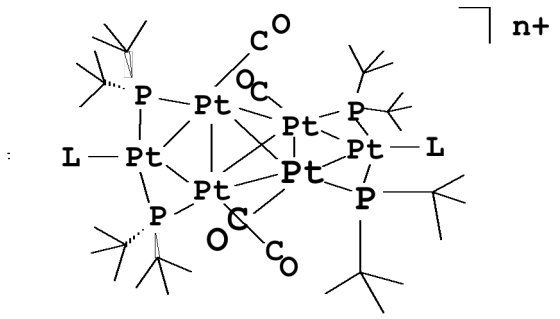

Figure 67. General structure of $[Pt_6(\mu\text{-}PBu^t_2)_4(CO)_4L_2]^{n+}$.

The $^{31}P\{^{1}H\}$ and $^{195}Pt\{^{1}H\}$ NMR spectra result from the sum of the subspectra arising from 22 groups of non-equivalent isotopomers (total number $2^6 = 64$), and nearly all the subspectra cannot be interpreted under simple first-order approximation. Except in some favorable case in which some signal is deceptively simple, in general the signals are predictably very complex and quite impossible to simulate. Both spectra, however, are useful for the characterization. In fact, the shape of the signal remains substantially unchanged when two new ligands are coordinated to the two apical platinum centers; on the contrary, the signal would drastically change if one or more CO coordinated to the internal platinum atoms were substituted. In the $^{31}P\{^{1}H\}$ of symmetrical $\{Pt_6\}X_2$ clusters the four P atoms are isochronous and therefore give only one signal (a central

singlet flanked by a complex set of Pt satellites), while unsymmetrical $\{Pt_6\}XY$ derivatives give two different signals. Analogously, the $^{195}Pt\{^1H\}$NMR spectra of $\{Pt_6\}X_2$ derivatives show two signals respectively attributed, basing on the relative intensities, to the four inner and to the two apical platinum centers; these signals are again doubled in unsymmetrical $\{Pt_6\}XY$ systems.

6 Appendix B

6.1 Cyclovoltammetric evaluation of intramolecular electronic communication.

The electrochemical behavior of the organometallic compounds depends on the complex nuclearity, on the nature of the metal centers and on the ligands features.[135]

The reduction and/or oxidation potentials can be quickly determined by cyclic voltammetry.[136] This analytic method allows to measure the current as a function of the potential applied to a stationary electrode, under full polarization conditions; the applied potential, which has the shape of a triangular wave, is, at first, linearly varied from the initial E_i to the final E_f value, at constant speed. Successively, the potential scan direction is inverted in order to return to the initial potential value (Figure 68).

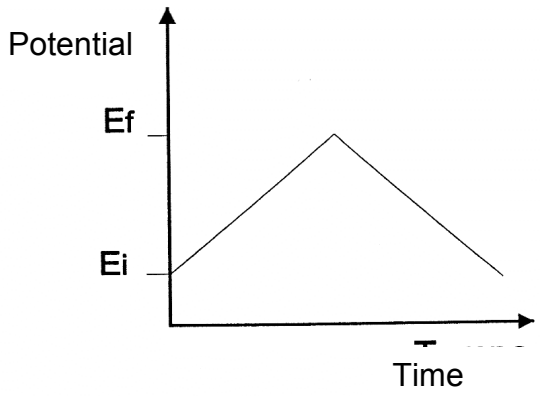

Figure 68. Potential scan *vs*. time in a cyclovoltammetric experiment.

In the cyclovoltammetric experiments, three different electrodes are used: a) the working electrode, made of inert materials (generally Pt, Au, and Hg), is the electrode on which the reactions occur; b) the reference electrode, with a well-known potential, is the internal reference; c) the auxiliary (or counter) electrode, generally a platinum wire, which ensure that the current does not pass through the reference electrode, thus preventing that the potential of the latter is interfered.

The voltammogram has a double wave shape (Figure 69), one for the anodic process (oxidation) and one for the cathodic process (reduction). Significant parameters in cyclic voltammetry are shown in Figure 69.

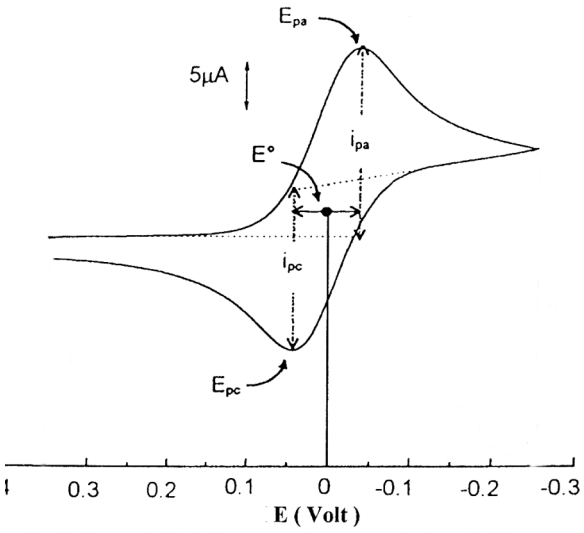

- E_{pc}: cathodic peak potential
- E_{pa}: anodic peak potential
- I_{pc}: cathodic current
- I_{pa}: anodic current

Figure 69. Basic parameters for a cyclic voltammogram.

Depending on the shape of the voltammogram it is possible to determine if the process is reversible, irreversible or quasi-reversible. The redox process reversibility can be chemical and electrochemical.

A general reduction process:

$$Ox + ne^- \longrightarrow Red$$

is chemically reversible when the process is not followed by chemical reactions; in this case the current intensity of the forward peak is the same as that of the return peak. The process is chemically irreversible when it is followed by chemical reactions; in this case the initial species disappear in favor of the formation of new compounds and the return peak in the voltammogram is absent. However, there could be competition between the rate of the chemical reaction which follows the redox process and the rate of potential scanning; in this case the process is chemically quasi-reversible and the return peak will be more and more intense upon increasing the scan potential rate.

Instead, the electrochemical reversibility concerns rate of electron transfer to the electrode: an electrode process is defined as electrochemically reversible when the electron transfer is fast enough to preserve the redox couple at the equilibrium, during the scan potential. In this case, the i_{pa}/i_{pc} ratio is *ca*. 1 and it is independent from the scan rate; moreover, the difference between the cathodic and the anodic peak potential, ΔE_p, is 59/*n* mV (where *n* is the number of the electrons involved in the redox process).

In the case of an electrochemically quasi-reversible process, the value of ΔE_p is higher than 59 mV and increases with the scan rate, while the i_{pa}/i_{pc} ratio commonly remains *ca*. 1. Finally, in an electrochemically irreversible process, the E_p value changes with the scan rate and the return peak is generally absent (Figure 70).

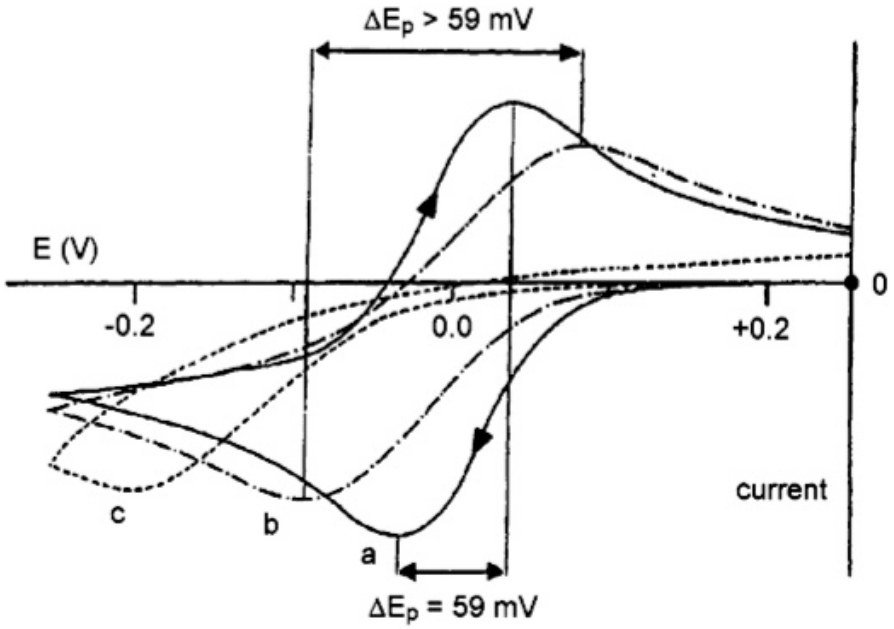

Figure 70. Qualitative behavior of the cyclic voltammetric profiles for a reduction process having features of: a) reversibility, b) quasi-reversibility and c) irreversibility.

The cyclovoltammetric technique allows to preliminarily evaluate the presence of electronic communication between two metal centers linked by a spacer.

As an example we consider the voltammetric profile after the removal of two electrons from a compound containing two metal centers, M, connected by an organic spacer. In the presence of electronic communication between the two metal atoms, the voltammogram would show two different peaks, E^1_{pa} and E^2_{pa}, originated by two subsequent monoelectronic oxidation processes (profile a, Figure 71). In fact, the

removal of the first electron from one metal center causes electron density variations, affecting the oxidation potential of the second metal center. When the spacer behaves as an insulator, the profile shows only one peak, due to the concurrent oxidation of both the metal atoms (bielectronic process, profile b, Figure 71).

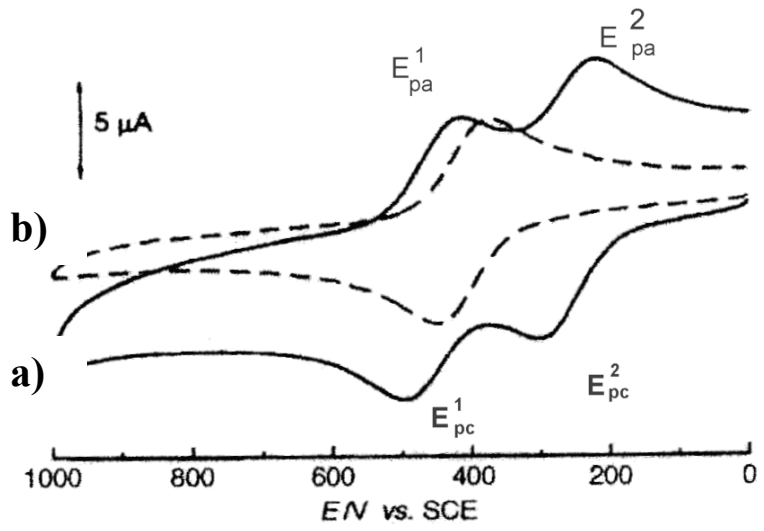

Figure 71. Representation of the cyclic voltammetric profiles expected for a dinuclear compound in which two metal centers are linked by a spacer, if electronic communication between them is present a) or not b).

The interaction extent between the metal centers is generally evaluated by measuring the equilibrium constant, K_{com}. In the dinuclear complex **I** in the example of equation (1), the removal of one electron from one of the two metal centers leads to the formation of a mixed valence complex (**MV**), which, successively, undergoes a further monoelectronic oxidation, generating the bi-oxidized species **II**.

$$\underset{\mathbf{I}}{M^{n}\text{–}\square\text{–}M^{n}} \underset{+e^-}{\overset{\mathbf{E^\circ_1}\ -e^-}{\rightleftharpoons}} \underset{\mathbf{MV}}{M^{n}\text{–}\square\text{–}M^{n+1}} \underset{+e^-}{\overset{\mathbf{E^\circ_2}\ -e^-}{\rightleftharpoons}} \underset{\mathbf{II}}{M^{n+1}\text{–}\square\text{–}M^{n+1}} \qquad (1)$$

The **I**, **II** and **MV** species are correlated by the *comproportionation* equilibrium, shown in equation (2), whose equilibrium constant, K_{com} [defined in equation (3)], is a function

of the difference between the potentials of the two redox processes reported in equation (1), ($\Delta E° = E°_2 - E°_1$).

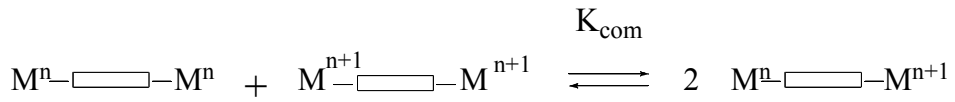

(2)

$$K_{com} = e^{\Delta E°F/RT} \qquad (3)$$

The concentration of the mixed valence specie **MV** tends to zero when $\Delta E°$ decreases and the electronic communication is efficient when high $\Delta E°$ (and, therefore, K_{com}) values are observed; in these cases it is generally possible to isolate the **MV** species.

The spectroscopic investigation of mixed-valence compounds in the near IR region represents an alternative way to get information about the electron transfer mechanisms and about the ability of the bridge to mediate electron transfer. In the near infrared region, a new band appears for the mixed-valence compound, which is absent in the neutral and in the dioxidized compounds. The band may be assigned to the intervalence charge transfer transition (IVCT) by the low energy and the large band-width. Such band occurs in all the solvents in which the system is soluble, and its position is independent of the solvent, suggesting that the compound can be classified as belonging to the Robin-Day's class III. According to this classification,[137] all the mixed-valence compounds may be classified in three different classes based on the intramolecular electronic delocalization between the two sites.

Class I: the two sites behave as independent. The physical and electronic properties of the compound are substantially identical to that of the isolated components. The system may be described as "valence trapped". No intervalence band is present.

Class II: the two sites interact weakly, there is partial electronic delocalization but the two sites are still distinguishable. One or more intervalence bands are present in the visible or near infrared region of the spectrum. The electrons are not equally delocalized between the two sites.

Class III: the electronic delocalization is maximum, the two sites result undistinguishable and the electrons are equally delocalized. Physical and electronic

properties and spectra result totally different from those exhibited by the two separated components. For example, in the Prussian Blue $Fe^{III}_4[Fe^{II}(CN)_6]_3$ the colour is totally different from that of the typical complexes of Fe(II) and Fe(III), respectively green and light yellow.

Anyway, the Robin and Day classification is not so strict as depicted above. For some compounds, especially those with an appreciable electronic communication between the donor and the acceptor sites, it is not so easy to classify them as a Class II or a Class III member. As pointed out by Meyer,[138] many mixed valence compounds may be classified in a fourth class which is intermediate between Class II and Class III. Such compounds exhibit some behavior typical of delocalized compounds and other peculiar of localized systems.

References and notes.

[1] a) J.A. Bertrand, F. A. Cotton, W. A. Dollase, *J. Am. Chem. Soc.*, **1963**, *85*, 1349. b) J. A. Bertrand, F.A. Cotton, W. A. Dollase, *Inorg. Chem.*, **1964**, *2*, 1166. c) F. A. Cotton, *Inorg. Chem.*, **1964**, *3*, 1217. d) F. A. Cotton, *Inorg. Chem.*, **1965**, *4*, 334. e) F. A. Cotton, C. B. Harris, *Inorg. Chem.*, **1965**, *4*, 55.

[2] a) G. Gonzales-Moraga, *Cluster chemistry*, Sprinter-Verlag, Berlin, **1993**. b) F. A. Cotton, G. Wilkinson, *Advanced Inorganic Chemistry*, Fifth Edition, John Wiley & Sons, New York, **1988**. c) C. Elschenbroich, A. Valzer, *Organometallics, A concise introduction*, VHC Publischers, Cambridge, **1989**. d) R. H. Crabtree, *The Organimetallic Chemistry of Transition Metals*, Second edition, John Wiley & Sons, New York, **1994**.

[3] M. H. Chisholm, Ed., *Early transition metal clusters with π-donor ligands*, VCH Publisher, Inc., New York, NY; Winheim, Germany and Cambridge, England.

[4] M. H. Chisholm, A. N. Machintosh, *Chem. Rev.*, **2005**, *105*, 2949.

[5] D. M. Mingos, D. J. Wales, *J. Organomet. Chem.*, **1990**, *349*, 679.

[6] a) K. Wade, *J. Chem. Soc. Chem. Comm.*, **1971**, *15*, 792. b) R. Manson, K. M. Thomas, D. M. P. Mingos, *J. Am. Chem. Soc.*, **1973**, *95*, 3802. c) D. M. P. Mingos, *Acc. Chem. Res.*, **1984**, *17*, 311. d) D. M. P. Mingos, *Polyhedra*, **1984**, *3*, 1289. e) K. P. Hall, D. M. P. Mingos, *Prog. Inorg. Chem.*, **1984**, *32*, 237. f) D. M. P. Mingos, M. J. Watson, *Adv. Inorg. Chem.*, **1992**, *39*, 327.

[7] J. Farges, M. F. de Feraudy, B. Raoult, G. Torchet, *J. Chem. Phys.*, **1986**, *84*, 3491.

[8] a) J. M. Bemis, L. F. Dahl, *J. Am. Chem. Soc.*, **1997**, *119*, 4545-4546. b) C. Femoni, M. C. Iapalucci, G. Longoni, P. H. Svensson, *Chem. Comm.*, **2004**, 2274. c) N. T. Tran, D. R. Powell, L. F. Dahl, *Chem. Eur. J.*, **2004**, *10*, 2318-2326. d) E. G. Mednikov, S. A. Ivanov, L. F. Dahl, *Angew. Chem. Int. Ed.*, **2003**, 323. e) A. Schnepf, R. Kappe, E. Weckert, H. Schnockel, *Chem. Eur. J.*, **2004**, *10*, 1977.

[9] N. T. Tran, D. R. Powell, L. F. Dahl, *Angew. Chem., Int. Ed.*, **2000**, *39*, 4121.

[10] a) F. Fabrizi de Biani, C. Femoni, M. C. Iapalucci, G. Longoni, P. Zanello, A. Cerotti, *Inorg. Chem.*, **1999**, *28*, 179. b) G. Schmid, *Chem. Rev.*, **1992**, *92*, 1709-1727.

[11] a) J. F. Berry, F. A. Cotton, T. Lu, C. A. Murillo, B. K. Roberts, X. Wang, *J. Am. Chem. Soc.* **2004**, *126*, 7082. b) F. A. Cotton, L. M. Daniels, C. A. Murillo, I. Pascual, *J. Am. Chem. Soc.,* **1997**, *119*, 10223. c) F. A. Cotton, L. M. Daniels, C. A. Murillo, I. Pascual, *Inorg. Chem. Commun.,* **1998**, *1*, 1. d) R. Clerac, F. A. Cotton, L. M. Daniels, K. R. Dunbar, K. Kirschbaum, C. A. Murillo, A. A. Pinkerton, A. J. Schultz, X. Wang, *J. Am. Chem. Soc.,* **2000**, *122*, 6226. e) R. Clerac, F. A. Cotton, L. M. Daniels, K. R. Dunbar, C. A. Murillo, I. Pascual, *Inorg. Chem.,* **2000**, *39*, 748. f) J. F. Berry, F. A. Cotton, C. S. Fewox, T. Lu, C. A. Murillo, X. Wang, *Dalton Trans.,* **2004**, 2297. g) J. F. Berry, F. A. Cotton, C. A. Murillo, *Dalton Trans.*, **2003**, 3015-3021. h) F. A. Cotton, *Inorg. Chem.*, **1998**, *37*, 5710. i) J. F. Berry, F. A. Cotton, C. A. Murillo, *Organometallics,* **2004**, *23*, 2503. l) J. F. Berry, F. A. Cotton, C. A. Murillo, B. K. Roberts, *Inorg. Chem*., **2004**, *43*, 2277. m) J. F. Berry, F. A. Cotton, P. Lei, T. Lu, C. A. Murillo, *Inorg. Chem*., **2003**, *42*, 3534.

[12] a)Y.-H. Chen, C.-C. Lee, C.-C. Wang, G.-H. Lee, S.-Y. Lai, F.-Y. Li, C.-Y. Mou, S.-M. Peng, *Chem. Commun.*, **1999**, 1667. b) S.-Y. Lai, T.-W. Lin, Y.-H. Chen, C.-C. Wang, G.-H. Lee, M.-H Yang, M.-K. Leung, S.-M. Peng, *J. Am. Chem. Soc.,* **1999,** *121,* 250. c) T.-B. Tsao, G.-H. Lee, C.-Y. Yeh, S.-M. Peng, *Dalton Trans.*, **2003**, 1465-1471. d) C.-C. Wang, W.-C. Lo, C.-C. Chou, G.-H. Lee, J.-M. Chen, S.-M. Peng, *Inorg. Chem.,* **1998,** *37,* 4059. e) S.-Y. Lin, I.- W. P. Chen, C.-H. Chen, M.-H. Hsieh, C.-Y. Yeh, T.-W. Lin, Y.-H. Chen, S.-M. Peng, *J. Phys. Chem. B,* **2004**, *108*, 959. f) S.-M. Peng, C.-C. Wang, Y.-L. Jang, Y.-H. Chen, F.-Y. Li, C.-Y. Mou, M.-K. Leung, *J. Magn. Magn. Mater.,* **2000**, *209*, 80. g) C. Y. Yeh,; Y.-L. Chiang, G.-H. Lee, S.-M. Peng, *Inorg. Chem*., **2002**, *41*, 4096. h) S.-J. Shieh, C.-C. Chou, G.-H. Lee, C.-C. Wang, S.-M. Peng, *Angew. Chem., Int. Ed. Engl*., **1997**, *26*, 56. i) J.-T. Sheu, C.-C. Lin, I. Chao, C.-C.Wang, S.-M. Peng, *J. Chem. Soc., Chem. Commun.,* **1996**, 315. l) E.-C. Yang, M.-C. Cheng, M.-S. Tsai, S.-M. Peng, *J. Chem. Soc., Chem. Commun.,* **1994**, 2377.

[13] a) J. K. Bera; Kim R.Dunbar, *Angew. Chem. Int. Ed.*, **2002**, *41*, 4453. b) E. Goto, R. A. Begum, S. Zhan, T. Tanase, K. Tanigaki, K. Sakai, *Angew. Chem. Int. Ed.*, **2004**, *43*,

5029. c) T. Zhang, M. Drouin, P. D. Harvey, *Inorg. Chem.,* **1999**, *38,* 957. d) C. E. Buss, K. R. Mann, *J. Am. Chem. Soc.,* **2002**, *124*, 1031. e) K. Matsumoto, S. Arai, M. Ochiai, W. Chen, A. Nakata, H. Nakai, S. Kinoshita, *Inorg. Chem.,* **2005**, *44*, 8552. f) T. Murahashi, T. Uemura, H. Kurosawa, *J. Am. Chem. Soc.,* **2003**, *125*, 8436. g) K. Mashima, A. Fukumoto, H. Nakano, Y. Kaneda, K. Tani, A. Nakamura, *J. Am. Chem. Soc.,* **1998**, *120,* 12151. h) B. E. Villarroya, C. Tejel, M.-M. Rohmer, L. A. Oro, M. A. Ciriano, M. Bénard, *Inorg. Chem.,* **2005**, *44*, 6536.

[14] a) S. Zacchini, *Eur. J. Inorg. Chem.*, **2011**, 4125-4145. b) C. Femoni, M. C. Iapalucci, G. Longoni, C. Tiozzo, J. Wolowska, S. Zacchini, E. Zazzaroni, *Chem. Eur. J.*, **2007**, *13*, 6544-6554.

[15] F. Fabrizi de Biani, C. Femoni, M. C. Iapalucci, G. Longoni, P. Zanello, A. Ceriotti, *Inorg. Chem.,* **1999**, *38*, 3721.

[16] a) C. Femoni, M. C. Iapalucci, F. Kaswalder, G. Longoni, S. Zacchini, *Coord. Chem. Rev.,* **2006**, *250*, 1580. b) D. Collini, C. Femoni, M. C. Iapalucci, G. Longoni, P. H. Svensson, P. Zanello, *Angew. Chem. Int. Ed.* **2002**, *41*, 3685.

[17] a) M. I. Bruce, N. N. Zaitseva, B. K. Nicholson, B. W. Skelton, A. H. White *J. Organomet. Chem.* **2008**, *693*, 2887. b) M. I. Bruce, M. L. Cole, C. R. Parker, B. W. Skelton, A. H. White *Organometallics* **2008**, *27*, 3352. c) M. I. Bruce, M. Gaudio, G. Melino, N. N. Zaitseva, B. K. Nicholson, B. W. Skelton, A. H. White *J. Cluster Sci.* **2008**, *19*, 147. d) M. I. Bruce, B. W. Skelton, A. H. White, N. N. Zaitseva *Organometallics* **2006**, *25*, 4817. e) M. I. Bruce, N. N. Zaitseva, P. J. Low, B. W. Skelton, A. H. White *J. Organomet. Chem.* **2006**, *691*, 4273. f) A. B. Antonova, M. I. Bruce, P. A. Humphrey, M. Gaudio, B. K. Nicholson, N. Scoleri, B. W. Skelton, A. H. White, N. N. Zaitseva, *J. Organomet. Chem.* **2006**, *691*, 4694. g) M. I. Bruce, N. N. Zaitseva, B. W. Skelton *J. Organomet. Chem.* **2006**, *691*, 759. h) M. I. Bruce, P. A. Humphrey, G. Melino, B. W. Skelton, A. H. White, N. N. Zaitseva, *Inorg. Chim. Acta* **2005**, *358*, 1453. i) A. B. Antonova, M. I. Bruce, B. G. Ellis, M. Gaudio, P. A. Humphrey, M. Jevric, B. K. Nicholson, G. J. Perkins, B. W. Skelton, B. Stapleton, A. H. White, N. N. Zaitseva, *Chem. Commun.* **2004**, 960. j) M. I. Bruce, M. E. Smith, N. N. Zaitseva, B. W. Skelton, A. H. White *J. Organomet. Chem.* **2003**, *670*, 170. k) M. I. Bruce, J.-F. Halet, S. Kalhal, P. J. Low, B. W. Skelton, A. H. White *J. Organomet.*

Chem. **1999**, *578*, 155. l) M. Akita, M. Terada, N. Ishii, H. Hirakawa, Y. Moro-Oka *J. Organomet. Chem.* **1994**, *473*, 175. m) S. M. Elder, B. H. Robinson, J. Simpson *J. Organomet. Chem.* **1990**, *398*, 165. n) R. J. Dellaca, B. R. Penfold *Inorg. Chem.* **1971**, *10*, 1269.

[18] (a) B. Ahrens, L. P. Clarke, N. Feeder, M. S. Khan, P. Li, J. N. Martin, P. R. Raithby *Inorg. Chim. Acta* **2008**, *361*, 3117. (b) N. T. Lucas, M. G. Humphrey, A. C. Willis *Acta Crystallogr., Sect. E: Struct. Rep. Online* **2005**, *61*, m463. (c) E. G. A. Notaras, N. T. Lucas, M. G. Humphrey, A. C. Willis, A. D. Rae *Organometallics* **2003**, *22*, 3659. (d) N. T. Lucas, E. G. A. Notaras, M. P. Cifuentes, M. G. Humphrey *Organometallics* **2003**, *22*, 284. (e) N. T. Lucas, E. G. A. Notaras, S. Petrie, R. Stranger, M. G. Humphrey *Organometallics* **2003**, *22*, 708. (f) R. D. Adams, O.-S. Kwon, B. Qu, M. D. Smith *Organometallics* **2001**, *20*, 5225.

[19] (a) L. Zhao, T. C. W. Mak, *Inorg. Chem.* **2009**, *48*, 6480. (b) L. Zhao, M. Du, T. C. W. Mak *Chem.Asian J.* **2007**, *2*, 1240. (c) M. I. Bruce, N. N. Zaitseva, B. W. Skelton, A. H. White *J. Organomet. Chem.* **2005**, *690*, 3268. (d) M. I. Bruce, B. G. Ellis, B. W. Skelton, A. H. White *J. Organomet. Chem.* **2000**, *607*, 137. (e) M. I. Bruce, P. J. Low, N. N. Zaitseva, S. Kalhal, J.-F. Halet, B. W. Skelton, A. H. White *J. Chem. Soc., Dalton Trans.* **2000**, 2939. (f) C. J. Adams, M. I. Bruce, E. Horn, B. W. Skelton, E. R. T. Tiekink, A. H. White *J. Chem. Soc., Dalton Trans.* **1993**, 3299.

[20] a) V. Calvo-Perez, M. Shang, G. P. A. Yap, A. Rheingold, T. P. Fehlner, *Polyhedron*, **1999**, *18*, 1869. b) M. I. Bruce, N. N. Zaitseva, B. W. Skelton, *J. Organomet. Chem.*, **2006**, *691*, 759.

[21] a) W. –Y. Yeh, T. W. Shiue, S. –M. Peng, G. –H. Lee, Organometallics, **2003**, 22, 2990. b) L. P. Clarke, J. M. Cole, J. E. Davies, A. French, D. F. Koentjono, P. R. Raithby, New J. Chem., **2005**, 29, 145. c) R. D. Adams, B. Qu, M. D. Smith, Organometallics, **2002**, 21, 4847. d) S. –G. Ang, X. Zhong, H. –G. Ang, Inorg. Chem., **2002**, 41, 3791. e) J. –P. K. Lau, W. T. Wong, Inorg. Chim. Acta, **2006**, 369, 3632.

[22] a) Y. –H. Tang, Y. –Y. Qin, Z. –J. Li, J. Zang, Y. Kang, R. –F. Hu, Y. –H. Wen, J. –K. Cheng, Y. –G. Yao, Bull. Chem. Soc. Japan, **2005**, 78, 626. b) G. Sakane, H. Kawasaki, T. Oomori, M. Yamasaki, H. Adachi, T. Shibahara, J. Cluster Sci., **2002**, 13, 75. c) V. P. Fedin, M. Sokolov, G. J. Lamprecht, R. Hernandez-Molina, M. –S. Seo, A.

V. Virovets, W. Clegg, A. G. Sykes, Inorg. Chem., **2001**, 40, 6598. d) R. –M. Yu S. –F., Lu, X. –Y. Huang, Q. J. Wu, J. –Q. Huang, Inorg. Chem., **1999**, 38, 3313.

[23] a) S. Sin, F. Di Salvo, *Chem. Mater.,* **2002**, *14*, 3448. b) S. –B. Yu, M. Droege, S. Downey, B. Segal, W. Newcomb, T. Sanderson, S. Crofts, S. Suravajjala, E. Bacon, W. Earley, D. Delecki, A. D. Watson, *Inorg. Chem.,* **2001**, *40*, 1576. c) M. J. Almond, M. G. B. Drew, H. Redman, D. A. Rice, *Polyhedron,* **2000**, *19*, 2127. d) M. N. Sokolov, A. V. Virovets, D. N. Dybtsev, O. A. Gerasko, V. P. Fedin, R. Hernandez-Molina, W. Clegg, A. G. Sykes, *Angew. Chem. Int. Ed.,* **2000**, *39*, 1659.

[24] a) M. I. Bruce, P. A. Humphrey, G. Melino, B. W. Skelton, A. H. White, N. N. Zaitseva, *Inorg. Chim. Acta,* **2005**, *358*, 1453. b) A. R. O'Connor, C. Nataro, A. L. Rheingold, *J. Organomet. Chem.,* **2003**, *679*, 72. c) K. M. Hanif, S. E. Kabir, M. A. Mottalib, M. B. Hursthouse, K. M. A. Malik, E. Risenberg, *Polyhedron,* **2000**, *19*, 1073. d) R. Dorta, H. Stoeckli-Evans, U. Bodensieck, G. Suss/Fink, *J. Organomet. Chem.,* **1998**, *553*, 307. e) P. M. Van Calcar, M. M. Olmstead, A. L. Balch, *Inorg. Chim. Acta,* **1998**, *270*, 28.

[25] a) M. I. Bruce, B. C. Hall, B. W. Skelton, M. E. Smith, A. H. White, *J. Chem. Soc., Dalton Trans.,* **2002**, 995. b) V. W.-W Yam, W. K.-M. Fung, K.-K. Cheung, *Chem. Commun.,* **1997**, 963.

[26] M.Izataki, O. Kitami, M. Tanabe, Y. Nishihara, K. Osakada, *J. Organomet. Chem.*, **2005**, *690*, 3957.

[27] a) L. Hao, G. J. Spivak, J. Xiao, J. J. Vittal, R. J. Puddephatt, *J. Am. Chem. Soc.,* **1995**, *117*, 7011. b) L. Hao, J. J. Vittal, R. J. Puddephatt, *Organometallics,* **1996**, *15*, 3115. c) L. Hao, J. J. Vittal, R. J. Puddephatt, *Inorg. Chem.,* **1996**, *35*, 269. d) G. J. Spivak, J. J. Vittal, R. J. Puddephatt, *Inorg. Chem.,* **1998**, *37*, 5474.

[28] a) D. G. Holah, A. N. Hughes, E. Krysa, V. R. Magnuson, *Organometallics*, **1993**, *12*, 4721. c) P.- C. Huang, F.- E. Hong, *J. Organomet. Chem.*, **2009**, *694*, 113. d) R. Vilar, S. E. Lawrence, S. Menzer, D. M. P. Mingos, D. J. Williams, *J. Chem. Soc., Dalton Trans.*, **1997**, 3305. e) D. Fenske, H. Fleischer, H Krautscheid, J. Magull, C. Oliver, S. Weisgerber, *Z. Naturforsch., B:Chem. Sci.*, **1991**, *46*, 1384. f) E. G. Mednikov, N. K. Eremenko, Yu. L. Slovokhotov, Yu. T. Struchkov, *Metalloorg. Khim. (Organomet. Chem. (USSR))*, **1989**, *2*, 1289.

[29] J. C. Salsman, C. P. Kubiak, Chapter 5 from *Spectroelectrochemistry,* edited by W. Kaim, A. Klein, Royal Society of Chemistry, Cambridge, **2008**.

[30] X. Lei, E. E. Wolf, T. P. Fehlner, *Eur. J. Inorg. Chem.,* **1998**, 1835.

[31] M. I. Bruce, N. N. Zaitseva, P. J. Low, B. W. Skelton, A. H. White, *J. Organomet. Chem.,* **2006**, *691*, 4273.

[32] a) U. Ritter, N. Winkhofer, R. Murugavel, A. Voigt, D. Stalke, H. W. Roesky, *J. Am. Chem. Soc.,* **1996**, *118*, 8580. b) R. L. Sturgeon, M. M: Olmstead, N. E. Shore, *Organometallics,* **1991**, *10*, 1649.

[33] a) N. T. Lucas, E. G. A. Notaras, M. P. Cifuentes, M. G. Humphrey, *Organometallics,* **2003**, *22*, 284. b) N. T. Lucas, E. G. A. Notaras, S. Petrie, R. Stranger, M. G. Humphrey, *Organometallics,* **2003**, *22*, 708. c) E. G. A. Notaras, N. T. Lucas, M. G. Humphrey, A. C. Willis, A. D. Rae, *Organometallics,* **2003**, *22*, 3659.

[34] a) B. K. Roland, H. D. Selby, M. D. Carducci, Z. Zheng, *J. Am. Chem. Soc.,* **2002**, *124*, 3222. b) J.-P. Lang, Q.-F. Xu, Z.-N. Chen, B. F. Abrahams, *J. Am. Chem. Soc.,* **2003**, *125,* 12682. c) R. C. Haushalter, *Angew. Chem., Int. Ed.,* **1985**, *24*, 432. d) R. D. Adams, D. Mannig, B. E. Segmuller, *Organometallics,* **1983**, *2*, 149. e) E. W. Ainscough, A. M. Brodie, R. K. Coll, A. J. A. Mair, J. M. Waters, *Inorg. Chim. Acta,* **1993**, *214*, 21. f) M. Ferrer, A. Julia, O. Rossell, M. Seco, M. A. Pelinghelli, A. Tiripicchio, *Organometallics,* **1997**, *16*, 3715. g) T. Shibahara, M. Sasaki, G. Sakane, *Inorg. Chim. Acta,* **1995**, *237*, 1. h) L. J. Arnold, K. M. Mackay, B. K. Nicholson, *J. Organomet. Chem.,* **1990**, *387*, 197.

[35] a) R. D. Archer, *Inorganic and Organometallic Polymers*, Wiley-VCH, **2001**. b) I. Manners, *Synthetic Metal-Containing Polymers*, Wiley-VCH, **2004**. c) D. Wöhrle, A. D. Pomogailo, *Metal Complexes and Metals in Macromolecules*, Wiley-VCH, **2003**. d) A. S. Abd-El-Aziz, C. E. Carraher Jr, C. U. Pittman Jr, M. Zeldin Eds, *Macromolecules Containing Metal and Metal-Like Elements*, Wiley-Interscience, **2006**.

[36] W.-M. Xue, F. E. Kühn, E. Herdtweck, Q. Li, *Eur. J. Inorg. Chem.*, **2001**, 213.

[37] a) R. Yoshida, T. Takahashi, T. Yamaguchi, H. Ichijo, *Adv. Mater.*, **1997**, *9*, 175-178. b) A. C. Arsenault, H. Mìguez, V. Kitaev, G. A. Ozin, I. Manners, *Adv. Mater.*, **2003**, *15*, 503-507.

[38] a) D. J. Caruana, A. Heller, *J. Am. Chem. Soc.,***1999**, *121*, 769-774. b) M. Albrecht, G. van Koten, *Adv. Mater.*, **1999**, *11*, 171-174. c) B. Wang, M. R. Wasielewski, *J. Am. Chem. Soc.*, **1997**, *19*, 12-21.

[39] a) A. N. Ajjou, H. Alper, *J. Am. Chem. Soc.*, **1998**, *120*, 1466-1468. b) T. J. Peckham, P. Nguyen, S. C. Bourke, Q. Wang, D. G. Harrison, P. Zoricak, C. Russel, L. M. Liable-Sands, A. L. Rheingold, A. J. Lough, I. Manners, *Organometallics*, **2001**, *20*, 3035-3043. c) C. Kollner, B. Pugin, A. Togni, *J. Am. Chem. Soc.*, **1998**, *120*, 10274-10275.

[40] A. M. Bradford, E. Kristof, M. Rashidi, D.-S. Yang, N. C. Payne, R. J. Puddephatt, *Inorg. Chem.*, **1994**, *33*, 2355-2363.

[41] B. F. G. Johnson, K. M. Sanderson, D. S. Shephard, D. Ozkaya, W. Zhou, H. Ahmed, M. D. R. Thomas, L. Gladden, M. Mantle, *Chem. Comm.*, **2000**,1317-1318.

[42] N. T. Lucas, M. G. Humprey, A. D. Rae, *Macromolecules*, **2001**, *34*, 6188-6195.

[43] F. Wang, Y.-H. Lay, M. Y. Han, *Org. Lett.*, **2003**, *5*, 4791-4794.

[44] F. L. Mulligan, D. C. Babbini, I. R. Davis, S. K. Hurst, G. S. Nichol, *Inorg. Chem.*, **2009**, *48*, 2708-2710.

[45] a) C. W. Allen, M. J. Bahadur, *Inorg. Organomet. Polym.,* **1998**, *8*, 23. b) B. S. Kang, D. H. Kim, T. S. Jung, E. K. Jang, Y. Pak, S. C. Shin, D.-S. Park, Y.-B. Shim, *Synth. Metals,* **1999**, *105*, 9. c) H. Kim, D.-S. Park, Y.-B. Shim, S. C. Shin, *J. Organomet. Chem.,* **2000**, *608*, 133. d) B. K. Roland, W. H. Flora, M. D. Carducci, N. R. Armstrong, Z. Zheng, *J. Clust. Sci.,* **2003**, *14*, 449. e) W. Y. Chan, S. B. Clendenning, A. Berenbaum, A. J. Lough, S. Aouba, H. E. Ruda, I. Manners, *J. Am. Chem. Soc.*, **2005**, *127*, 1765-1772. f) X. Yan, S. Cheng, L. Sun, X. Chen, J. Qin, *Polymer*, **2012**, *5*, 241-247.

[46] F. Fabrizi de Biani, A. Ienco, F. Laschi, P. Leoni, F. Marchetti, L. Marchetti, C. Mealli, P. Zanello, *J. Am. Chem. Soc.*, **2005**, *127*, 3076.

[47] P. Leoni, F. Marchetti, L. Marchetti, M. Pasquali, S. Quaglierini, *Angew. Chem., Int. Ed.*, **2001**, *40*, 3617.

[48] P. Leoni, S. Manetti, M. Pasquali, A. Albinati, *Inorg. Chem.*, **1996**, *35*, 6045.

[49] C. Cavazza, F, Fabrizi de Biani, T. Funaioli, P. Leoni, F. Marchetti, L. Marchetti, P. Zanello, *Inorg. Chem.*, **2009**, *48*, 1385-1397.

[50] a) V. W.-W. Yam, K. M.-C. Wong, *Top. Curr. Chem.*, **2005**, vol. 257, 1-32. b) N. J. Long, C. K. Williams, *Angew. Chem. Int. Ed.*, **2003**, *42*, 2586-2617. c) M. S. Khan, M.

R. A. Al-Mandhary, M. K. Al- Suti, F. R. Al-Battashi, S. Al-Saadi, B. Ahrens, J. K. Bjernemose, M. F. Raithby, M. Younus, N. Chawdhury, A. Kohler, E. A. Marseglia, E. Tedesco, N. Feeder, S. J. Teat, *Dalton Trans.*, **2004**, 2377-2385.

[51] a) W.-Y. Wong, *J. Inorg. Organomet. Polym. Mater.*, **2005**, *15*, 197. b) W.-Y. Wong, C.-L. Ho, *Coord. Chem. Rev.*, **2006**, 2627. c) W.-Y. Wong, Chapter 6 in *Frontiers in Transition Metal-Containing Polymers*, A. S. Abd-El-Aziz, I. Mannes Eds, Wiley-Interscience, **2007**, 369.

[52] a) F. Paul, C. Lapinte, *Coord. Chem. Rev.*, **1998**, *178-180*, 431. b) M. I. Bruce, *Coord. Chem. Rev.*, **1997**, *166*, 91. c) P. Blenkiron, G. D. Enright, P. J. Low, J. F. Corrigan, N. J. Taylor, Y. Chi, J.-Y. Saillard, A. J. Carty, *Organometallics*, **1998**, *17*, 2447.

[53] C. Bonaccorsi, F. Fabrizi de Biani, P. Leoni, F. Marchetti, L. Marchetti, P. Zanello, *Chem. Eur. J.*, **2008**, *14*, 847-856.

[54] P. Leoni, F. Marchetti, L. Marchetti, M. Pasquali, *Chem. Commun.*, **2003**, 2372.

[55] A. Albinati, P. Leoni, L. Marchetti, S. Rizzato, *Angew. Chem., Int. Ed.*, **2003**, *42*, 5990.

[56] P. Leoni, L. Marchetti, S. K. Mohapatra, G. Ruggeri, L. Ricci, *Organometallics*, **2006**, *25*, 4226-4230.

[57] a) S. K. Mohapatra, PhD Thesis, *Hindered Platinum Clusters as Organometallic Synthons*, University of Pisa, **2008**. b) V. Bonuccelli, Master Thesis, *Sintesi e caratterizzazione di sistemi contenenti due o più unità cluster esanucleari di platino*, University of Pisa, **2009**.

[58] A. Albinati, F. Fabrizi de Biani, P. Leoni, L. Marchetti, M. Pasquali, S. Rizzato, P. Zanello, *Angew. Chem., Int. Ed.*, **2005**, *44*, 5701-5705.

[59] E. Leary, H. Van Zalinge, S. J. Higgins, R. J. Nichols, F. Fabrizi de Biani, P. Leoni, L. Marchetti, P. Zanello, *Phys. Chem. Chem. Phys.*, **2009**, *11*, 5198.

[60] a) T. Hirao, *Coord. Chem. Rev.*, **2002**, *226*, 81-91. b) P. Zanello, R. Cini, A. Cinquantini, P. L. Orioli, *J. Chem. Soc., Dalton Trans.*, **1983**, 2159. c) T. Hirao, *Macromol. Symp.*, **2002**, *186*, 75. d) Q. Wang, L. Yu, *J. Am. Chem. Soc.*, **2000**, *122*, 11806. e) P. G. Pickup, *J. Mater. Chem.*, **1999**, *9*, 1641.

[61] *Unpublished results.*

[62] P. Leoni, L. Marchetti, V. Bonuccelli, S. K. Mohapatra, A. Albinati, S. Rizzato, *Chem. Eur. J.*, **2010**, *16*, 9468-9477.

[63] G. A. Lawrance, *Chem. Rev.*, **1986**, *86*, 17-33.

[64] a) P. J. Stang, M. H. Kowalski, M. D. Schiavelli, D. Longford, *J. Am. Chem. Soc.*, **1989**, *111*, 3347. b) J. Manna, C. J. Kuhel, J. A. Whiteford, P. J. Stang, D. C. Muddiman, S. A. Hofstadler, R. D. Smith, *J. Am. Chem. Soc.*, **1997**, *119*, 11611. c) M. Ferrer, A. Gutierrez, M. Mounir, O. Rossell, E. Ruiz, A. Rang, M. Engeser, *Inorg. Chem.*, **2007**, *46*, 3395. d) R. K. Merwin, D. M. Roddick, *J. Organom. Chem.*, **1995**, *487*, 69.

[65] A. J. De Koning, P. H. Budzelaar, J. Boersma, G. J. M. Van de Kerk, *J. Organomet. Chem.*, **1980**, *199*, 153-169.

[66] P. Krumholz, *J. Am. Chem. Soc.*, **1951**, *73*, 3487-3492.

[67] D. E. Richardson, H. Taube, *J. Am. Chem. Soc.*, **1983**, *105*, 40.

[68] a) J. Hershel, J. A. Krause Bauer, W. B. Connick, *Inorg. Chem.*, **2004**, *43*, 725-733. b) E. Tfouni, A. Marcos de Souza Macedo, L. Nunes Cardoso, K. Queiroz Ferreira, E. Cristina de Oliveira, Z. Novais da Rocha, *Inorg. Chim. Acta*, **2005**, *358*, 2909-2920.

[69] D. Taher, B. Walfort, G. van Koten, H. Lang, *Inorg. Chem. Commun.*, **2006**, *9*, 955-958.

[70] J. J. Turner, F.-W. Grevels, S. M. Howdle, J. Jacke, M. T. Haward, W. E. Klotzbucher, *J. Am. Chem. Soc.*, **1991**, *113*, 8347-8353.

[71] T. Ito, T. Hamaguchi, H. Nagino, T. Yamaguchi, H. Kido, I. S. Zavarine, T. Richmond, J. Washington, C. P. Kubiak, *J. Am. Chem. Soc.*, **1999**, *121*, 4625-4632.

[72] H. W. Kroto, J. R. Heath, S. C. O'Brien, R. F. Curl, R. E. Smalley, *Nature*, **1985**, *318*, 162.

[73] a) M. Prato, *J. Mater. Chem.*, **1997**, *7*, 1097-1109. b) T. Da Ros, M. Prato, *Chem. Commun.*, **1999**, 663-669.

[74] P. M. Allemand, K. C. Khemani, A. Koch, F. Wudl, K. Holczer, S. Donovan, G. Gruner, J. D. Thompson, *Science*, **1991**, *253*, 301-303.

[75] J. H. Schon, C. Kloc, R. C. Haddon, B. Batlogg, *Science*, **2000**, *288*, 656-658.

[76] a) F. Wudl, *Acc. Chem. Res.*, **1992**, *25*, 157. b) R. Taylor, D. R. M. Walton, *Nature*, **1993**, *363*, 685. c) A. Hirsch, *Angew. Chem., Int. Ed. Engl.*, **1993**, *32*, 1138. d) A. Hirsch, *The Chemistry of the Fullerenes*, Thieme, Stuttgart, **1994**. e) F. Diedeirich, L.

Isaacs, D. Philip, *Chem. Soc. Res.*, **1994**, *23*, 243. f) A. Hirsch, *Synthesis*, **1995**, 865. g) R. Taylor, *The chemistry of Fullerenes*, World Scientific, Singapore, **1995**. h) F. Diederich, C. Thilgen, *Science*, **1996**, *271*, 317.

[77] R. C. Haddon, *Acc. Chem. Res.*, **1992**, *25*, 127.

[78] R. C. Haddon, *Science*, **1993**, *261*, 1545.

[79] K. Komatsu, Y. Murata, N. Takimoto, S. Mori, N. Sugita, T. S. M. Wan, *J. Org. Chem.*, **1994**, *59*, 6101-6102.

[80] S. A. Vail, P. J. Krawezuk, D. M. Guldi, A. Palkar, L. Echegoyen, J. P. C. Tomé, M. A. Fazio, D. I. Schuster, *Che. Eur. J.*, **2005**, *11*, 3375-3388.

[81] N. Bucci, T. J. J. Muller, *Tetrahedron Letters*, **2006**, *47*, 8329-8332.

[82] Y. Murata, M. Suzuki, K. Komatsu, *Org. Biomol. Chem.*, **2003**, *1*, 2624-2625.

[83] a) M. Prato, M. Maggini, C. Giacometti, G. Scorrano, G. Sandonà, G. Farnia, *Tetrahedron*, **1996**, *52*, 5221. b) C. Atienza, B. Insuasty, C. Seoane, N. Martìn, J. Ramey, G. M. A. Rahaman, D. M. Guldi, *J. Mater. Chem.*, **2005**, *15*, 124. c) S. R. Wilson, S. MacMahon, F. T. Tat, P. D. Jarowski, D. I. Schuster, *Chem. Commun.*, **2003**, 226-227.

[84] M. Maggini, G. Scorrano, M. Prato, *J. Am. Chem. Soc.*, **1993**, *115*, 9798-9799.

[85] O. Tsuge, S. Kanemasa, *Adv. Heterocycl. Chem.*, **1989**, *45*, 231.

[86] D. M. Guldi, M. Prato, *Acc. Chem. Res.*, **2000**, *33*, 695-703.

[87] a) A H. H. Stephens, M. L. H. Green, *Adv. Inorg. Chem.*, **1997**, *44*, 1-43. b) A. L. Balch, L. L. Olmstead, *Chem. Rev.*, **1998**, *98*, 2123-2165. c) K. Lee, H. Song, J. T. Park, *Acc. Chem. Res.*, **2003**, *36*, 78-86. d) Y.-J. Cho, T. K. Ahn, H. Song, K. S. Kim, C. Y. Lee, W S. Seo, K. Lee, S. K. Kim, D. Kim, J. T. Park, *J. Am. Chem. Soc.*, **2005**, *127*, 2380-2381. e) B. K. Park, G. Lee, K. H. Kim, H. Kang, C. Y. Lee, M. A. Miah, Y.-K. Han, J. T. Park, *J. Am. Chem. Soc.*, **2006**, *128*, 11160-11172. f) B. K. Park, C. Y. Lee, J. Jung, J. H. Lim, Y. –K. Han, C. S. Hong, J. T. Park, *Angew. Chem. Int. Ed.*, **2007**, *46*, 1436-1439.

[88] Y.-K. Han, K. H. Kim, J. C. Kim, B. K. Park, J. T. Park, *Eur. J. Inorg. Chem.*, **2010**, 1530-1535.

[89] Y. Matsuo, E. Nakamura, *Organometallics*, **2003**, *22*, 2554-2563.

[90] M. Sawamura, Y. Kuninobu, M. Toganoh, Y. Matsuo, M. Yamanaka, E. Nakamura, *J. Am. Chem. soc.*, **2002**, *124*, 9354.

[91] M. Sawamura, Y. Kuninobu, E. Nakamura, *J. Am. Chem. Soc.*, **2000**, *122*, 12407.

[92] a) M. Sawamura, H. Iikura, E. Nakamura, *J. Am. Chem. Soc.*, **1996**, *118*, 12850. b) M. Sawamura, H. Iikura, A. Horai, E. Nakamura, *J. Am. Chem. Soc.*, **1998**, *120*, 8285. c) M. Sawamura, M- toganoh, Y. Kuninobu, S. Kato, E. Nakamura, *Chem. Lett.*, **2000**, 270. d) M. Sawamura, H. Iikura, T. Ohama, U. E. Hackler, E. Nakamura, *J. Organomet. Chem.*, **2000**, *599*, 32. e) M. Sawamura, M. Toganoh, H. Iikura, Y. Matsuo, A. Hirai, E. Nakamura, *J. Mater. Chem.*, **2002**, *12*, 2109.

[93] H. Iikura, S. Mori, M. Sawamura, E. Nakamura, *J. Org. Chem.*, **1997**, *62*, 7912.

[94] H. Song, Y. Lee, Z.-H. Choi, K. Lee, J. T. Park, J. Kwak, M.-G. Choi, *Organometallics*, **2001**, *20*, 3139-3144.

[95] a) H.-F. Hsu, J. R. Shapley, *J. Am. Chem. Soc.*, **1996**, *118*, 9192-9193. b) H.-F. Hsu, J. R. Shapley, *J. Organomet. Chem.*, **2000**, *599*, 97-105.

[96] a) J. T. Park, H. Song, J.-J. Cho, M.-K. Chung, J.-H. Lee, I.-H. Suh, *Organometallics*, **1998**, *17*, 227-236. b) H. Song, K. Lee, J. T. Park, M.-G. Choi, *Organometallics*, **1998**, *17*, 4477-4483. c) H. Song, K. Lee, J. T. Park, H. Y. Chang, M.-G. Choi, *J. Organomet. Chem.*, **2000**, *599*, 49-56.

[97] a) K. Lee, H.-F. Hsu, J. R. Shapley, *Organometallics*, **1997**, *16*, 3876-3877. b) K. Lee, J. R. Shapley, *Organometallics*, **1998**, *17*, 3020-3026.

[98] K. Lee, C. H. Lee, H. Song, J. T. Park, h. Y. Chang, M.-G. Choi, *Angew. Chem., Int. Ed.*, **2000**, *39*, 1801-1804. b) K. Lee,Z.-H. Choi, Y.-J. Cho, H. Song, J. T. Park, *Organometallics*, **2001**, *20*, 5564-5570.

[99] K. Lee, H. Song, B. Kim, J. T. Park, s. Park, M.-G. Choi, *J. Am. Chem. Soc.*, **2002**, *124*, 2872-2873.

[100] B. M. Illescas, N. Martín, Charter 36 from *Handbook of Nanophysics: Clusters and Fullerenes*, 2, edited by K. D. Sattler, CRC Press, Boca Raton (Florida), **2011**.

[101] M. Maggini, A. Donò, G. Scorrano, M. Prato, *J. Chem. Soc., Chem. Commun.*, **1995**, 845.

[102] D. Armspach, E. C. Constable, F. Diederich, C. E. Housecroft, J.-F. Nierengarten, *Chem. Commun.*, **1996**, 2009.

[103] a) M. Maggini, A. Karlsson, G. Scorrano, G. Sandonà, G. Farnia, M. Prato, *J. Chem. Soc., Chem. Commun.*, **1994**, 589. b) M. Prato, M. Maggini, C. Giacometti, G. Scorrano, G. Sandonà, G. Farnia, *Tetrahedron*, **1996**, *52*, 5221.

[104] W. B. Austin, N. Bilow, W. J. Kelleghan, K. S. Y. Lau, *J. Org. Chem.*, **1981**, *46*, 2280-2286.

[105] a) R. Bender, P. Braunstein, A. Dedieu, P. D. Ellis, B. Huggins, P. D. Harvey, E. Sappa, A. Tiripicchio, *Inorg. Chem.*, **1996**, *35*, 1223. b) R. Bender, P. Braustein, A. tiripicchio, M. Tiripicchio Camellini, *Angew. Chem., Int. Ed.*, **1985**, *24*, 861.

[106] a) A. Bondi, *J. Phis. Chem.*, **1964**, *68*, 441-451. b) A. Bondi, *Physical Properties of Molecular Crystal, Liquids and Glasses*, Wiley, New York, **1968**.

[107] P. Leoni, F. Marchetti, M. Pasquali, L. Marchetti, A. Albinati, *Organometallics*, **2002**, *21*, 2176-2182.

[108] J. Li, H. Grennberg, *Chem. Eur. J.*, **2006**, *12*, 3869.

[109] J. Lewis, N. J. Long, P. R. Raithby, G. P. Shields, W.-Y. Wong, M. Younus, *J. Chem. Soc., Dalton Trans.*, **1997**, 4283-4288.

[110] P. Zanello, F. Laschi, M. Fontani, C. Mealli, A. Ienco, K. Tang, X. Jin, L. Li, *J. Chem. Soc., Dalton Trans.*, **1999**, 965-970.

[111] a) L. Echegoyen, L. E. Echegoyen, *Acc. Chem. Res.*, **1998**, *31*, 593-600. b) T. Suzuki, Y. Maruyama, T. Akasaba, W. Ando, K. Kobayashi, S. Nagase, *J. Am. Chem. Soc.*, **1994**,*116*, 1359-1363.

[112] T. J. Wadas, R. J. Lachicotte, R. Eisenberg, *Inorg. Chem,*, **2003**, *42*, 3772-3778.

[113] Y. Shirai, Y. Zhao, L, Cheng, J. M. Tour, *Org. Lett.*, **2004**, *6*, 2129.

[114] D. M. Guldi, M. Maggini, G. Scorrano, M. Prato, *J. Am. Chem. Soc.*, **1997**, *119*, 974-980.

[115] a) D. M. Guldi, S. Gonzales, N. Martin, A. Anton, J. Garin, J. Orduna, *J. Org. Chem.*, **2000**, *65*, 1978-1983. b) K. Simonsen, V. Konovalov, T. Konovalova, T. Kawai, M. Cava, L. Kispert, R. Metzger, J. Becher, *J. Chem. Soc., Perkin Trans. 2*, **1999**, 657-665.

[116] A. M. Arif, D. E. Heaton, R. A. Jones, C. M. Nunn, *Inorg. Chem.*, **1987**, *26,* 4228.

[117] P. W. Dyer, J. Fawcett, M. J. Hanton, D. M. P. Mingos*,* A.-M. Williamson, *Dalton Trans.*, **2004**, 2400.

[118] M. T. Reetz, E. Bohres, R. Goddard, M. C. Holthausen, W. Thiel *Chem. Eur. J.*, **1999**, *5*, 2101

[119] M. M. Dell'Anna, P. Mastrorilli, C. F. Nobile, B. Calmuschi-Cula, U. Englert M. Peruzzini *Dalton Trans.*, **2008**, 6005.

[120] P. Leoni, S. Manetti, M. Pasquali, *Inorg. Chem*., **1995**, *34*, 749-752.

[121] P. Leoni, M. Sommovigo, M. Pasquali, P. Sabatino, D. Braga, *J. Organomet. Chem.*, **1992**,*423*, 263-270.

[122] P. Leoni, G. Chiaradonna, M. Pasquali, F. Marchetti, *Inorg. Chem.*, **1999**, *38*, 253-259.

[123] Allen, F. H. *Acta Cryst.*, **2002**, *B58*, 380-388.

[124] S. Arifhodzic-Radojevic, A. D. Burrows, N. Choi, M. McPartlin, D. M. P. Mingos, S. V. Tarlton, R. Vilar, *J. Chem. Soc., Dalton Trans.*, **1999**, 3981-3988.

[125] P. Leoni, E. Vichi, S. Lencioni, M. Pasquali, E. Chiarentin, A. Albinati, *Organometallics*, **2000**, *19*, 3062-3068.

[126] N. G. Connelly, W. E. Geiger, *Chem. Rev.*, **1996**, *96*, 877-910.

[127] a) A. I. Vogel, *Textbook of Practical Organic Chemistry*, fifth edition, Longman Scientific and Technical, Harlow, UK, **1989**. b) D. D. Perrin, W. L. F. Armarego, *Purification of Laboratory Chemical*, third edition, Pergamon Press, **1988**.

[128] R. B. King, M. B. Bisnette, *J. Organomet. Chem*., **1967**, *8*, 287.

[129] J. Li, H. Grennberg, *Chem. Eur. J.*, **2006**, *12*, 3869.

[130] M. Krejčik, M. Daněk, F. Hartl, *J. Electroanal. Chem*., **1991**, *317*, 179.

[131] A. J. Carty, S. A. MacLaughlin, D. Nucciarone, "Phosporus-^{31}P NMR Spectroscopy in Stereochemical Analisys: Organic Compounds and Metal Complexes", J. B. Verkade. L. D. Quin Editori, VCH, Weinheim, **1987**.

[132] a) A. Albinati, F. Lianza, M. Pasquali, M. Sommovigo, P. Leoni, P. S. Pregosin, H. Rüegger, *Inorg.Chem.*, **1991**, 30, 4690; b) P. Leoni, M. Pasquali, M. Sommovigo, F. Laschi, P. Zanello, A. Albinati, F. Lianza, P. S. Pregosin, H. Rüegger, *Organometallics*, **1993**, 12, 4503; c) P. Leoni, M. Pasquali, M. Sommovigo, F. Laschi, P. Zanello, A. Albinati, F. Lianza, P. S. Pregosin, H. Rüegger, *Organometallics*, **1994**, 13, 4017; d) M. Sommovigo, M. Pasquali, F. Marchetti, P. Leoni, T. Beringhelli, *Inorg. Chem*, **1994**, 33, 2651; e) M. Sommovigo, M. Pasquali, F. Marchetti, P. Leoni, U. Englert, *Inorg. Chem*, **1994**, 33, 2686; f) P. Leoni, *Organometallics*, **1993**, 12,2432.

[133] a) P. S. Pregosin, *Coord. Chem. Rev,*, **1982**, 44, 247; b) P. S. Pregosin, *Ann. Rep. NMR Spectroscopy*, **1986**, 285.

[134] M. P. Brown, R. J. Puddephatt, M. Rashidi, K. R. Seddon, *J.Chem.Soc., Dalton Trans.,* **1978**, 516.

[135] C. J. Jones, *Chem. Soc. Rev.*, **1998**, *27*, 286.

[136] a) D. A. Skogg, J. J. Leary, *Chimica Analitica Strumentale*, forth edition, EdiSES, Napoli, **1992**. b) P. Zanello, *Inorganic Electrochemistry*, RSC Ed., **2003**.

[137] M. B. Robin, P. Day, *Adv. Inorg. Chem. Radiochem.*, **1967**, *10*, 247.

[138] K. D. Demadis, C. M. Hartsham, J. Meyer, *Chem. Rev.*, **2001**, *101*, 2655.